UNIVERSIDADE ESTADUAL PAULISTA "JÚLIO DE MESQUITA FILHO"
FACULDADE DE ENGENHARIA
CAMPUS DE ILHA SOLTEIRA

BRUNA SILVEIRA PAVLACK

DAMAGE QUANTIFICATION USING POLYNOMIAL CHAOS-KRIGING

Ilha Solteira
2022

BRUNA SILVEIRA PAVLACK

DAMAGE QUANTIFICATION USING POLYNOMIAL CHAOS-KRIGING

A Thesis submitted to the Faculdade de Engenharia de Ilha Solteira - UNESP in partial fulfillment of the requirements for obtaining the Doctorate in Mechanical Engineering.
Knowledge area: Solid Mechanics

Advisor: Prof. Dr. Samuel da Silva
Co-advisor: Prof. Dr. Americo Barbosa da Cunha Junior

Ilha Solteira

2022

FICHA CATALOGRÁFICA
Desenvolvido pelo Serviço Técnico de Biblioteca e Documentação

P338d

Pavlack, Bruna Silveira.
Damage quantification using Polynomial Chaos - Kriging / Bruna Silveira Pavlack.-- Ilha Solteira: [s.n.], 2022

117 f. : il.

Dissertação (mestrado) - Universidade Estadual Paulista. Faculdade de Engenharia de Ilha Solteira. Área de conhecimento: Mecânica dos Sólidos, 2022

Orientador: Samuel da Silva
Coorientador: Americo Barbosa da Cunha Junior
Inclui bibliografia

1. Structural health monitoring. 2. Composite structures. 3. Propagation of uncertainties. 4. Damage detection. 5. Damage quantification. 6. Polynomial Chaos-Kriging method.

Raiane da Silva Santos
Supervisora Técnica de Seção
Seção Técnica de Referência, Atendimento ao usuário e Documentação
Diretoria Técnica de Biblioteca e Documentação
CRB/8 - 9999

unesp

UNIVERSIDADE ESTADUAL PAULISTA

Câmpus de Ilha Solteira

CERTIFICADO DE APROVAÇÃO

TÍTULO DA TESE: Damage quantification using Polynomial Chaos-Kriging

AUTORA: BRUNA SILVEIRA PAVLACK
ORIENTADOR: SAMUEL DA SILVA
COORIENTADOR: AMERICO BARBOSA DA CUNHA JUNIOR

Aprovada como parte das exigências para obtenção do Título de Doutora em ENGENHARIA MECÂNICA, área: Mecânica dos Sólidos pela Comissão Examinadora:

Prof. Dr. SAMUEL DA SILVA (Participaçao Virtual)
Departamento de Engenharia Mecanica / Faculdade de Engenharia de Ilha Solteira - UNESP

Prof. Dr. ELÓI JOÃO FARIA FIGUEIREDO (Participaçao Virtual)
Engenharia Mecânica / Universidade Lusófona de Humanidades e Tecnologias

Prof. Dr. ALEXANDRE ABRAHÃO CURY (Participaçao Virtual)
Mecânica Aplicada e Computacional / Universidade Federal de Juiz de Fora - UFJF

Profa. Dra. MARCELA RODRIGUES MACHADO (Participaçao Virtual)
Departamento de Engenharia Mecânica / Universidade de Brasília (UnB)

Prof. Dr. NEY ROITMAN (Participaçao Virtual)
Departamento de Engenharia Civil / Universidade Federal do Rio de Janeiro (UFRJ)

Ilha Solteira, 24 de junho de 2022

To my parents José and Cleusa and
to my siblings Alana, Gabrieli and Gabriel
for unconditional love and for being always present,
regardless of physical distance.

To my husband Diogo for his love,
patience and partnership on this journey.

To all my teachers, who believe and fight for a quality public education.

ACKNOWLEDGMENTS

Since August 2018 I have dedicated my efforts to be able to present in this thesis a modest contribution to the area of solid mechanics, but none of this would be possible without the people who helped me along this path. That's why I want to express my eternal gratitude in the following paragraphs.

First of all, I thank God, who gave me the life and faith to carry on in difficult times. Nothing I've achieved so far would be possible without my parents. To you José and Cleusa, my immense gratitude. Thank you for the love you have always given me and for even without studying, having fought so hard for me and my siblings to learn. My gratitude to my siblings Alana, Gabrieli and Gabriel, who are always by my side, sharing moments of joy and afflictions. And to my husband, Diogo, for his love, patience and advice. None of this would be possible without your unconditional support.

I thank and dedicate this thesis to all my teachers, from primary education to higher education. Thank you so much for believing in quality public education and contributing to my formation! In particular, I thank my advisor Samuel da Silva and co-advisor Americo Cunha. Thank you for introducing me to the world of Structural Health Monitoring. I am very grateful for all the teachings and patience in the course of this work. I would also like to thank Prof. David Garcia Cava for his collaboration in this work and for providing the dataset of the wind turbine blade. I am also immensely grateful all the professors of the Department of Mechanical Engineering at FEIS - Unesp for their classes. Finally, I am grateful to the examination committee for the comments and contributions.

I would like to thank all my colleagues from the Nucleus of Modeling and Experimentation with Computers (NUMERICO) and the Group of Intelligent Materials and Systems (GMSINT). Thank you for all the contributions and sharing of ideas during these doctoral years! Special thanks to Jessé Paixão, João Pedro Canisso, and Luccas Miguel for our work developed together. I would also like to thank my friends, Alessandra, Caroline, Débora, Elisângela, Eva, Fagner, Gabriele, Gláucia, Jéssica, Jocélia, Luthiana, Mariana, Silvia, and Vitor, for always staying by my side, encouraging and supporting. Thank you so much for your friendship!

I would like to acknowledge the institutional support of Federal Institute of Mato

Grosso do Sul and Paulista State University “Júlio de Mesquita Filho” and financial support from CAPES.

My sincere gratitude to everyone I have not mentioned, but who contributed directly or indirectly to the realization of this work! Hope you enjoy reading!

"Ninguém ignora tudo. Ninguém sabe tudo. Todos nós sabemos alguma coisa. Todos nós ignoramos alguma coisa. Por isso aprendemos sempre."

Paulo Freire ($\star$1921, †1997).

ABSTRACT

Society increasingly craves the generation of clean and affordable energy. An alternative to this is energy from the wind, wind energy. In this sense, there is an increase in the number of wind farms and, consequently, the number of wind turbines in operation. Since wind turbines are large structures, their visual inspection can present a high number of false alarms that can cause significant human life risks. In this scenario, it is essential to develop Structural Health Monitoring methodologies in wind turbines to detect and quantify damage and, consequently, avoid failures and accidents. This work presents a data-driven vibration methodology for Structural Health Monitoring. The key idea is to apply a Polynomial Chaos-Kriging metamodel for damage quantification. The investigation seeks to quantify the damage severity, described by a specific type of debonding in a composite wind turbine blade as a damage index function, assuming the uncertainties. The blade was instrumented with ten accelerometers on the trailing edge, ten accelerometers on the leading edge, and an electromechanical actuator, which generates the impact on the structure. The obtained metamodel demonstrates the ability to capture the trend that relates the damage indices and the damage size at the simulated points. Subsequently, a global sensitivity analysis is performed to identify the influence of each accelerometer on the global damage index. The sensitivity analysis method used is the Sobol' indices. The results obtained from the Sobol' indices are satisfactory, as they demonstrate that the sensors located in the damage path have greater sensitivity and influence on the global damage index. Studies of this nature are essential, as they make it possible to optimize the location of sensors for better detection of damage and contribute to cost reduction. Finally, a methodology for damage detection on the blade is also proposed, using a confidence interval of 95% of a Kriging model obtained from the transmissibility function between two sensors in the healthy condition. The detection probabilities obtained for the damage conditions were satisfactory.

Keywords: Structural Health Monitoring. Composite structures. Propagation of uncertainties. Damage detection. Damage quantification. Polynomial Chaos-Kriging method. Sensitivity analysis. Sobol' indices.

RESUMO

Cada vez mais a sociedade almeja pela geração de energia limpa e acessível. Uma alternativa para isso é a energia proveniente dos ventos, a energia eólica. Neste sentido, há um aumento no número de parques eólicos e, consequentemente, um aumento no número de aerogeradores em operação. Devido ao fato dos aerogeradores serem estruturas grandes, sua inspeção visual pode apresentar grandes riscos à vida humana. Neste cenário, é muito importante o desenvolvimento de metodologias de Monitoramento da Saúde Estrutural em aerogeradores, com o intuito de detectar e quantificar danos, e consequentemente evitar falhas e acidentes. Neste trabalho é apresentada uma metodologia de Monitoramento da Saúde Estrutural, baseada em vibração orientada por dados, para quantificação de danos utilizando um metamodelo obtido a partir do método Polinômio do Caos-Krigagem. A investigação busca quantificar a severidade do dano, descrito por um tipo específico de descolamento em uma pá de turbina eólica de compósito, em função de um índice de dano, levando-se em consideração as incertezas. A pá foi instrumentada com dez acelerômetros na borda superior, dez acelerômetros na borda inferior e um atuador eletromecânico, o qual gera o impacto na estrutura. O metamodelo obtido demonstra ser capaz de capturar a tendência que relaciona os índices de dano e o tamanho do dano nos pontos simulados. Posteriormente, é realizada a análise de sensibilidade global para identificar a influência de cada acelerômetro em um índice de dano global. O método de análise de sensibilidade utilizado é os índices de Sobol. Os resultados obtidos dos índices de Sobol são satisfatórios, pois demonstram que os sensores localizados no caminho do dano possuem maior sensibilidade e influência no índice de dano global. Estudos dessa natureza são fundamentais, pois possibilitam otimizar a localização dos sensores para melhor detecção de danos e contribuir para a redução de custos. Por fim, também é proposta uma metodologia para detecção de danos na pá, por meio de um intervalo de confiança de 95% de um modelo Krigagem obtido a partir da função de transmissibilidade entre dois sensores, na condição saudável. As probabilidades de detecção obtidas para as condições de dano foram satisfatórias.

Palavras-chave: Monitoramento da Saúde Estrutural. Estruturas de material compósito. Propagação de incertezas. Detecção de dano. Quantificação de dano. Metódo Polinômio de Caos-Krigagem. Análise de sensibilidade. índices de Sobol.

LIST OF FIGURES

LIST OF TABLES

LIST OF ACRONYMS

AK-MCS	-	Adaptive Kriging-Monte Carlo Simulation
AR	-	Autoregressive
CFRP	-	Carbon Fiber Reinforced Polymer
DI	-	Damage index
FEM	-	Finite Element Method
FFT	-	Fast Fourier Transform
FG-CNT	-	Functionally graded carbon nanotube
FRF	-	Frequency response function
FV	-	Feature Vector
GPR	-	Gaussian Process Regression
GSA	-	Global sensitivity analysis
LARS	-	Least Angle Regression
LE	-	Leading Edge
LOO	-	leave-one-out
MC	-	Monte Carlo
MD	-	Mahalanobis distance
NARX	-	Nonlinear AutoRegressive with eXogenous input model
OPCK	-	Optimal Polynomial Chaos-Kriging
PC	-	Principal Component
PCA	-	Principal Component Analysis
PC-Kriging	-	Polynomial Chaos-Kriging
PCE	-	Polynomial Chaos Expansion
PDF	-	Probability Density Function
PSD	-	Power Spectral Density
PZT	-	Piezoeletric transducer
RC	-	Reconstructed Component
RMSE	-	Root Mean Squared Error
ROC	-	Receiver Operating Characteristic
SAR	-	Specific Absorption Rate
SB-VAWT	-	Straight blade vertical axis wind turbine
SCADA	-	Supervisory Control and Data Acquisition

SHM	-	Structural Health Monitoring
SPCK	-	Sequential Polynomial Chaos-Kriging
TE	-	Trailing Edge
UQ	-	Uncertainty Quantification
VSHM	-	Vibration Structural Health Monitoring

LIST OF SYMBOLS

$\mathbf{A}$	-	Experimental matrix known of the model
$\mathcal{A}$	-	Subset of the polynomial indexes
$\beta^T f(x)$	-	Mean value of the Gaussian distribution
$\mathbf{C}_Z$	-	Covariance matrix of the embedded matrix
$\mathbb{C}$	-	Damping matrix of a system
$\mathcal{D}$	-	Cardinality of set $\mathcal{A}$
$\mathcal{D}_i$	-	Local damage index corresponding to the i-th path
$\mathcal{DI}$	-	Global damage index
$\mathcal{D}_T$	-	Probabilistic threshold
$\mathcal{D}_x$	-	support of the vector distribution $\mathbf{X}$
$\mathbf{E}_X$	-	Matrix of eigenvectors
$f_{\mathbf{X}}$	-	PDF relative to $\mathbf{X}$
$f(t)$	-	Input force vector
h_i	-	i-th component of the vector
k	-	Independent input parameters
$\mathbb{K}$	-	Stiffness matrix of a system
M	-	Number of realizations of the signal vector
$\mathbb{M}$	-	Mass matrix of a system
$\mathcal{M}$	-	Computational model
$\mathcal{M}^{PC}$	-	Truncated computational model
$\mathbb{N}$	-	Set of natural numbers
p	-	Vector dimension
$\mathbb{R}$	-	Set of real numbers
$\mathcal{R}$	-	Correlation function
$\mathbf{R}$	-	Matrix of reconstructed components
S_i	-	First-order Sobol' indices
S_{ij}	-	Second-order Sobol' indices
S_i^T	-	Total Sobol' indices
$\mathcal{S}$	-	Vector of damage severity
$\mathbf{T}_B$	-	Baseline feature matrix
$\mathbf{T}_i$	-	Feature vector

$T_{(S_i,S_j)}$	-	Transmissibility of sensor s_i and s_j
$x(t)$	-	Contains the responses of each degree-offreedom of the system
$\mathcal{X}$	-	Initial experimental design
x_i	-	i-th element of the vector of damage indices
x_j	-	j-th element of the vector of damage indices
$\mathbf{X}$	-	Input vector
$\check{\mathbf{X}}$	-	Full embedded matrix of the reference state
Y	-	Model output
$\mathcal{Y}$	-	Initial experimental design response
y	-	PCE coefficients
$\mathbb{Z}$	-	Set of integers
$\mathbf{Z}$	-	Matrix containing signal vectors corresponding to the healthy condition
$\check{\mathbf{Z}}$	-	Full embedded matrix of the reference state
$\mathcal{Z}(.,.)$	-	Zero mean, unit variance, and a stationary Gaussian process
W	-	Number of legged copies used in the embedding operation

GREEK LETTERS

α	-	Index of the components of the polynomial
δ	-	Kronecker delta
ϵ	-	Truncation error
ϵ_{LOO}	-	Leave-one-out error
ϵ_{gen}	-	Generalized error
$\epsilon_{gen_{emp}}$	-	Empirical error
ϵ_{val}	-	validation error
κ	-	Threshold defined by a risk of false alarm probability
μ^{PC}	-	Mean value of a PCE
μ_B	-	Mean vector of the baseline feature matrix
ϕ	-	Orthonormal polynomials
Ψ	-	Orthonormal polynomials
Π	-	Tensor product
σ^2	-	Variance
Σ	-	Covariance matrix of the training data in the baseline condition associated with Mahalanobis squared distance
Σ_Z	-	Covariance of baseline feature matrix
θ	-	Hyperparameter vector of kernel function
Ω	-	Describes outcomes of the underlying probability space with a correlation family
ω	-	Frequency

CONTENTS

1 INTRODUCTION

This chapter presents the motivation of the thesis, pointing out the main challenges of Structural Health Monitoring (SHM) problems in nonlinear systems and composite materials, considering the presence of uncertainties. Objectives are presented, the main contributions of the thesis are also addressed, and the chapter ends with the outline of the work.

1.1 MOTIVATION

SHM methods are used to diagnose and extract meaningful information about the health from a structure of interest, based on the measured data from sensors distributed and permanently installed along the structure (LARROSA; LONKAR; CHANG, 2014). In the last years, many SHM methods have reached the right level in detecting and locating with reliably the presence and propagation of the damage in structural systems. SHM techniques have four functional levels of the classification proposed by Rytter (1993): Level 1 – damage detection, Level 2 – damage location, Level 3 – damage quantification, and Level 4 – remaining useful life estimate. The first three levels are also categorized as diagnosis and the last as prognosis in the literature. All levels are significant for structural health. However, it should note that performing level 1 is critical because it can avoid failures and accidents by detecting damage. In the literature, there are fewer works from levels 2, 3, and 4 than from level 1, as these levels are more challenging to obtain. Because of the above, it is concluded that SHM techniques are essential because they consist of detecting damage in initial states, thus intervening in its propagation and, consequently, preventing an accident from occurring. Worden *et al.* (2015) show an overview of different SHM strategies.

All mechanical systems in operation end up having a nonlinear vibration regime at some time of their operating cycle; this is due to the existence and appearance of numerous mechanisms such as clearances, friction, materials with complex constitutive relationships, flexibility, excessive loading, high operating speeds, etc. (VIRGIN, 2000; WORDEN; TOMLINSON, 2001). There are no general dynamic analysis methods in nonlinear mechanical systems as in linear cases. However, the literature is already very

mature and aware of the need to consider these effects both in the design and adjustment phases, structural analysis, modification, and optimization (GOGE *et al.*, 2005; KERSCHEN *et al.*, 2006; TANG *et al.*, 2015). In the last decade, there has been a shift in emphasis to accommodate the growing industrial need for tools capable of handling complex nonlinearities in larger-scale structures. In Noël and Kerschen (2017) the main developments in the study of nonlinear systems since 2006 were researched. To illustrate the techniques, they used a satellite structure.

The problem of SHM in nonlinear systems is organized in two basic formulations (BORNN; FARRAR; PARK, 2010). In the first formulation, the system is assumed to be linear before damage occurs. After the appearance or nucleation of some damage, some nonlinear effect on the structure's response is induced. Damage are typical failure modes caused by impact, cracks (FRISWELL; PENNY, 2002), delamination (MANDAL; WADADAR; BANERJEE, 2015) or rubbing (ZENG *et al.*, 2015), which are essentially nonlinear effects. Thus, the detection process detects nonlinearity in the system responses in this procedure. The design is more complicated in the second formulation but closer to industrial interest cases. It is considered that engineering systems can already operate in a nonlinear manner before structural variation occurs. In these situations, the inherent nonlinearities need to be considered before the damage appears not to be mistaken for damage.

Villani, Silva and Cunha Jr (2019b) observed that when a structure vibrates, assuming an uncertain propagation[1], it is difficult to distinguish whether the variations observed in indices extracted from the signals to assess the health a structure occurred due to damage or natural variability of these inherent uncertainties of geometry, boundary conditions, etc. It was found that there is a need to assume and propagate these uncertainties in the prediction models or even in the classic metrics for checking the structural state, aiming at the detection and classification of the correct structural condition of the system under analysis. The results obtained in Villani, Silva and Cunha Jr (2019b) and Villani *et al.* (2019) showed that the use of stochastic models, and in this case models via Volterra series, made the decision-making method for damage detection more robust, raising the level of statistical reliability, which was confirmed by the Receiver Operating Characteristic (ROC) curves. It is worth remembering that these problems were quite complicated because the structure vibrates in a nonlinear regime of motion. The damage present also induces nonlinear vibrations, in this case, emulating breathing crack. Thus, if it is

[1]Either due to measurement noise or variation of manufacturing, operational or environmental parameters.

done unsupervised, the classification problem demands a lot from the numerical models of evaluation, even more so if there are uncertainties in the parameters being propagated. However, the entire process of reproducing the uncertainty of the stochastic model used in Villani, Silva and Cunha Jr (2019b) was simulated by the Monte Carlo method, which requires a large amount of data for sampling to ensure convergence. This represents a significant disadvantage since many samples' need dramatically increases the computational cost of processing in a scenario closer to the real, even more than they need for much experimental realization to have the stochastic model estimated from the experimental data. It should also be noted that the high number of achievements to access makes the method impractical in an industrial context. With this, there is a practical need to have a faster and more straightforward approach to obtain these metamodels[2] of the structures to be monitored to detect damage in this scenario with uncertainties (SARGSYAN, 2017).

The Monte Carlo method is widely used for the propagation of uncertainties. However, this method requires many samples, as has been highlighted before. Fortunately, the literature has shown alternative ways to propagate uncertainty in models from random inputs with lower sampling costs. One of these ways is the Polynomial Chaos Expansion (PCE) method. The PCE has been shown to represent the uncertainties in the physical input parameters from orthogonal functions that propagate the uncertainties to the model outputs with simulations that require less sampling than the Monte Carlo method. Another advantage is that classic auto-regressive models can be combined with the PCE method to identify stochastic metamodels used in SHM. Among the uncertainties, we can highlight entries such as environmental parameters, the temperature that can be measured, or even variation of excitation frequencies in the propagation of waves in the composite material, propagation path, etc. (BOGOEVSKA *et al.*, 2017; SPIRIDONAKOS; CHATZI; SUDRET, 2016).

In Umesh and Ganguli (2013) the PCE was used to study the effect of uncertainty on the vibration control of a smart composite material plate with piezoelectric sensors or actuators. The composite material properties and the piezoelectric coefficients were considered independent and normally distributed random variables. Spiridonakos and Chatz (2014) used the PCE to describe the propagation of uncertainties in a stochastic system and to evaluate changes in the conditions of the structural system and independent components. This work showed how PCE could be used to detect damage. In Mai (2016) has been demonstrated that methods using PCE can be applied to dynamic systems with uncertain parameters and or uncertain excitation. A more general approach has been

[2]Reduced models, based on approximations of the rigorous model.

investigated to solve problems of mechanical systems subject to stochastic excitations. The system dynamics is a nonlinear stochastic autoregressive model with exogenous input (NARX), whose stochastic parameters are modeled with PCEs.

In this sense of using the PCE, a very interesting method and still little explored in the literature is the Polynomial Chaos-Kriging (PC-Kriging) method, which results from the combination of PCE and Kriging. This combination results in technique metamodeling more accurately than the PCE and Kriging separately (SCHÖBI *et al.*, 2014). The Kriging method, also known as Gaussian Process Regression (GPR), is a non-parametric Bayesian approach that has the advantages of working on small datasets and providing measurements that consider the predictions' uncertainties.

Another motivation for this thesis's development is to obtain of SHM methods to be used in composite material structures, which is an application of current interest. These structures are much more complicated than metallic cases because anisotropy is an inherent property. Also, these structures' manufacturing processes are almost handcrafted and with countless uncertainties in the elastic parameters, causing a lot of variation in the fundamental characteristics extracted when calculating a damage metric, such as wave propagation speed, propagation time waves, and amplitudes, ridges, etc. Composite materials are commonly made using carbon fiber, glass, Kevlar, or similar fibers. Generally, this material's most common failure modes are anisotropic and multiple, such as delamination, matrix breakage, and fiber detachment reducing stiffness (ADAMS; ADAMS, 1989). This makes fault identification and prediction more difficult. One way to avoid catastrophic failures in composite material structures is to use SHM methods to observe minor defects and inspect larger areas. García-Macías *et al.* (2016) made a study based on the stochastic representation of plates reinforced with FG-CNT[3] and analyzed the propagation of their uncertainty in the response. The finite element method (FEM) was used to study the individual and interactive effects of mechanical properties (matrix/CNTs) and classification profiles via power-law distributions. The impact of stochastic uncertainties on the composite material's global properties was represented using probability theory.

Despite the enormous resistance and the excellent weight/resistance ratios, the composite material structures can present damage mechanisms that cause very complex failures caused by low-speed impact and damages that are not superficially selected. Therefore, the application of an SHM method based only on the data of temporal responses, measured by accelerometers or PZTs (piezoelectric transducer), involving the propagation of waves is welcome and has already been the object of study in the Group of Materials

[3]Functionally graded carbon nanotube.

and Intelligent Systems - GMSINT[4] of UNESP, with good results already published in the literature (VILLANI *et al.*, 2019; VILLANI; SILVA; CUNHA JR, 2019; VILLANI, L. G. G.; SILVA, S. da; CUNHA JR, A., 2019; PAIXÃO; SILVA, 2019). In these structures, it is also essential to consider the uncertainties to detect the variations caused by damages and to be able to quantify the delamination.

Another fact is that currently, the society aims for a future where energy generation is increasingly clean and accessible, which is Goal 7 of the UN 2030 Agenda (ONU, 2015). Thus, there is an expansion in offshore wind turbines because the generation of wind energy is considered clean energy, making studies in this area necessary. Additionally, the maintenance of wind turbine blades involves, in the most part, methods based on visual inspection, which can be dangerous and expensive (CAVA; TCHERNIAK, 2019). In Piauí, Brazil, in February 2020, a wind turbine's blades came off, causing a severe accident. Fortunately, there were no injured people, but this accident could have been fatal. The company reported that the blades had undergone maintenance and were unable to identify the causes of the accident[5] (Figure 1). Therefore, a system for monitoring wind turbines' conditions is of great industrial interest, demanding further development of methodologies for detection and quantification of damage to these structures (CIANG; LEE; BANG, 2008).

Figure 1: Accident in which a wind turbine's blades came off, on the coast of Piauí - Brazil.

Source: Globo.com (2020).

[4]Of Portuguese Grupo de Materiais e Sistemas Inteligentes.
[5]News available at <https://g1.globo.com>.

Given all the above motivations, this work proposes the construction of metamodels, using the PC-Kriging method, to quantify the size of the damage in a practical application, which is a composite wind turbine blade. Afterwards, a sensitivity analysis of the location of the sensors is carried out in the composite blade to optimize the use of accelerometers and consequently reduce costs. Finally, the use of the transmissibility function, between the output data in the healthy condition of two sensors, for damage detection is proposed. This study may represent a significant advance in the techniques of SHM concerning the quantification of damages and sensitivity analysis in structures of composite material that works in a nonlinear regime, being thus challenging to model in a parametric way and subject to the significant variation of parameters due to the uncertainties inherent. Figure 2 shows a graphical abstract of the research structure developed in this thesis.

Figure 2: Graphical abstract of the research developed in the thesis.

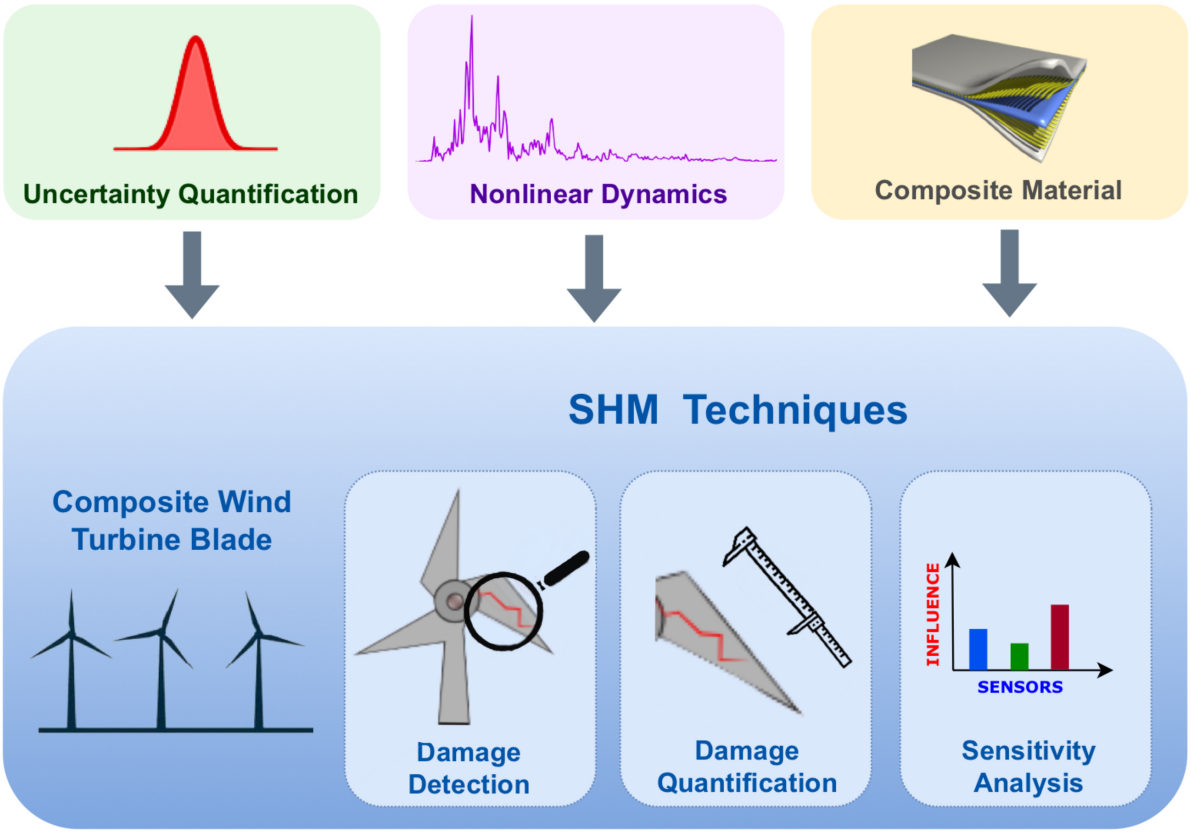

Source: Prepared by the author.

1.2 OBJECTIVES

The main objective of this thesis is to investigate new SHM methodologies for composite material structures, specifically a composite wind turbine blade, considering the uncertainties. The specific objectives can be summarized as follows:

- To propose and investigate a basis for application in SHM involving damage quantification in a structure of composite wind turbine blade from the construction of metamodels combining models of time series with the quantification of uncertainties, be it temperature or condition of operation, measured or not, but propagated by Polynomial Chaos-Kriging;
- Perform a sensitivity analysis of the location of sensors on the blade;
- To investigate the use of transmissibility function for damage detection in the composite wind turbine blade, using a Kriging metamodel.

1.3 MAIN CONTRIBUTIONS

The main contributions of the present work are:

- Study and review of the PCE, Kriging, PC-Kriging, and sensitivity analysis methods. A comparison of the use of the PCE method with the Monte Carlo method can be found in Pavlack *et al.* (2020);
- Proposal of a methodology for quantifying damage to large wind turbine blades. For this, we used the PC-Kriging method, which defines a trend curve that associates a damage index with an estimate of the damaged area, considering the uncertainties. Part of the results and discussions of chapter 4 of this thesis is published in Pavlack *et al.* (2022);
- Conducting a sensitivity analysis of the location of sensors on a wind turbine blade, aiming to optimize the use of accelerometers and reduce costs in developing SHM methodologies;
- Proposal of a methodology for damage detection in a wind turbine blade using transmissibility function between two sensors, with the healthy condition data, to obtain a Kriging metamodel, where the confidence interval of 95% is a threshold for detection of the damaged state.

1.4 OUTLINE

This thesis is structured into the following chapters:

- **Chapter 1 - INTRODUCTION:** presents the motivation of the research, objectives, and the main contributions.
- **Chapter 2 - A BRIEF STATE-OF-THE-ART REVIEW:** illustrates the main contributions in the literature on the use of metamodels to quantify damage to wind turbine blades, sensitivity analysis to optimize sensor location in the experiment, and the use of a metamodel generated from transmissibility function for damage detection.
- **Chapter 3 - METHODS FOR OBTAINING METAMODELS AND SENSITIVITY ANALYSIS:** reports the importance of considering the uncertainties in the models of mechanical systems. The methods PCE, Kriging, and PC- Kriging are presented and how these methods obtain a metamodel to propagate uncertainties. It also covers the theory of global sensitivity analysis and a way to perform the analysis, Sobol' indices.
- **Chapter 4 - PC-KRIGING METAMODEL FOR QUANTIFICATION OF THE DEBONDING AREA IN LARGE WIND TURBINE BLADES:** investigate the performance of a data-driven methodology for quantification damage based on the use of a metamodel obtained from the PC-Kriging method. The investigation seeks to quantify the severity of the damage, described by a specific type of debonding in a composite wind turbine blade as a function of a damage index. The damage indexes used are computed using a data-driven vibration Structural Health Monitoring (VSHM) methodology.
- **Chapter 5 - SENSITIVITY ANALYSIS OF SENSOR LOCATION AND USE OF TRANSMISSIBILITY FUNCTION FOR DAMAGE DETECTION IN A WIND TURBINE BLADE:** performs the sensitivity analysis, using the Sobol' indices, of a global damage index (DI) to obtain the sensors with the most influential data in the DI. After that, the transmissibility function between the sensors is calculated, and a methodology for damage detection is proposed based on a metamodel obtained from the transmissibility function of healthy data.
- **Chapter 6 - FINAL CONCLUSIONS:** comprises the main conclusions and a path forward for future work.

2 A BRIEF STATE-OF-THE-ART REVIEW

This chapter reviews the state of the art about the main topics covered in this thesis. First of all, we discuss metamodels to quantify damage to wind turbine blades, sensitivity analysis to optimize sensor location, and the use of transmissibility function for damage detection.

2.1 DAMAGE QUANTIFICATION IN WIND TURBINE BLADES

The significant growth experienced by the wind energy industry and its costs per kilowatt-hour has made this sector highly competitive. Therefore, a system for monitoring wind turbines' conditions is of great industrial interest, demanding further development of methodologies for detecting and quantifying damage to these structures (CIANG; LEE; BANG, 2008). Most wind turbine blades are manufactured using composite material, so they have a complex internal structure. Thus, the Structural Health Monitoring (SHM) of wind turbine blades is essential for reasons of reliability and safety since the maintenance of blades, in large part, involves a method based on visual execution, which can be dangerous and expensive (CAVA; TCHERNIAK, 2019). Fortunately, there has been significant development of techniques using wave or vibration responses to extract characteristics from damage and thus diagnose the current state of the wind turbine blades. However, the user needs to decide whether there is an upcoming structural failure or whether the system can be kept in operation under monitoring to track the progress of the damage and its impact on the condition of the structure, after detecting the initial delamination damage in a region of the monitored structure (PAIXÃO *et al.*, 2021).

Structural Health Monitoring methods are used to diagnose and extract meaningful information about the health from a structure of interest, based on the measured data from sensors distributed and permanently installed along with the structure (LARROSA; LONKAR; CHANG, 2014). As already commented in section 1.1, the damage quantification is not yet extensively addressed by the scientific community. Still, improving structures' safety and useful life is crucial, thus motivating the scientific community to develop some damage quantification methods. Paixão, Silva and Figueiredo (2020) used AutoRegressive (AR) models on Lamb wave signals measured on a composite material

plate to calculate damage-sensitive features for calculating indexes using the Mahalanobis square distance. Quantification was achieved by learning a defined curve and using cubic spline functions to predict the delamination area. Silva *et al.* (2020) executed a similar idea when manipulating the possibility of extrapolating these trend curves to future prognostic states when the delamination grows in the same place and with a similar effect. These studies demonstrated that the resources that use AR models precisely correlate with the structural state and a smooth tendency that allows using cubic spline functions.

Many studies have addressed experiments in wind turbines in the literature, but there is a lack of methodologies to quantify their damage. One of the difficulties quantifying wind turbine blades' damage is that these structures work under variability (temperature, climate, etc.). Therefore, it is of great importance to consider uncertainty quantification. A method with valid results in obtaining uncertainty quantification models is the Polynomial Chaos Expansion (PCE). The PCE method with application in engineering was introduced in Ghanem and Spanos (1990). They proposed a new convergent orthogonal expansion method to solve material variability problems. The material property was modeled as a random field. The results found had a good agreement with the results obtained through a Monte Carlo simulation. In Ghanem and Spanos (1991), the PCE was used to quantify the uncertainty applied to some problems involving mechanical systems. The use of different types of orthogonal polynomials to represent non-Gaussian processes was introduced in Xiu and Karniadakis (2002), which presents a method for solving stochastic differential equations based on Galerkin projections on a polynomial chaos basis. They represented stochastic processes based on an Askey family of orthogonal polynomials that reduced the system's dimensionality and led to the exponential convergence of the error. This new methodology, which is reviewed in Xiu (2010), presents satisfactory computational cost and precision results. One of the significant advantages of using the PCE is its rapid convergence and expressing the final solution as a random process and not just as a set of statistics. Bogoevska *et al.* (2017) mention that operational structures such as wind turbines have complex dynamic behavior that challenges the applicability of existing SHM strategies for condition evaluation. Thus, Bogoevska *et al.* (2017) proposes a structure based on the symbiotic treatment of environmental/operational variables acting on the structure's vibration response. A probabilistic model of the PCE was used for uncertainty quantification in the identified structural performance indicators. Avendaño-Valencia *et al.* (2017) emphasized that effective fatigue monitoring and prediction algorithms for structures such as wind turbines require an accurate representation of their dynamic response on the short and long-term scale. The long term can be achieved

in a computationally efficient way through metamodels. That article discussed a two-step methodology. The first consisted of projecting the Power Spectral Density (PSD) of the measured dynamic response of the wind turbine linearly in an alternative representation space through Principal Component Analysis (PCA). In the second stage, the coefficients of the PCA-based projection were used as a vector of characteristics, represented by a probability density model in the characteristic space, which is associated with environmental/operational variables measured by the Supervisory Control and Data Acquisition (SCADA) of the wind turbine through the PCE. The proposed methodology facilitated the detection of different wind turbine modes, although it can still be used for fatigue simulation and prediction only by sampling from the resource space. This methodology was demonstrated with actual data measured on a wind turbine located in Lübbenau, Germany, measured over three months.

2.1.1 Polynomial Chaos-Kriging Method

In this thesis work, the methodology discussed for quantifying the size of damage like trailing edge debonding of a wind turbine blade is based on obtaining a metamodel using the Polynomial Chaos-Kriging (PC-Kriging) method. PCE and Kriging are two popular non-intrusive metamodeling techniques (they do not modify or adapt the original model equations). The PCE replaces the computational model with a series of orthonormal polynomials in the input variables, where the polynomials are chosen in coherence with the probability distributions of these input variables (GHANEM; SPANOS, 1991; GHANEM; OWHADI; HIGDON, 2017). The Kriging method assumes that the computational model behaves as a realization of a Gaussian random process whose parameters are estimated from the available computer executions, that is, input vectors and response values (LATANIOTIS; MARELLI; SUDRET, 2015). The PC-Kriging presents itself as a new non-intrusive metamodel approach combining PCE and Kriging. The PCE is close to the computational model's global behavior, while Kriging is responsible for its local variability. Combining these two methods leads to better accuracy, or at least as good, as either method alone (SCHÖBI *et al.*, 2014; SCHÖBI; SUDRET; WIART, 2015). That is why the choice of applying both methods as a combined approach in this work.

Some works were carried out using the combination of the PCE and Kriging methods, and thus it was possible to identify some advantages and disadvantages of this combination. The PC-Kriging method's main advantages are the ease of model construction, the low computational cost, the analytical calculation of classical statistical measures of the quantity of interest, and simplicity compared to other machine learning techniques.

However, the PC-Kriging is very sensitive to data quality, just like any other machine learning technique, and impossible to apply to large problems, these being some of its disadvantages (SCHÖBI; SUDRET, 2014; DU; LEIFSSON, 2020). In Kersaudy *et al.* (2015), the Specific Absorption Rate (SAR) was evaluated using a surrogate model to reduce the computational cost. Thus, it was considered a sparse representation of the PCE using minimal angle regression as a selection algorithm to retain the most influential polynomials. The selected polynomials are used as regression functions for the universal Kriging model. This combination proposal was applied to three benchmark examples, and the performances were compared with a standard Kriging model and a sparse PCE classic. The combination of the methods showed an adequate performance. In the literature, some studies used PC-Kriging for quantification problems considering uncertainties. In Schöbi, Sudret and Marelli (2016), a new structural reliability method was developed based on the PC-kriging approach, which was coupled to an active learning algorithm known as adaptive Kriging-Monte Carlo Simulation (AK-MCS). The problem was formulated so that the calculation of small probabilities of failure and extreme quantiles were unified. Dubreuil *et al.* (2018) carried out a parametric study of engineering models under uncertainty, using the PC-Kriging approach. The advantage of the approach developed in that article was the reduction in computational cost, which was demonstrated in several numerical examples and illustrated in the parametric study of an aircraft wing under uncertainty.

2.2 SENSITIVITY ANALYSIS IN WIND TURBINE BLADES AND OTHER COMPOSITE MATERIAL STRUCTURES

To the best of our knowledge, few works in the literature propose the sensitivity analysis in composite wind turbine blades. A study on this topic is available in Echeverría, Mallor and Miguel (2017). In that work, it is commented that the implementation of efficient blade designs gains relevance as wind turbine developments require longer blades. So, Echeverría, Mallor and Miguel (2017) identified the design variables that affect the performance of the wind turbine. The number of variables was first determined to accurately represent the project. A methodology based on statistical tests of hypotheses applied to airfoil approach errors is presented to assess the accuracy. Afterward, a study is carried out to evaluate the sensitive blade variables in the performance of the wind turbine, for which a global sensitivity analysis is performed using multivariable linear regressions and methods based on variance. As a result, a list of variables is deduced that can be discarded in an optimization model without affecting the performance of the wind

turbine.

In Almohammadi *et al.* (2012), the flow field characteristics and predicted power coefficient of a straight blade vertical axis wind turbine (SB-VAWT) were investigated using computational fluid dynamics modeling using 2D simulations. In the mesh phase, three parameters were investigated, and in the simulation phase, two other parameters were investigated. Significant differences were observed in the flux field characteristics and the predicted power coefficient for some of these parameters, leading to unreliable predictions if not considered in detail. As a result, the sensitivity analysis performed on the parameters suggests which parameters should be focused on in the modeling process.

Thapa and Missoum (2022) performed the uncertainty quantification and global sensitivity analysis (GSA) on a blade from the National Renewable Energy Laboratory 5 Megawatt wind turbine, using the Polynomial Chaos Expansion-based approach. The authors comment that the performance and reliability of wind turbine blades are negatively affected due to uncertainties, so it is important to consider the uncertainties during the design phase. However, performing UQ of composite blades is computationally expensive, so a PCE-based approach is used. Afterward, the GSA is performed, using the Sobol' indices to identify the most influential random parameters in the formulation.

A range of works in the literature perform sensitivity analysis in composite structures because the existing uncertainties in these structures make reliability and sensitivity analysis highly necessary. Bodjona and Lessard (2015) report that bonded/bolted joints in composites are more robust and more durable. Still, there is limited understanding of how load sharing between the adhesive and screws works and how it can be most effectively achieved. For this reason, the work carried out by Bodjona and Lessard (2015) presents a GSA of a computer model of a single-bolt, single-lap composite joint containing an elastic-plastic adhesive. This work is a continuation of the study developed in Bodjona *et al.* (2015), which presents the development and validation of the model. The purpose of the sensitivity analysis was to quantify the influence of different joint design parameters on load sharing. As a result, it was found that the adhesive yield strength is the most critical factor. The joint E/D ratio, adhesive hardening slope, and adhesive thickness were other significant factors influencing load sharing. In Liu and Paavola (2018) a sensitivity analysis is also performed, but for composite laminated plates and shells, which have shear deformation.

One of the methods to perform the GSA is the Sobol' indices (in chapter 3 is presented in more detail). In Carneiro and Antonio (2020) Sobol' indices are used to reduce the

dimension of the uncertainty space, improving efficiency towards global convergence of reliability assessment in composite laminated structures with multiple components. As the uncertainty space in these structures easily becomes oversized and not all random variables are relevant, a GSA is necessary to identify the most critical parameters. According to Zhou *et al.* (2021), local sensitivity can measure how local perturbations of the input variables' distribution parameters affect structural reliability, while global sensitivity can measure the contributions of input variables to reliability over their entire uncertainty range. Recently, they used an adaptive Kriging-based approach to estimate failure probability and local and global sensitivity of composite structures. The Kriging model is combined with numerical simulation to analyze the reliability and sensitivity of a composite beam and composite plate. After, the methodology is applied to a composite radome (used for aeronautical purposes). As a result, the reliability of the radome is obtained, and the input parameters that are important for the reliability of the radome are identified. In that work, it is concluded that the approach based on adaptive Kriging offers a viable tool for evaluating the reliability of composite structures.

2.3 DAMAGE DETECTION USING TRANSMISSIBILITY FUNCTIONS

Some works explore the use of transmissibility functions in the literature for damage detection. In Chesne and Deraemaeker (2013) a critical review of the state-of-the-art is carried out, highlighting the main difficulties in using transmissibility functions to detect and locate damage. This review highlights the importance of choosing the frequency bands, the effects of the environment, and the dependence on the location of the force. In the second part of the work, a damage detection study was carried out using the transmissibility function in non-dispersive systems, such as mass-spring systems. The methodology performed obtained a good localization of the damage only when the excitation force was located exactly next to the damage, which is a very rare case in practice. In the other cases, the damage location was obtained by restricting the frequency band to frequencies lower than the first eigenfrequency. This work also concluded that the analytical results obtained for non-dispersive systems could not be extended to more general dispersive systems (e.g., beams and plates), as the location of the damage is not guaranteed, even when the excitation force is close to the damage. Finally, the paper showed that the transmissibility functions are sensitive to damage; besides, it is difficult to use them unsupervised.

Maia *et al.* (2011) cite the importance of developing methods that are capable of

simultaneously detecting the existence of the damage and quantifying its extent. In that sense, they propose a methodology to detect and quantify structural damage, using the transmissibility of responses measured along with the structure. For this, numerical simulations were presented, and a comparison was made with the results using frequency response functions. To validate the proposed methodology, experimental tests are carried out.

The proposed approach was validated on data from a physics-based numerical model and experimental data from a three-story aluminum frame structure. After that, a damage indicator was defined to detect and identify the severity of the damage. For both numerical and experimental simulations, the damage indicator results performed better than those obtained in Rizos *et al.* (2008), Fassois and Sakellariou (2007) and Rizos *et al.* (2008), primarily when non-linearity occurs, which is the closest case to the real thing. Zhou *et al.* (2015a) illustrated that the transmissibility of the system responses and the transmissibility coherence can be extracted and analyzed.

According to Zhou *et al.* (2015b) if we consider transmissibility as a damage-sensitive characteristic, it will vary according to the damage level. Furthermore, the Mahalanobis distance can distinguish a healthy condition from a damaged condition in a structure. For this reason, in the study developed in Zhou *et al.* (2015b) a damage detection approach is proposed using the Mahalanobis distance with structural data in the form of transmissibility. The work results demonstrate a good ability to detect damage using transmissibility.

An approach to detect structural damage using transmissibility together with hierarchical clustering and similarity analysis was proposed in Zhou *et al.* (2017). Hierarchical cluster analysis is adopted to discriminate damaged scenarios from an unsupervised perspective, taking transmissibility as a characteristic to distinguish damaged from undamaged patterns. Simulated results are performed on a ten-floor structure and experimental tests on a free beam to validate this work. The results obtained show a satisfactory performance in damage detection and potential application in actual engineering situations. Zhou, Maia and Wahab (2018) also proposed a methodology for damage detection using the transmissibility functions and obtaining good results in the detection performance. The transmissibility was extracted from the structural responses, and the main features were selected by principal component analysis to reduce the computational cost. Afterward, damage indicators are built for both healthy and damaged conditions. Finally, a numerical simulation with a clamped-clamped beam and a four-story structure is adopted to validate the proposed methodology.

In Ulriksen, Tcherniak and Damkilde (2015) a vibration-based damage detection method to an operating Vestas V27 wind turbine blade is explored. This blade was analyzed in four stages: healthy and three damaged. The blade is subjected to controlled actuator hits in each state, producing forced vibrations measured by twelve accelerometers. The dimensionality of the acceleration data is reduced by employing PCA. Then a reduced set of selected principal scores are used as damage characteristics in the Mahalanobis metric to detect damage-induced anomalies. In this work, the importance of choosing an adequate frequency band to develop the methodology is commented. For this, the authors used a band-pass filter from 900 Hz to 1300 Hz after analyzing the behavior of the collected data.

2.4 SCOPE OF THE THESIS

This chapter presented a brief review of the state-of-the-art, covering topics related to damage quantification and sensitivity analysis in composite wind turbine blades and other composite material structures. Methodologies using the PC-Kriging method and works in the literature using transmissibility function for damage detection were also discussed. With the literature review, it became clear the importance of considering the uncertainties in composite material structures and how the sensitivity analysis can help optimize models and implementations.

Quantifying severity is not an easy task. As seen in the literature review, there are not many methods to quantify wind turbine blade damage, one of this thesis's contributions. The thesis proposes a methodology for damage quantification using a PC-Kriging metamodel in a composite wind turbine blade. In chapter 4, a PC-Kriging metamodel achieved a reasonable prediction of damage severity. However, the location of the actuator and accelerometers influenced the performance of the metamodel. For this reason, a sensitivity analysis of the location of the sensors is carried out using the Sobol' indices, presented in chapter 5 .

Finally, this work also proposes a methodology for damage detection in a composite wind turbine blade. The proposal is based on obtaining a Kriging metamodel from the transmissibility functions between two sensors, where the confidence interval of 95% is a threshold for damage detection. As already mentioned in the motivation and literature review, the development of SHM methods is significant for society and of great industrial interest, thus justifying the relevance of the studies developed in this thesis.

3 METHODS FOR OBTAINING METAMODELS AND SENSITIVITY ANALYSIS

In this chapter, some methods for obtaining metamodels that consider uncertainties and sensitivity analysis methods are discussed. Section 3.1 presents the Polynomial Chaos Expansion, Kriging, and Polynomial Chaos-Kriging methods. Section 3.2 details a technique to perform sensitivity analysis, the Sobol' indices. Finally, section 3.3 comments about the toolbox used in this work to implement the mentioned methods.

3.1 METHODS FOR OBTAINING METAMODELS

Mathematical models, obtained from experiments in the engineering area, can approximate real behavior to a certain level of accuracy. Our goal should be to achieve the highest level of accuracy possible. Many uncertainties are introduced in the experiments, for example, observation errors and random disturbance of some experimental conditions, environmental conditions, etc. Therefore, uncertainties in obtaining the model must be considered to reduce the physical system's discrepancies and the mathematical model. Different types of uncertainties can present themselves in a given problem and interact with each other, affecting the modeling and engineering design. Therefore, it is essential to quantify the errors to interpret the results (ABSIL *et al.*, 2016; ZHANG; YIN; WANG, 2020).

In recent years, the research in uncertainty quantification (UQ) has been valued and supported by academia and industry (WANG; JIANG, 2015). Different UQ approaches were developed, such as sensitivity analysis, Monte Carlo simulation, response surface approaches, classical statistical confidence limits assessment, Dempster-Shafer theory, and Bayesian inference (ZHANG; YIN; WANG, 2020).

In Sudret (2018), a framework for the quantification of uncertainties is presented, which can be seen in Figure 3. In this scheme, the following steps are considered for uncertainty quantification: system modeling, quantification of uncertainties variables, propagation of uncertainties, and sensitivity analysis. In step 1, the system is modeled based on physical principles and also the random variables are considered, obtaining the system modeling. In step 2, the objective is to represent the uncertain parameters based

on the available data and information. The experimental data are evaluated, and the distribution of each parameter is determined. In step 3, the objective is to estimate the uncertainty of the output variable $Y = \mathcal{M}(X)$ and thus obtain the statistics and joint probability density function (PDF) of the parameters. Finally, in step 4, input parameters are identified whose uncertainty has no impact on output variability. Input parameters are also determined to reduce output variability when defined as deterministic. This stage performs a screening of the parameters to obtain a new model that presents better results for propagating uncertainties. Various methods are available in the literature to propagate uncertainties in mechanical systems. This study will focus on Polynomial Chaos Expansion (PCE), Kriging, and Polynomial Chaos-Kriging (PC-Kriging) methods. The algorithm of these methods will be presented and their advantages and disadvantages. These methods are chosen because they have a low computational cost, as they do not depend on the sample value if compared, for example, with the Monte Carlo method.

Figure 3: Framework for uncertainty quantification.

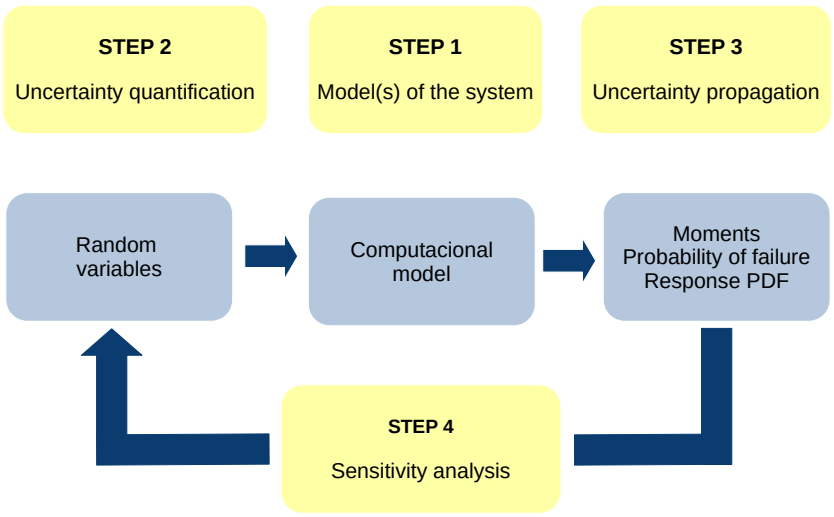

Source: Adapted from Sudret (2018).

PCE, Kriging, and PC-Kriging are methods for obtaining a surrogate model. The surrogate model can represent a complex phenomenon, with a large number of input parameters (TRIPATHY; BILIONIS, 2018), with a lower computational cost. These models, also known as the response surface or metamodel, have a set of easy-to-evaluate mathematical functions that approximate the real model based on input-output samples. Metamodels treat the computational model as a black box and only need input and output values for the quantity of interest. Gradually, deterministic models are being replaced by stochastic models (MARELLI, S.; SUDRET, B., 2015). However, there is a cost to deal

with a large amount of information in stochastic models. When using methods such as, for example, the Monte Carlo method, there will be a need for a large number of samples, increasing the computational cost of the simulations and also the identification parameters with experimental data, given the greater demand for samples. In this sense, the PCE, Kriging, and PC-Kriging prove to be powerful techniques for obtaining metamodels in propagating uncertainties. These methods can provide statistical information, such as mean and variance, without generating an expensive sampling process. The PCE, Kriging, and PC-Kriging methods are presented in detail below.

3.1.1 Polynomial Chaos Expansion

The PCE was introduced at the beginning of century XX with the pioneering work of Wiener (1938). The PCE method with application in engineering was introduced in Ghanem and Spanos (1990). They proposed a new approach using convergent orthogonal expansion to solve material variability problems. The material property was modeled as a random field. The results found had a good agreement with the results obtained through a Monte Carlo simulation. In Ghanem and Spanos (1991), the PCE was used to quantify the uncertainty applied to some problems involving mechanical systems. The use of different types of orthogonal polynomials to represent non-Gaussian processes first appeared in Xiu and Karniadakis (2002), which presents a method for solving stochastic differential equations based on Galerkin projections on a polynomial chaos basis. They represented stochastic processes based on an Askey family of orthogonal polynomials, which reduced the system's dimensionality and led to the exponential convergence of the error. Soize and Ghanem (2004) observed that random variables, on which uncertainties may depend in a model, can be defined as a measure space in relation to the solution to the mathematical problem. So, Soize and Ghanem (2004) shed light on the mathematical structure of this space, where cases of dependent and independent random variables are addressed. For this, bases are developed in the product space that can be viewed as generalizations of the standard polynomial chaos approximation. The use of different types of orthogonal polynomials[6] to represent non-Gaussian processes was defined in Xiu (2010). This new methodology applied by Xiu (2010) presented satisfactory results in terms of computational cost and precision when compared to the Monte Carlo method. One of the significant advantages of using the PCE is its rapid convergence and expressing the final solution as a random process and not just as a set of statistics.

[6]Family of polynomials so that any two distinct polynomials are orthogonal to each other under some inner product.

According to MARELLI, S.; SUDRET, B. (2015), be an input vector $\mathbf{X} \in \mathbb{R}^M$, $M-$dimensional consisting of random variables and $X = (X_1, \cdots, X_M)$ with a given PDF $f_{\mathbf{X}}$, and a computational model of finite variance with output $Y = \mathcal{M}(X)$, with $Y \in \mathbb{R}$ and $\mathcal{M} : \mathbf{X} \in \mathcal{D}_{\mathbf{X}} \subset \mathbb{R}^M \mapsto \mathbb{R}$ is the computational model of interest, where $\mathcal{D}_{\mathbf{X}}$ is the support of the vector distribution $\mathbf{X}$, such as illustrated in Figure 4. The Polynomial Chaos Expansion $\mathcal{M}(\mathbf{X})$ is given by

$$Y = \mathcal{M}(\mathbf{X}) = \sum_{\alpha \in \mathbb{N}^M} y_\alpha \Psi_\alpha(\mathbf{X}), \tag{1}$$

being that $\Psi_\alpha(\mathbf{X})$ are orthonormal polynomials[7] about f_X, $\alpha \in \mathbb{N}^M$ is the index of the components of the polynomial Ψ_α and $y_\alpha \in \mathbb{R}$ are the coefficients.

Figure 4: Computational model under uncertainty.

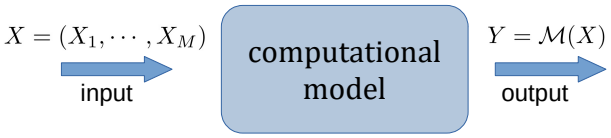

Source: Prepared by the author.

It is necessary to work with finite expansion for computer simulation in applied situations. Therefore, the sum of Eq. (1), frequently, needs to be truncated to a finite sum, given by

$$Y \equiv \mathcal{M}(\mathbf{X}) \approx \mathcal{M}^{PC}(\mathbf{X}) = \sum_{\alpha \in \mathcal{A}} y_\alpha \Psi_\alpha(\mathbf{X}) + \epsilon, \tag{2}$$

being that $\mathcal{A} \subset \mathbb{N}^M$ is a subset of the polynomial indexes and ϵ is the truncation error. The truncation method will be presented in the **truncation method** part.

Construction of the Polynomial Base

The polynomial base $\Psi_\alpha(\mathbf{X})$ of the Eq. (2) is traditionally built from orthonormal polynomials $\phi_j^{(i)}(x_i)$ that satisfy (KAINTURA; DHAENE; SPINA, 2018; MARELLI, S.; SUDRET, B., 2015):

$$\left\langle \phi_j^{(i)}(x_i), \phi_k^{(i)}(x_i) \right\rangle = \int_{\mathcal{D}_{X_i}} \phi_j^{(i)}(x_i) \phi_k^{(i)}(x_i) f_{X_i}(x_i) dx_i = \delta_{jk}, \tag{3}$$

[7] Polynomials orthogonal to each other and have norms equal to 1.

being that i identifies the input variable for which they are orthogonal, as well as the corresponding polynomial family, j and k correspond to the degree of the polynomial, $f_{X_i}(x_i)$ represents the input distribution and δ_{jk} is the Kronecker delta.

The polynomials $\Psi_\alpha(\mathbf{X})$ can be represented as a tensor product:

$$\Psi_\alpha(x) = \Pi_{i=1}^{M} \phi_{\alpha_i}^{(i)}(x_i). \tag{4}$$

Due to the orthonormal relationship in Eq. (3), it also follows that the polynomials constructed in Eq. (4) are orthonormal:

$$\langle \Psi_\alpha(x), \Psi_\beta(x) \rangle = \delta_{\alpha\beta}, \tag{5}$$

being that $\delta_{\alpha\beta}$ is an extension of the Kronecker delta for the multi-dimensional case.

Family of orthogonal polynomials

To improve the convergence of the PCE method, different classes of orthogonal polynomial bases are used depending on the nature of the random variables studied, as can be seen in Table 1.

Table 1: Correspondence of orthogonal polynomials and probability density functions of different random variables.

Process type	Random variables	Orthogonal polynomial
Continuous	Gaussian	Hermite
	Gamma	Laguerre
	Beta	Jacobi
	Uniform	Legendre
Discrete	Poisson	Charlier
	Binomial	Krawtchouk
	Negative Binomial	Meixner
	Hypergeometric	Hahn

Source: Xiu and Karniadakis (2002).

Truncation method

The simplest and most generic case of using a truncation criterion is to consider only polynomials with a maximum total degree p, that is

$$\mathcal{A} \equiv \mathcal{A}^{M,p} = \{\alpha \in \mathbb{N}^M : \| \alpha \| = \sum_{i=1}^{M} \alpha_i \leq p\}. \tag{6}$$

This standard truncation criterion becomes ineffective on high dimension problems, so that Blatman (2009) developed two methods that significantly reduce cardinality $\mathcal{D} = card\left(\mathcal{A}^{M,p}\right) = \frac{(M+p)!}{(M!p!)}$ of the finite set of multi-indexes. The methods are: maximum interaction and hyperbolic truncation.

Calculating the Coefficients

There are many methods for calculating the coefficients y_α from PCE to the base given in Eq. (2). The development of the PCE method is similar to the analysis of deterministic finite elements since it uses notions of projection, orthogonality, and weak convergence. This type of formulation is called the Galerkin method. This method converts the original system of differential equations of motion, known as a weak formulation system, resulting in a linear system of equations that allows determining the coefficients of the system's response in random space. Therefore, it is necessary to know the shape of the parameter by a physics law to obtain the differential equations that describe this model. The Galerkin method is considered an intrusive method. Intrusive methods require new programming for the stochastic model. In contrast, non-intrusive methods can use the code of the deterministic model and, therefore, do not require new programming of the model.

Non-intrusive methods were implemented as alternatives to the Galerkin method. The expansion coefficients are estimated using a set of sample data from the input parameters of the analysis model and their associated responses. The non-intrusive character of these methods is precisely because the equations that govern the model are not modified or adapted. In general, intrusive methods have faster convergence but are difficult to implement (often impossible for real situations). Non-intrusive methods, however, have slower convergence but are easy to implement. A non-intrusive method is the Stochastic Placement method, which consists of constructing an interpolation of the variable of interest and calculating this interpolation from the pre-determined points of the stochastic space.

If you have the Eq. (2), considering n samples and $P \in \mathbb{Z}$, the coefficients y_α can be obtained by solving

$$\begin{bmatrix} \Psi_0(X_1) & \Psi_1(X_1) & \Psi_2(X_1) & \cdots & \Psi_{P-1}(X_1) \\ \vdots & \vdots & \vdots & \ddots & \vdots \\ \Psi_0(X_n) & \Psi_1(X_n) & \Psi_2(X_n) & \cdots & \Psi_{P-1}(X_n) \end{bmatrix} \begin{Bmatrix} y_0(t) \\ \vdots \\ y_{P-1}(t) \end{Bmatrix} \approx \begin{Bmatrix} Y_1(t) \\ \vdots \\ Y_n(t) \end{Bmatrix} \Leftrightarrow \Psi\mathbf{y} \approx \mathbf{Y}, \tag{7}$$

via least squares regression. In complex cases, where the system cannot be evaluated many times, it is common to specify how many times one wants to analyze and consider the metamodel that has the least error. Or, it is also possible to specify a value of $\epsilon_{LOO} < \varepsilon$ and so get n, but analytically it is impossible to resolve.

Error estimation

After the metamodel is built, its accuracy can be quantified by estimating the generalized error, which is given by

$$\epsilon_{gen} = \mathbb{E}[(\mathcal{M}(\mathbf{X}) - \mathcal{M}^{PC}(\mathbf{X}))^2]. \tag{8}$$

In practice, this error is calculated empirically so that

$$\epsilon_{gen_{emp}} = \frac{1}{n}\sum_{i=1}^{n}\left(\mathcal{M}(\mathbf{X}) - \mathcal{M}^{PC}(\mathbf{X})\right)^2. \tag{9}$$

The generalized error ϵ_{gen} is underestimated by the empirical error $\epsilon_{gen_{emp}}$ (BLATMAN, 2009). This is due to the so-called overfitting phenomenon, in which the empirical error systematically decreases with the increasing degree of the polynomial base. In contrast, the generalized error can increase. It is extremely important to use an error indicator that is less prone to overfitting. Thus, it is necessary to use the cross-validation leave-one-out (LOO) error.

Cross-validation is a technique that consists of building N metamodels $\mathcal{M}^{PC}$, each created in a reduced experimental project $\mathcal{X}\backslash\mathbf{x}^{(i)} = \{\mathbf{x}^{(j)}, j = 1, ..., N, j \neq i\}$ and comparing your forecast on excluded points $\mathbf{x}^{(i)}$ with the real value $y^{(i)}$ (BLATMAN; SUDRET, 2010). The cross-validation error leave-one-out can be given by

$$\epsilon_{LOO} = \frac{1}{n}\sum_{i=1}^{n}\left(\mathcal{M}(\mathbf{x}^{(i)}) - \mathcal{M}^{PC}(\mathbf{x}^{(i)})\right)^2. \tag{10}$$

The calculation of the LOO error appears to be computationally costly since it requires training and validating the N PCE models. However, due to the linear regression formula of the PCE, the LOO error can be calculated using algebraic derivations of a single PCE model $\mathcal{M}^{PC}$ built with the entire sample set $\mathcal{X}$ this way (BLATMAN, 2009):

$$\epsilon_{LOO} = \sum_{i=1}^{N}\left(\frac{\mathcal{M}(\mathbf{x}^{(i)}) - \mathcal{M}^{PC}(\mathbf{x}^{(i)})}{1 - h_i}\right)^2 \tag{11}$$

where h_i is the i-th component of the vector given by $\mathbf{h} = diag\left(\mathbf{A}(\mathbf{A}^T\ \mathbf{A})^{-1}\mathbf{A}^T\right)$, where $\mathbf{A}$ is an experimental matrix known of the model.

PCE Moments

Due to the orthonormality of the polynomial base, the first two moments of the PCE are obtained from its coefficients. In particular, the mean value of a PCE is

$$\mu^{PC} = \mathbb{E}\left[\mathcal{M}^{PC}(X)\right] = y_0, \tag{12}$$

where y_0 is the coefficient of the base term, $\Psi_0 = 1$.

Likewise, the PCE variance is:

$$\sigma^2 = \mathbb{E}\left[\left(\mathcal{M}^{PC}(X) - \mu^{PC}\right)^2\right] = \sum_{\substack{\alpha \in \mathcal{A} \\ \alpha \neq 0}} y_\alpha^2, \tag{13}$$

where the sum is the coefficients of the non-constant terms in the base.

3.1.2 Kriging

Kriging, also known as the Gaussian process, is a stochastic interpolation method that uses Gaussian processes to interpolate complex functions. This method was used for the first time in geostatistics by kriging (KRIGE, 1951), and formalized in MATHERON (1963). Later, the Kriging method began to be used in the context of metamodeling and computational experiments. In the work of Sacks *et al.* (1989), Kriging was used to represent an input/output mapping of an expensive computational model.

Gaussian processes are of interest due to their regression and machine learning classification applications. In Santner, Williams and Notz (2003), you can find an in-depth introduction to Kriging as a metamodeling tool. In RASMUSSEN, C. E.; WILLIAMS, C. K. I. (2006) the Kriging is presented as a regression and classification tool.

In the Kriging method is assumed that the model output is $Y = \mathcal{M}(x)$ and that is the realization of a Gaussian process indexed by $x \in \mathcal{D}_X \subset \mathbb{R}^M$. The Kriging model is described by the following equation (SANTNER; WILLIAMS; NOTZ, 2003; SCHÖBI; MARELLI; SUDRET, 2017):

$$Y \approx \mathcal{M}^K(x) = \beta^T f(x) + \sigma^2 \mathcal{Z}(x, \Omega), \tag{14}$$

where $\beta^T f(x)$ is the mean value of the Gaussian distribution, σ^2 is a variance, and $\mathcal{Z}(x, \Omega)$ is a zero mean, unit variance, and a stationary Gaussian process that is characterized by a correlation function $\mathcal{R}$ and its hyperparameters θ.

The algorithm for obtaining a Kriging metamodel has the following steps:

- Select the functional basis of the Kriging trend;
- Select the appropriate correlation function $\mathcal{R}(x, x'; \theta)$;
- Obtain an estimate of the hyperparameters θ and the variance of the Gaussian process σ^2, if they are unknown (which is usually the case). This involves setting up an optimization problem and resolution of it;
- Use the ideal value of θ, and the rest of the unknown Kriging parameters (σ^2, β) can be calculated.

Trend types

The trend corresponds to the mean of the Kriging metamodel; that is, it is the term $\beta^T f(x)$ in Eq. (14). According to the complexity of the trend function, there are three popular kriging models (STEIN, 1999), being them simple, ordinary, and universal Kriging.

- **Simple Kriging:** the trend is described by

$$\beta^T f(x) = \sum_{j=1}^{P} f_j(x), \tag{15}$$

where f_j's are arbitrary and specified, the coefficients β are all 1's.

- **Ordinary Kriging:** the trend has a constant yet unknown value and is described by

$$\beta^T f(x) = \beta_0 f_0(x) = \beta_0, \tag{16}$$

where, by convention, $f_0(x) = 1$.

- **Universal Kriging:** the trend is a linear combination of prescribed arbitrary functions and is described by

$$\beta^T f(x) = \sum_{j=0}^{P} \beta_j f_j(x). \tag{17}$$

The functions f_j's can be polynomials, constants, or user-defined functions. This case is the one with the most flexible and general formulation. The simple and ordinary Kriging are special cases of universal Kriging (LATANIOTIS; MARELLI; SUDRET, 2015; ZHANG; YIN; WANG, 2020).

Correlation functions

The correlation function, also known as the kernel or covariance function, is very important in the Kriging method because it contains assumptions about the approximation function. It tests the similarity between observations and new points.

The conditions for a function $\mathcal{R}(x, x')$ to be a correlation function is:

- The correlation matrix is positive semi-definite for any choice of number of sample points N of the experimental project;
- The function is symmetric.

Correlation function types

In general, a correlation function can be expressed in the form $\mathcal{R}(x, x'; \theta)$, where θ is a vector that contains a set of parameters (LATANIOTIS; MARELLI; SUDRET, 2015).

Several correlation families can be found in the literature, such as Linear, Exponential, Gaussian (also called squared exponential), and Matérn autocorrelation function (RASMUSSEN; WILLIAMS, 2005). Below you can see some of the correlation families.

- **Linear:**

$$\mathcal{R}(x, x'; \theta) = max\left(0, 1 - \frac{|x - x'|}{\theta}\right). \tag{18}$$

- **Exponential:**

$$\mathcal{R}(x, x'; \theta) = exp\left[-\frac{|x - x'|}{\theta}\right]. \tag{19}$$

- **Gaussian:**

$$\mathcal{R}(x, x'; \theta) = exp\left[-\frac{1}{2}\left(\frac{|x - x'|}{\theta}\right)^2\right]. \tag{20}$$

- **Matérn:**

$$\mathcal{R}(x, x'; \theta, v) = \frac{1}{2^{v-1}\Gamma(v)}\left(2\sqrt{v}\frac{|x - x'|}{\theta}\right)\kappa_v\left(2\sqrt{v}\frac{|x - x'|}{\theta}\right), \tag{21}$$

where θ is the correlation function scale parameter, $v \geq 1\frac{1}{2}$ is the shape parameter, Γ is the Euler's Gamma function, and κ_v is the modified Bessel function of the second kind.

When the input dimension is greater than the M input variables, the multidimensional correlation function can be constructed from one-dimensional correlation families: Ellipsoidal and Separable.

- Ellipsoidal correlation functions is calculated as follows:

$$\mathcal{R}(x, x'; \theta) = R(h); \quad h = \left[\sum_{i=1}^{M}\left(\frac{x_i - x'_i}{\theta_i}\right)^2\right]^{0.5}, \tag{22}$$

where $h = \dfrac{|x - x'|}{\theta}$ (RASMUSSEN, C. E.; WILLIAMS, C. K. I., 2006).

- Separable correlation function is calculated as follows (SACKS *et al.*, 1989; DUBOURG, 2011):

$$\mathcal{R}(x, x'; \theta) = \prod_{i=1}^{M} R(x_i, x'_i, \theta_i). \tag{23}$$

These types of functions represent an anisotropic case; that is, there is a single scale parameter for each input dimension.

Isotropic correlation functions

A multidimensional correlation function is called isotropic when the parameter θ has a single scale associated with all input dimensions. That is, this function has the same behavior in all dimensions. For each type of correlation function, the isotropy is defined as follows:

- Isotropic ellipsoidal correlation function:

$$\mathcal{R}(x, x'; \theta) = \mathcal{R}(h); \quad h = \frac{1}{\theta}\left[\sum_{i=1}^{M} (x_i - x_i')^2\right]^{0.5}. \tag{24}$$

- Isotropic separable correlation function:

$$\mathcal{R}(x, x'; \theta) = \prod_{i=1}^{M} R(x_i, x_i', \theta). \tag{25}$$

Estimation methods

The hyperparameters θ of the Kriging metamodel are generally unknown and must be estimated. The estimate is obtained by solving an optimization problem. Generally, two estimation methods are the most used: maximum-likelihood estimation and cross-validation estimation.

The purpose of maximum-likelihood estimation is to find the set of Kriging parameters β, σ^2, θ, and if applied, σ_n^2, so that the likelihood of observations $\mathcal{Y} = \{\mathcal{M}^{(1)}, \cdots, \mathcal{M}^{(N)}\}^T$ be maximized, and $\mathcal{Y}$ have a multivariate Gaussian distribution. Depending on the presence and nature of the noise, different optimization problems can be configured. In the cross-validation estimation method, the idea is to obtain the Kriging parameters β, σ^2, θ, and, if applicable, σ_n^2, that minimizes the cross-validation error. As in the case of maximum-likelihood estimation, depending on the presence and nature of the noise, different optimization problems based on the cross-validation estimation can also be set up.

Error estimation

The predictive accuracy of the Kriging metamodel can be assessed using a leave-one-out (LOO) cross-validation error or validation error.

The leave-one-out (LOO) cross-validation error is calculated on the initial experimental design $\mathcal{X}$, and its corresponding responses $\mathcal{Y} = \mathcal{M}(\mathcal{X})$ as follow (LATANIOTIS; MARELLI; SUDRET, 2015):

$$\epsilon_{LOO} = \frac{1}{N}\left[\frac{\sum_{i=1}^{N}\left(\mathcal{M}(x_i) - \mu_{\hat{Y},(-i)}(x_i)\right)^2}{var\mathcal{Y}}\right], \tag{26}$$

where $\mu_{\hat{y},(-i)}(x_i)$ denotes the Kriging metamodel that is obtained using all the points of the experimental design $\mathcal{X}$, except x_i.

The validation error is calculated as the relative generalization error on an independent set of data $\mathcal{D}_{val} = \{(x^i_{val}, y^i_{val}), i = 1, \cdots, N_{val}\}$ as follows (LATANIOTIS; MARELLI; SUDRET, 2015):

$$\epsilon_{var} = \frac{N_{val} - 1}{N_{val}} \left[\frac{\sum_{i=1}^{N_{val}} \left(\mathcal{M}\left(x^{(i)}_{val}\right) - \mathcal{M}^K\left(x^{(i)}_{val}\right)\right)^2}{\sum_{i=1}^{N_{val}} \left(\mathcal{M}\left(x^{(i)}_{val}\right) - \hat{\mu}_{Y_{val}}\right)^2} \right], \tag{27}$$

where $\hat{\mu}_{Y_{val}} = \frac{1}{N_{val}} \sum_{i=1}^{N_{val}} \mathcal{M}\left(x^{(i)}_{val}\right)$ is the sample mean of the validation set responses. This error measure is important when comparing the performance of different metamodels in the same validation set.

3.1.3 Polynomial Chaos-Kriging

In general, Kriging focuses on the computational model's local behavior, resulting in high prediction accuracy close to the sample point of the experimental design. Still, its overall behavior may not be as accurate. To compensate for this, Schöbi *et al.* (2014) proposed a new approach that combines the PCE and Kriging methods, the Polynomial Chaos-Kriging (PC-Kriging). It is a metamodeling algorithm and is based on the PCE technique. The PC-Kriging uses the regression type PCE to capture the global behavior of the computational model and the interpolation type Kriging to capture the variations. This combination results in a more efficient metamodeling technique than PCE and Kriging separately (SCHÖBI *et al.*, 2014).

The PC-Kriging method works as follows; the Kriging interpolates the local variations of model Y depending on the points of the experiment. At the same time, the PCE is very close to the global behavior of model Y. A more accurate metamodel is developed by combining these techniques' global and local approaches. The PC-Kriging is defined as a universal Kriging model that consists of a set of orthonormal polynomials (SCHÖBI; SUDRET; MARELLI, 2016; SCHÖBI; SUDRET; WIART, 2015; KERSAUDY *et al.*, 2015):

$$Y \approx \mathcal{M}^{(PCK)}(X) = \sum_{\alpha \in \mathcal{A}} y_\alpha \Psi_\alpha(X) + \sigma^2 \mathcal{Z}(x, \Omega), \tag{28}$$

where $\sum_{\alpha \in \mathcal{A}} y_\alpha \Psi_\alpha(X)$ is a weighted sum of orthonormal polynomials that describe the trend of the PC-Kriging model, σ^2 is the variance and $\mathcal{Z}(x, \Omega)$ is the zero mean. Therefore, PC-Kriging can be interpreted as a universal model of Kriging with a specific trend.

The construction of the metamodel by PC-Kriging consists of two stages: (i) the

determination of a set of polynomials that defines the trend and (ii) the resolution of the ideal correlation parameters and the trend parameters. The polynomials that define the trend are calculated using the PCE by employing the Least Angle Regression (LARS) algorithm. The trend parameters and correlation parts are calculated as in the universal Kriging algorithm by using a gradient-based optimization algorithm to solve the log-likelihood function's maximization. These two steps are processed in series, as the set of polynomials can be determined independently of Kriging's settings (SCHÖBI; SUDRET; WIART, 2015; KERSAUDY *et al.*, 2015; SCHÖBI; SUDRET; MARELLI, 2016; SCHÖBI; MARELLI; SUDRET, 2017).

After configuring the PC-Kriging metamodel, its accuracy in new data can be assessed using the validation error. This is calculated as the relative generalization error in an independent set of inputs and outputs $[\mathcal{X}_{val}, \mathcal{Y}_{val} = \mathcal{M}(\mathcal{X}_{val})]$:

$$\epsilon_{val} = \frac{N-1}{N} \left[\frac{\sum_{i-1}^{N} \left(\mathcal{M}(x_{val}^{(i)}) - \mathcal{M}^{PCK}(x_{val}^{(i)}) \right)^2}{\sum_{i=1}^{N} \left(\mathcal{M}(x_{val}^{(i)}) - \hat{\mu} y_{val} \right)^2} \right], \tag{29}$$

where $\hat{\mu} y_{val} = \frac{1}{N} \sum_{i=1}^{N} \mathcal{M}(x_{val}^{(i)})$ is the sample mean of the validation set response. This error measure is useful for comparing the performance of different surrogate models when evaluated in the same validation set.

The PC-Kriging algorithm can be done in two ways: sequential and optimal. In sequential PC-Kriging (SPCK), the set of polynomials and the Kriging metamodel are determined sequentially. First, the PCE determines the ideal set of polynomials based on LARS. Every set of polynomials is incorporated into the PC-Kriging equation. Then the PC-Kriging metamodel is calibrated as a usual Kriging model, including the calculation of the coefficients y_α. In the optimal PC-Kriging (OPCK), the model is obtained iteratively. As in SPCK, the ideal set of polynomials is determined by LARS. The LARS algorithm results in a dispersion of the group of polynomials classified according to their correlation with the current residual in each LARS iteration (in decreasing order). Each polynomial is then added individually to the trend of a PC-Kriging model. In each iteration, a new PC-Kriging model is calibrated. The PC-Kriging models are compared using their LOO error estimators at the end of this process. In Schöbi, Sudret and Wiart (2015), the performances of the Kriging, PCE, SPCK, and OPCK methods, in terms of generalization of relative error in the analytical reference functions, are compared. The results showed that PC-Kriging is better than, or at least as good as, Kriging and PCE methods separately for small experimental projects, in the sense of low dimension. Moreover, it was concluded that OPCK is preferable to SPCK because it reduces the number of polynomials in the

regression part and reduces the metamodel's complexity.

3.2 SENSITIVITY ANALYSIS

To analyze the influence of each variability input data on the system's response of interest, global sensitivity analysis (GSA) is a powerful tool. The GSA can be defined by a variance decomposition method, which aims to decompose the output variance as the sum of each input variable's contributions or combinations. There are several techniques of GSA available in the literature, such as the Borgonovo, Morris method, so on, and Sobol' indices (SALTELLI *et al.*, 2008). In this work, we will focus on the Sobol' indices method.

3.2.1 Sobol' indices

A GSA method that has recently been explored by engineering is the Sobol' indices, defined in Sobol (1993), and has the idea of determining the expansion of the computational model in increasing dimensional sums in terms of conditional variances. One of its main advantages is dealing with non-linear and non-parameterized models and providing a quantitative and qualitative classification.

Given a mathematical model $\mathcal{M}$ that has k independent input parameters gathered into an input vector $\mathbf{X}$ and an output scalar Y such that:

$$Y = \mathcal{M}(\mathbf{X}) \quad , \quad \mathbf{X} = \{X_1, X_2, \ldots, X_k\} \tag{30}$$

. According to Sobol (1993), you can define Y in decomposition into sums of different dimensions. To simplify the notation, all of the following equations will assume that the input variables are uniform and that the input set support is $\mathcal{D}_X = [0,1]^k$. Therefore Y is defined by:

$$Y = \mathcal{M}_0 + \sum_{i=1}^{k} \mathcal{M}_i\left(X_i\right) + \sum_{i<j}^{k} \mathcal{M}_{ij}\left(X_i, X_j\right) + \cdots + \mathcal{M}_{1\ldots k}\left(X_1 \ldots X_k\right), \tag{31}$$

where all sums of the expansion can be computed by integrals recursively, the first term $\mathcal{M}_0$ is constant and equal to the expected value:

$$\mathcal{M}_0 = \int_{\mathcal{D}_x} \mathcal{M}\left(\mathbf{X}\right)\, d\mathbf{X} \tag{32}$$

The other terms $\mathcal{M}_i(X_i)$ and $\mathcal{M}_{ij}(X_i, X_j)$ are the conditional mean values for the param-

eters i and ij $(i \neq j)$, respectively:

$$\mathcal{M}_i(X_i) = \int_0^1 \cdots \int_0^1 \mathcal{M}\left(\mathbf{X}\right)\ d\mathbf{X}_{\sim i} - \mathcal{M}_0, \tag{33}$$

$$\mathcal{M}_{ij}(X_i, X_j) = \int_0^1 \cdots \int_0^1 \mathcal{M}\left(\mathbf{X}\right)\ d\mathbf{X}_{\sim ij} - \mathcal{M}_0 - \mathcal{M}_i(X_i) - \mathcal{M}_j(X_j). \tag{34}$$

The notation $\sim$ indicates that the variables are deleted. The Eq. 31 has the property of orthogonality in terms of conditional means as defined by Homma and Saltelli (1996). In this way, it is possible to define the Sobol' decomposition in terms of conditional variances (SOBOL, 1993). Thus, we obtain the first-order Sobol' indices, which quantify the additive effect of each input separately concerning the total variance,

$$S_i = \frac{Var[\mathcal{M}_i(X_i)]}{Var[\mathcal{M}(\mathbf{X})]}, \tag{35}$$

and the interaction effects of the inputs, as a second-order index:

$$S_{ij} = \frac{Var[\mathcal{M}_{ij}(X_i, X_j)]}{Var[\mathcal{M}(\mathbf{X})]}. \tag{36}$$

Higher-order Sobol' indices take into account the effects of the interactions of the various parameters and are defined in the same way. The total Sobol' indices is the sum of all Sobol' indices involving each variable. From the computational point of view, the total indices are calculated by

$$S_i^T = 1 - S_{\sim i} \tag{37}$$

where the notation $\sim$ indicated which variables are excluded in the summands of the Sobol' indices. The result of the Sobol' indices for a given parameter varies from 0 to 1. The closer to the value 1, the greater the influence of the analyzed parameter.

PCE-based Sobol' indices

Sobol' indices are usually calculated using a Monte Carlo (MC) simulation. This approach can be computationally expensive due to the small convergence rate. An alternative way to calculate Sobol' indices is by building a surrogate model defined by PCE. The Sobol' indices calculated by the PCE can be seen in Crestaux, Maitre and Martinez (2009) and Palar *et al.* (2018).

The output response PCE expression is given by Eq. (2). System output uncertain

response statistics can be calculated using PCE. Therefore, the mean output response from the system is:

$$\hat{\mu}(Y) = \mathbb{E}\left[\mathcal{M}^{PCE}(X)\right] = y_0. \tag{38}$$

Likewise, the variance is obtained as:

$$\widehat{Var}(Y) = \mathbb{E}\left[\left(\mathcal{M}^{PCE}(X) - \hat{\mu}\right)^2\right] = \sum_{\alpha \in \mathcal{A}} y_\alpha^2 \tag{39}$$

Therefore, as a post-processing technique, Sobol' indices can be determined only with PCE coefficients, so the first-order indices is:

$$S_i^{PCE} = \sum_{\substack{\alpha \in \mathcal{A}_i \\ \alpha \neq 0}} y_\alpha^2 \Bigg/ \sum_{\alpha \in \mathcal{A}} y_\alpha^2. \tag{40}$$

And, the second-order Sobol' indices is:

$$S_{ij}^{PCE} = \sum_{\substack{\alpha \in \mathcal{A}_{ij} \\ \alpha \neq 0}} y_\alpha^2 \Bigg/ \sum_{\alpha \in \mathcal{A}} y_\alpha^2. \tag{41}$$

3.3 UQLAB

To solve propagation uncertainties, you can use the UQLab, a software structure based on Matlab and designed to develop uncertainties quantification techniques and algorithms. UQLab is a framework that offers an extensive arsenal of types of analysis and integrated algorithms. It consists of open-source scientific modules that are connected to UQLabCore to carry out the propagation of uncertainties through Monte Carlo sampling, sensitivity analysis, reliability analysis (calculation of probabilities of rare events), building surrogate models (PCE, Kriging, and PC-Kriging methods), Bayesian techniques for inverse problems, etc. (MARELLI; SUDRET, 2014).

UQLab was developed at ETH Zurich (Switzerland) under Professor Bruno Sudret and Ph.D. Stefano Marelli's supervision. In this work, UQLab was used to implement the methodologies of damage quantification, through the PC-Kriging metamodel, sensitivity analysis using Sobol' indices, and to obtain the Kriging metamodel of the transmissibility function for damage detection in a composite wind turbine blade. To implement the methodologies, we enter the input and output information of the metamodels and the necessary configurations for the methods used.

4 POLYNOMIAL CHAOS-KRIGING METAMODELS FOR QUANTIFICATION OF THE DEBONDING AREA IN LARGE WIND TURBINE BLADES

This chapter investigates the performance of a data-based methodology for quantifying damage based on a metamodel obtained from the Polynomial Chaos-Kriging (PC-Kriging) method. The investigation seeks to quantify the severity of the damage, described by a specific type of debonding in a wind turbine blade as a function of a damage index. The damage indexes are calculated using a data-based Vibration Structural Health Monitoring (VSHM) methodology. Debonding damage from the blade is introduced artificially, and the blade is excited with an electromechanical actuator that raises a mechanical impulse causing the blade to impact. The acceleration responses' vibrations are measured by accelerometers distributed along the track and blade of the wind turbine. A metamodel is obtained using the PC-Kriging method based on damage indexes, trained with the blade's healthy condition and four damage conditions, and tested with the other two damage conditions. The PC-Kriging presents promising results for capturing the good tendency for the severity of the damage as a function of the damage index. This study complements the damage detection analyzes performed previously on the same structure in Cava and Tcherniak (2019).

The main contribution of this chapter is to propose a PC-Kriging framework for damage quantification. To the best of the authors' knowledge, this methodology is not yet explored in the context of SHM; despite its great potential for damage quantification, once it considers the propagation of uncertainties in the model with a relatively low computational cost, becoming something viable for the industrial context. In particular, this work explores applying the PC-Kriging method for quantification damage to a composite wind turbine blade using a data-driven methodology. There is no similar application in the SHM literature using this method to quantify the delaminated area in our limited knowledge.

This chapter is organized as follows: section 4.1 presents the methodologies used for the detection and quantification of damage; section 4.2 shows the experimental apparatus used to simulate damage in the wind turbine blade; section 4.3 presents the results obtained, and in section 4.4 the main conclusions are highlighted.

4.1 SHM APPROACH

The damage detection methodology used in Cava and Tcherniak (2019) followed the idea of Vibration-based Structural Health Monitoring (VSHM), which measures vibration responses from an artificial excitation. Thus, the structure's health/current state can be analyzed by monitoring its vibration response changes. The methodology was applied to an SSP 34 m wind turbine blade. Conventional classification of VSHM methodologies is the division between model-based (MAES *et al.*, 2016) and non-model-based (or data-driven) methods (LOVE, 2002; AVENDAÑO-VALENCIA; CHATZI; SPIRIDONAKOS, 2015). In the methodology of this work, a data-driven approach is used. Non-model-based methods depend exclusively on the data measured from the structure under study. These methods also involve constructing a model, but that model is based on data rather than numerical or analytical models (AVENDAÑO-VALENCIA; CHATZI; SPIRIDONAKOS, 2015). The structure's initial state measurements are considered reference states, where these observations can be compared with the structure measurements in operation. Any deviation of the new observations from the reference state might be considered an indication of damage. In Tcherniak and Mølgaard (2015), an analysis of an unsupervised methodology was carried out, which combined the correlation between the signals measured from different accelerometers. This study demonstrated that methodologies based on data-driven techniques have a great potential for detecting damage on large structures. Currently, many data-driven methodologies are being developed (TCHERNIAK; MøLGAARD, 2017; BULL; ULRIKSEN; TCHERNIAK, 2018; CAVA; TCHERNIAK; BRANNER, 2018); for example, in Soize and Orcesi (2020), a machine learning approach was presented using only an experimental database consisting of a small number of records to detect changes in the rigidity of engineering structures.

4.1.1 Damage detection methodology

The methodology presented in this study to obtain a damage index (DI) is available in Cava and Tcherniak (2019). This methodology is considered a simple nonparametric method for data compression and information extraction. The procedure is divided into four steps: data collection, the reference state, feature extraction, and the inspection phase for decision-making. Figure 5 provides a flowchart of the methodology steps. Below is a brief description of each step of the damage detection methodology.

Data collection

Figure 5: Flowchart of vibration-based methodology for damage detection in wind turbine blades proposed by Cava and Tcherniak (2019).

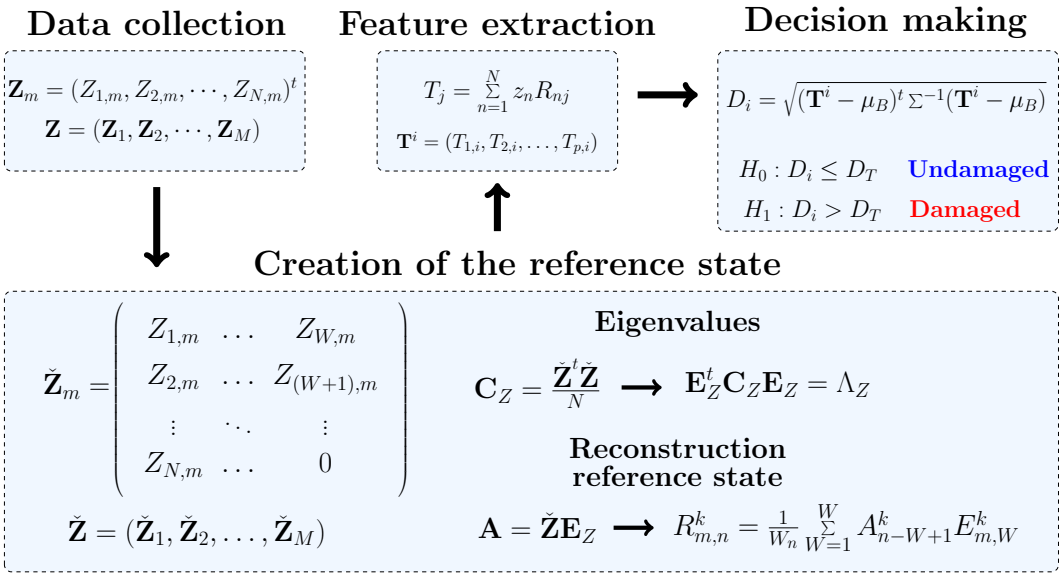

Source: Prepared by the author.

The first step is to collect the data from the structure/system. Acceleration signals are measured and discretized into a vector. Each measured signal is first standardized to have zero mean and unit variance and, secondly, transformed into the frequency domain. Each signal vector realization is arranged in the columns of the matrix $\mathbf{Z}$, i.e.,

$$\mathbf{Z} = (\mathbf{Z}_1, \mathbf{Z}_2, \ldots, \mathbf{Z}_M)\,. \tag{42}$$

The matrix $\mathbf{Z}$ is constructed from signal vectors obtained on the pristine/healthy state of the wind turbine blade, and it is used for creating the reference state.

Creation of the reference state

A reference state is created based on the matrix $\mathbf{Z}$, where the observation signal vectors can be compared. First, each vector signal $\mathbf{Z}_m$ is embedded into a matrix $\check{\mathbf{Z}}_m$ by W-lagged copies of itself. All matrices $\check{\mathbf{Z}}_m$ are used to create the full embedded matrix $\check{\mathbf{Z}}$, i.e.,

$$\check{\mathbf{Z}} = \left(\check{\mathbf{Z}}_1, \check{\mathbf{Z}}_2, \ldots, \check{\mathbf{Z}}_M\right). \tag{43}$$

The covariance matrix of $\check{\mathbf{Z}}$, which defines the covariance between the different signal

vector realizations, is estimated by

$$\mathbf{C}_Z = \frac{\check{\mathbf{Z}}^t \check{\mathbf{Z}}}{N}. \tag{44}$$

The eigendecomposition of $\mathbf{C}_Z$ yields λ_k and $\mathbf{E}^k$ eigenvectors in the same order as their corresponding eigenvalues. Each eigenvalue defines the partial variance in the direction of its corresponding eigenvector. A matrix $\mathbf{E}_Z$ contains all eigenvectors $\mathbf{E}^k$. Each Principal Component (PC) $\mathbf{A}^k$ associated with each eigenvector $\mathbf{E}^k$ is calculated by projecting the matrix $\check{\mathbf{Z}}$ onto $\mathbf{E}_Z$. The Reconstructed Components (RCs) are calculated by convolving the PCs with the associated $\mathbf{E}^k$. The RCs are then arranged in columns into the matrix $\mathbf{R}$. Therefore, $\mathbf{R}$ can be used as the reference state of the structure/system to which the observation signal vectors are compared.

Feature extraction

A Feature Vector (FV) is obtained for each new observation signal vector, which will be subjected to damage evaluation by comparing its similarity to the reference state defined by $\mathbf{R}$. An FV is calculated by multiplying an observation signal vector $\mathbf{z}$ with each RC in the reference state $\mathbf{R}$, as shown in (45) where $j = 1, \ldots W$.

$$T_j = \sum_{n=1}^{N} z_n R_{nj} \tag{45}$$

Each T_j value represents the inner product between an observation signal vector and each RC. All T_j are arranged into a vector $\mathbf{T}$ with dimension W. The FV $\mathbf{T}$ characterizes the observation signal vector onto the feature space.

Inspection phase and decision making

The baseline feature matrix $\mathbf{T}_B$ is created. Once the baseline is defined, an observation FV is then compared with the baseline $\mathbf{T}_B$. Using the Mahalanobis distance damage index is obtained,

$$\mathcal{D}_i = \sqrt{(\mathbf{T}^i - \boldsymbol{\mu}_B)^t \boldsymbol{\Sigma}^{-1} (\mathbf{T}^i - \boldsymbol{\mu}_B)}, \tag{46}$$

where $\boldsymbol{\mu}_B$ is the mean row of the baseline feature matrix $\mathbf{T}_B$; $\boldsymbol{\Sigma}$ is its corresponding covariance matrix, and $\mathcal{D}_i$ is the damage index.

To label an observation as an outlier or inlier, it is necessary to set a threshold against which damage rates can be assessed. A probabilistic point D_T based on the probability

density function (PDF) of the distances measured by the baseline FVs for the baseline matrix is calculated $\mathbf{T}_B$. As the damage indexes are always positive ($\mathcal{D}_i > 0$), a lognormal probability density function was used to approximately adjust the data considered as a training set, to define a limit to distinguish between observations of the healthy and damaged structure. The D_T limit is calculated by the inverse of the lognormal cumulative density. Thus, the definition of whether or not there is damage is given by the decision below:

$$\mathbf{H_0} : \mathcal{D}_i \leq D_T \quad \Rightarrow \quad \text{Undamage wind turbine blade}$$

$$\mathbf{H_1} : \mathcal{D}_i > D_T \quad \Rightarrow \quad \text{Damaged wind turbine blade}$$

4.1.2 Damage quantification methodology

After detecting the initial trailing edge debonding in the wind turbine blades using a data-driven approach, the user needs to decide if there is an imminent structural failure or if the system can be kept in operation under monitoring to track the damage progression and its impact on structural safety conditions. Therefore, it is imperative to obtain the quantification of the debonding length.

In this work, the proposed algorithm for damage quantification is divided into two stages: learning and validation. In the learning stage, the damage conditions and the healthy condition of the blade are known. After obtaining the damage index, it is used as an input in a metamodel that has the damage size as an output. In the validation step, the structural condition of the blade is not known. In this way, first the damage index is obtained and it is verified by the threshold if the structure is damaged or not. If damage is detected in the structure, then the damage index is entered as an input in the learned metamodel, which responds to the damage size. In Figure 6 it is possible to see a schematic representation of the algorithm for debonding quantification in wind turbine blade.

Computer simulation of many modern engineering and applied sciences problems have a high computational cost. In this context, metamodeling tries to reduce computational costs and perform sophisticated analyzes, such as reliability analysis and design optimizations (SCHÖBI; MARELLI; SUDRET, 2017). One method for obtaining metamodels is investigated: PC-Kriging, which combines the methods PCE and Kriging.

The idea of applying PC-Kriging in the damage quantification level is to employ a

Figure 6: Algorithm for debonding quantification in wind turbine blade.

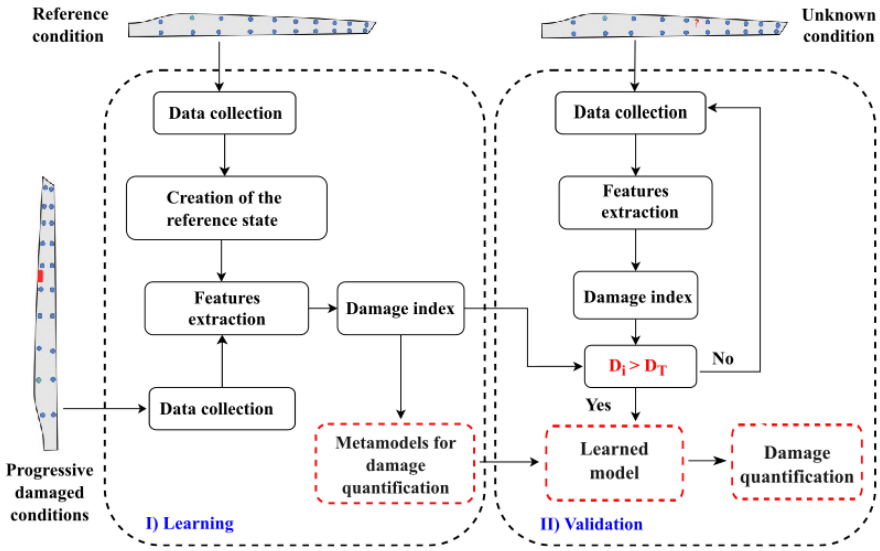

Source: Prepared by the author.

metamodel to capture the trend between the local damage index and damage size, which has been observed by Cava and Tcherniak (2019). The local damage index is used as input, and the damage size is used as an output to construct a PC-Kriging model. The PC-Kriging can be described as

$$\mathcal{S} \cong \sum_{\alpha \in \mathcal{A}} y_\alpha \Psi_\alpha(\mathcal{D}_i) + \sigma^2 \mathcal{Z}(\mathcal{D}_i, \Omega), \tag{47}$$

where $\mathcal{D}_i \in \mathbb{R}$ is the local damage index with a given Probability Density Function (PDF) f_X, $\mathcal{S}$ is the damage size, with $\mathcal{S} \in \mathbb{R}$. The $\sum_{\alpha \in \mathcal{A}} y_\alpha \Psi_\alpha(\mathcal{D}_i)$ is a weighted sum of orthonormal polynomials that describes the PC-Kriging model trend, where $\Psi_\alpha(\mathcal{D}_i)$ are orthonormal polynomials in relation to f_X, $\alpha \in \mathcal{A}$ are the indices and y_α are the corresponding coefficients; σ^2 is the variance of the process, and $\mathcal{Z}((\mathcal{D}_i), \Omega)$ is a Gaussian random process with zero mean. Ω describes outcomes of the underlying probability space with a correlation family $\mathcal{R}$ and its hyperparameters θ. That is, the correlation function $\mathcal{R} = \mathcal{R}(x, x', \theta)$ describes the correlation between two samples of the input space. For example, x and x' depends on the hyperparameters θ (LATANIOTIS; MARELLI; SUDRET, 2015).

In the first stage of the PC-Kriging metamodel construction, the polynomials set defining the trend through the PCE are defined using the LARS algorithm. In the second stage, the ideal correlation and tendency parameters are calculated the same way in the universal Kriging algorithm. For this study results, an optimal PC-Kriging approach

is used; that is, the metamodel is obtained iteratively, and the one chosen is the one that minimized the LOO error. The optimal PC-Kriging is chosen because it already has better performance in the literature than the sequential PC-Kriging (SCHÖBI; SUDRET; WIART, 2015). Figure 7 shows a schematic representation of the Optimal PC-Kriging algorithm.

Figure 7: Schematic representation of the Optimal Polynomial Chaos-Kriging algorithm in wind turbine blade.

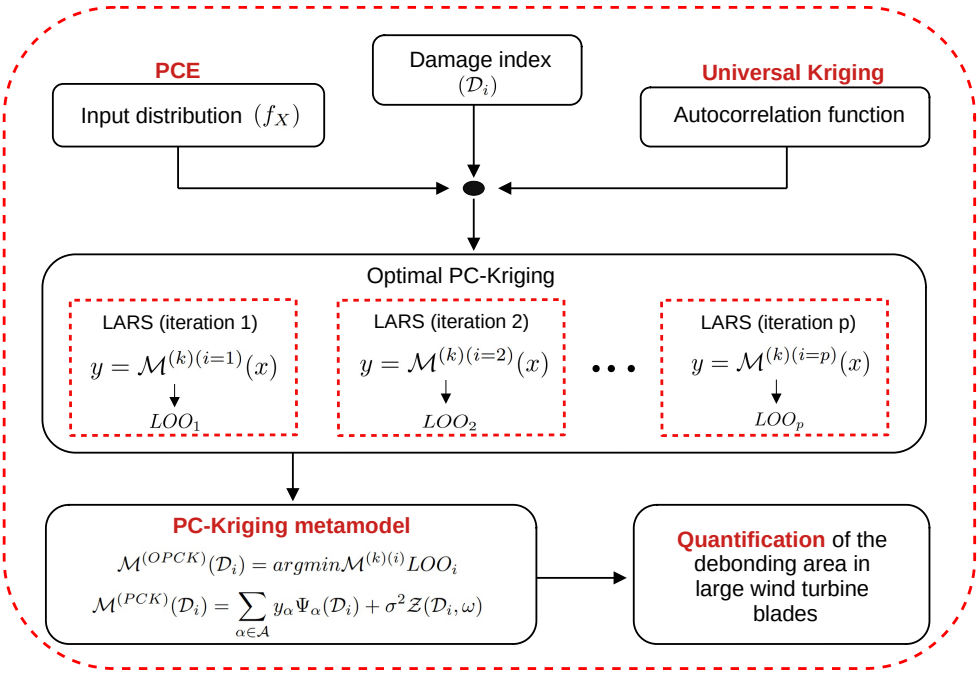

Source: Prepared by the author.

4.2 EXPERIMENTAL APPLICATION

The dataset used in the practical application proposed in this work belongs to Bruel & Kjaer. This dataset has been explored recently to validate different methodologies (CAVA; TCHERNIAK, 2019; CAVA; TCHERNIAK; BRANNER, 2018; ULRIKSEN *et al.*, 2016; CRESPO, 2016; TCHERNIAK; MØLGAARD, 2015; LARSEN *et al.*, 2014). A brief description of the experimental setup will be provided below. A detailed description of the experimental setup can be found in Nielsen *et al.* (2010) and Eder *et al.* (2015).

The experimental application of the methodology proposed was performed in the SSP 34 m wind turbine blade. SSP-Technology A/S manufactured the blade, and the

experiments were performed on a test rig at the Wind Energy department, the Technical University of Denmark. The blade of the wind turbine and the experiment's facilities can be seen in Figure 8(b).

Figure 8: Experimental setup of the SSP 34 meters wind turbine blade manufactured by SSP-Technology A/S. The blade was instrumented with 10 accelerometers along the leading edge (LE) and 10 along the trailing edge (TE) and was excited by an electromechanical actuator. The debonding damage was artificially introduced into the blade.

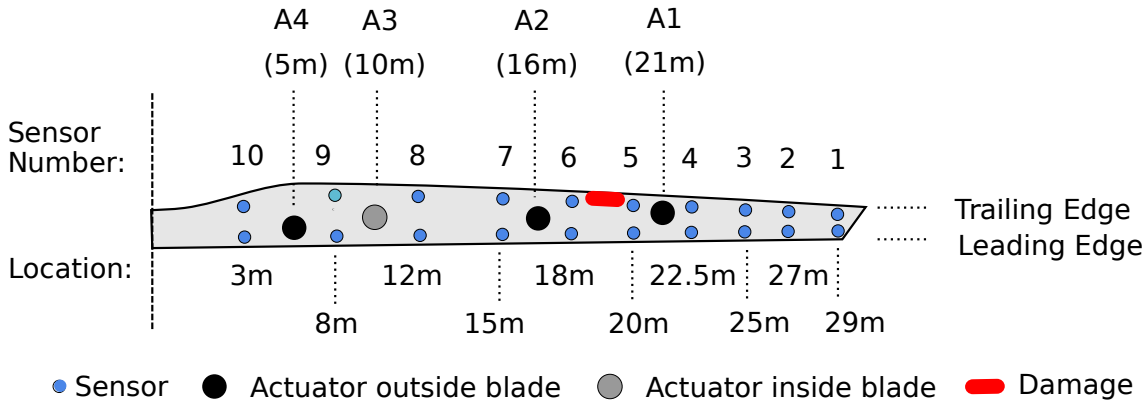

(a) Accelerometers, damage and actuator locations scheme.

(b) Test rig set-up.

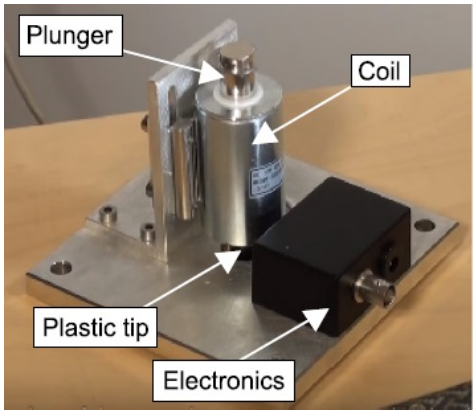

(c) Electromechanical actuator.

Source: Adapted from Cava and Tcherniak (2019).

The experimental application hardware consists of an electromechanical actuator and accelerometers. The actuator is an electromechanical device consisting of two main parts: a steel plunger and a coil. Driven by an electrical pulse, the coil shoots the plunger towards the structure; after the hit, the plunger returns to its initial position by spring. Figure 8(c) show the electromechanical actuator used to generate the impact in the structure, and it was placed on the surface outside of the blade at the positions indicated in Figure 8(a). From some pre-tests, it is observed that even one actuator can excite the entire blade (TCHERNIAK; MØLGAARD, 2015).

The blade was also instrumented with twenty triaxial accelerometers, model Bruel & Kjaer Type 4524-B, positioned as represented in the scheme in Figure 8(a). Ten accelerometers were placed on the trailing edge (TE) and ten on the leading edge (LE). Only the acceleration in the direction normal to the blade surface, which coincides with the flap-wise motion of the blade, was utilized. The acceleration signals were recorded by a distributed data acquisition unit based on several 12 channel data acquisition modules Bruel & Kjaer Type 3053-B, and data recording software Bruel & Kjaer Type 7708 (LARSEN *et al.*, 2014). The unit also contains a signal generator, which was set to generate a rectangular pulse, which, after amplification, was fed to the actuator, resulting in an actuator hit. The data acquisition was triggered by this pulse, set to collect vibration data for a few milliseconds before and a few seconds after the pulse. Using the trigger significantly reduces the amount of data collected for the analysis (TCHERNIAK; MØLGAARD, 2015).

One of the main types of damage in wind turbine blades is the adhesive joint debonding (MONTESANO; CHU; SINGH, 2016). This type of damage occurs when an adhesive bond between the laminates of the pressure and suction sides of the blade breaks can happen on both leading and trailing edges. Small debonding size can grow up to a level at which repair is impossible, and the entire blade should be replaced (CAVA; TCHERNIAK, 2019). Damage of this nature has been introduced into the turbine blade. First, holes through the adhesive between the blade's pressure and suction sides were drilled. Then, the holes were merged using a saw and a chisel, forming an opening that was gradually extended from 20 cm up to 120 cm by increments of 20 cm. The debonded parts were connected by bolts, placed at 10 cm intervals (see Figure 9(b)). The healthy condition was then simulated by tightening all the bolts, and then the accelerometers measured when the blade was excited by actuator A1. After a few seconds, when the impact response had decayed, the blade was excited by actuator A2, and the signals were measured. Similarly, it occurred when the blade was excited by actuators A3 and A4. The progressive damaged conditions were reproduced by loosening some bolts. The series of measurements were repeated, firstly for the damaged condition with an opening of 20 cm (D20), and later for damaged conditions with an opening of 40 cm (D40), 60 cm (D60), 80 cm (D80), 100 cm (D100) and 120 cm (D120). The location of the damage can be seen in Figure 8(a).

Experimental data is always contaminated by noise, so it was necessary to repeat the measurements several times. In this experiment, the time between the actuator impacts varied from one to five minutes to speed up the validation. The time between measurements can be increased in real applications, depending on industrial requirements. In

Figure 9: Damage introduced in SSP 34 m wind turbine blade.

(a) Damage introduced by chisel in the trailing edge.

(b) Damage bolted to control the damage size and any additional anomalies introduced by the impact that generates the damage.

Source: Adapted from Cava and Tcherniak (2019).

the experiment, acceleration signals were collected for the blade's impact response under healthy and progressive damaged conditions, totaling 386 signals collected for seven simulated structural conditions, as can be seen in Table 2. It should be noted that in carrying out this experiment, the execution of the test, for a set of observations, was carried out without really controlling it; for this reason, the number of signals is different for each structural condition (CAVA; TCHERNIAK, 2019).

Table 2: Number of signals measured on each experimental test.

Condition	Damage size	Number of signals
H	-	53
D20	20 cm	70
D40	40 cm	61
D60	60 cm	60
D80	80 cm	49
D100	100 cm	54
D120	120 cm	39
Total		386

Source: Adapted from Cava and Tcherniak (2019).

4.3 RESULTS AND DISCUSSIONS

This section presents the damage detection results and quantification of the trailing edge debonding area. To obtain the results is used the software MATLAB. For damage quantification results is used the toolbox UQLab. It is used to estimate the trailing edge debonding size, using the damage index, and optimizing the PC-Kriging model.

4.3.1 Damage detection

The methodology for damage detection described previously is applied in the SSP 34 m wind turbine blade dataset. The dataset provides acceleration signals collected from sensors placed on the trailing and leading edges. In Cava and Tcherniak (2019), the authors defined the parameters chosen for the best methodology performance, which are employed in this work. In creating the reference state, it is considered a $M = 10$ signal vector realization with a sliding window size of $W = 10$. The feature vector dimension is set to $p = 5$. The baseline matrix construction is performed using $s = 26$ feature vectors of dimension $p = 5$ extracted from healthy condition signals. In the inspection phase, the risk of false alarm probability is set to $\kappa = 0.01$ in the lognormal density function. The choice of $\kappa = 0.01$ is because this way we will have a low false alarm probability. A detailed discussion of each one of these parameters on the methodology performance can be found in Cava and Tcherniak (2019).

Figure 10 presents a comparison between the measured and reconstructed spectrum frequency of the reference state considering the signal collected by the sensor 1 and actuator location at A1. As can be observed, using 5 principal components allows an adequate reconstruction of the spectrum frequency, which is used as the reference state.

Figures 11-18 show the damage index by damage size obtained from accelerometers in the TE and LE for actuator positions A1, A2, A3, and A4. The damage detection results present three scenarios: i) damage indexes can detect and track the damage's severity; ii) the damage is not well detected, as it has many false negatives. However, as the damage increases, there is a tendency for the damage indexes, so the damage's progression is somehow detected. In this case, there is a time-dependent feature for damage detection; iii) a final scenario is when the damage indexes cannot detect the damage or track its progress. For the actuator in position A1, it can be seen in Figure 11 that, in general, the sensors were able to detect the damage well. As for the accelerometers in the LE, only sensors 6, 7, and 8 were able to detect the damage, but they presented some false

Figure 10: Reconstructed reference state and measured spectrum frequency under healthy condition obtained from signals measured by sensor 1 in trailling edge and actuator location at A1.

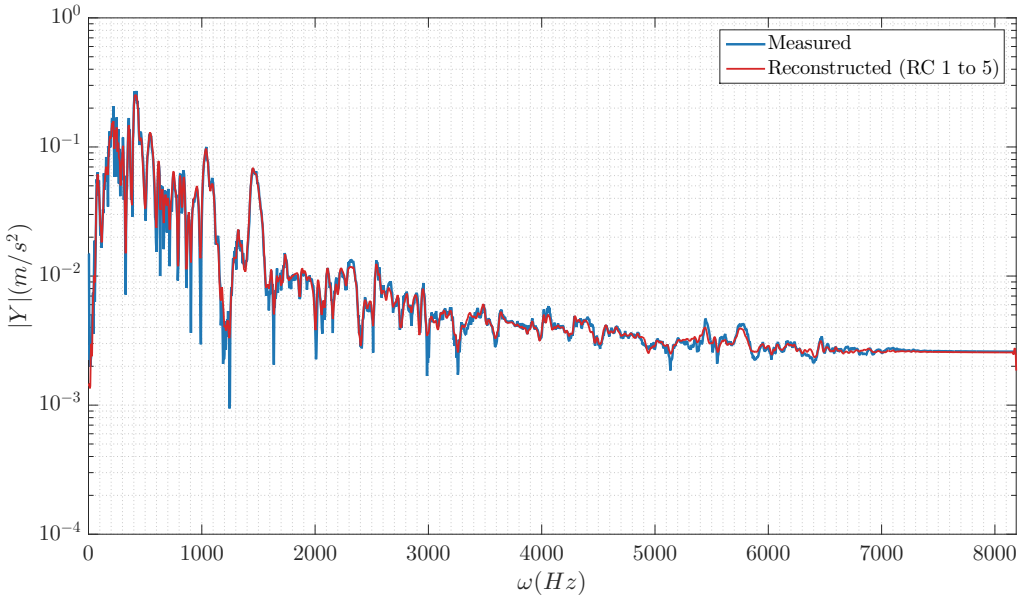

Source: Prepared by the author.

negatives, as can be seen in the Figure 12. For actuators in positions A2 and A3, it can be seen in Figures 13-16 that sensors, both in TE and LE, did not obtain a good detection of damage. Finally, Figure 17 and Figure 18 show the results obtained for the actuator in position A4. In this position of the actuator, the sensors in the TE have better detection of damage, highlighting sensors 1, 2, 3, and 4. It is possible to observe that the accelerometers along the TE detected the damage better than the accelerometers along with the LE in all actuator positions.

Figure 11: Damage index ($\mathcal{D}_i$) by damage size ($\mathcal{S}$) for accelerometers in the trailing edge (TE) with actuator in position A1. The damage index in the healthy (●) and damaged (x) conditions. The dashed line (---) corresponds to the threshold defined by a risk of false alarm probability equal set to $\kappa = 0.01$.

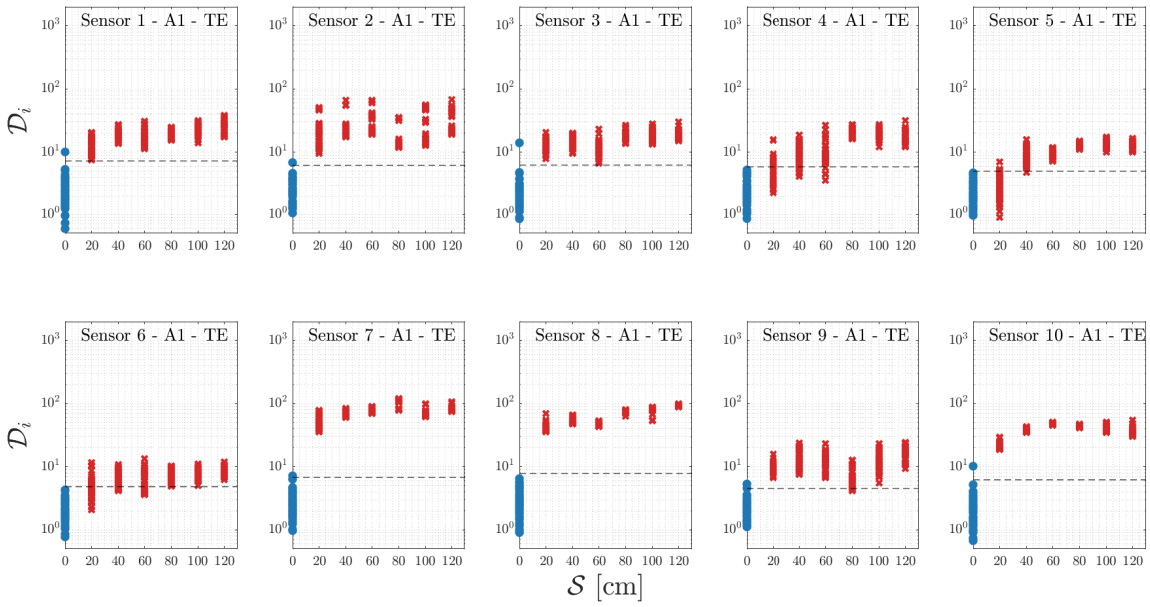

Source: Prepared by the author.

Figure 12: Damage index ($\mathcal{D}_i$) by damage size ($\mathcal{S}$) for accelerometers in the leading edge (LE) with actuator in position A1. The damage index in the healthy (●) and damaged (x) conditions. The dashed line (---) corresponds to the threshold defined by a risk of false alarm probability equal set to $\kappa = 0.01$.

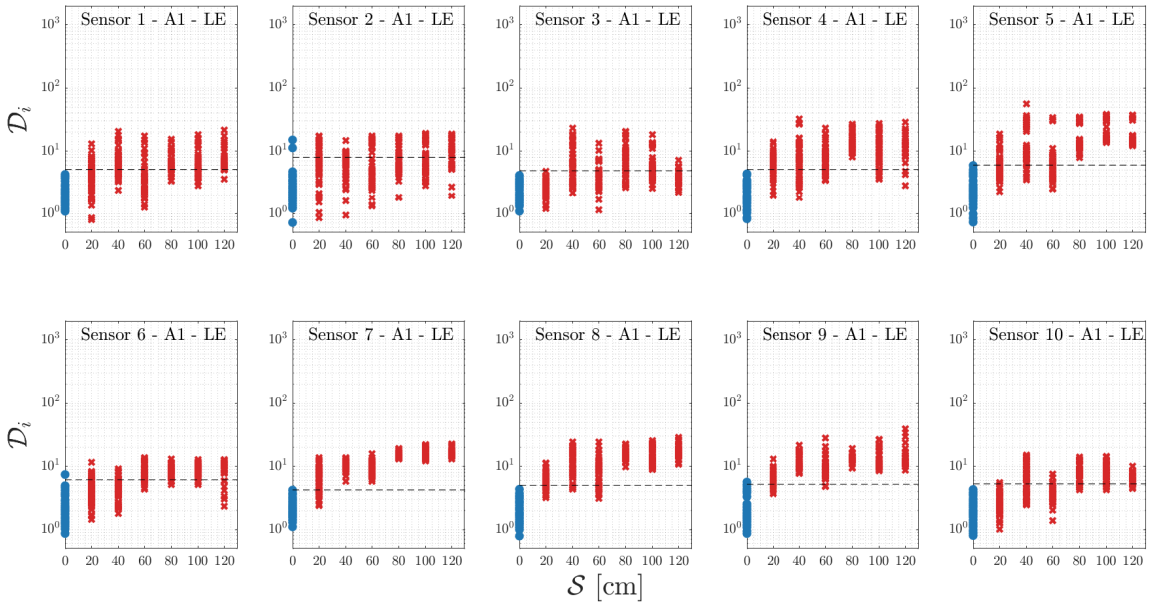

Source: Prepared by the author.

Figure 13: Damage index ($\mathcal{D}_i$) by damage size ($\mathcal{S}$) for accelerometers in the trailing edge (TE) with actuator in position A2. The damage index in the healthy (●) and damaged (x) conditions. The dashed line (---) corresponds to the threshold defined by a risk of false alarm probability equal set to $\kappa = 0.01$.

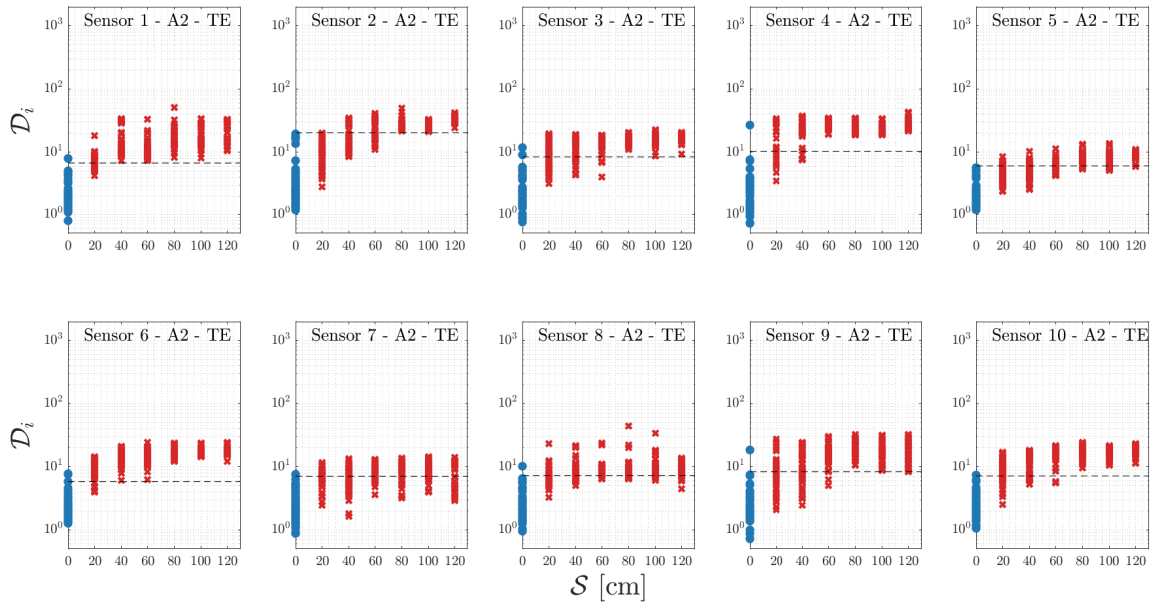

Source: Prepared by the author.

Figure 14: Damage index ($\mathcal{D}_i$) by damage size ($\mathcal{S}$) for accelerometers in the leading edge (LE) with actuator in position A2. The damage index in the healthy (●) and damaged (x) conditions. The dashed line (---) corresponds to the threshold defined by a risk of false alarm probability equal set to $\kappa = 0.01$.

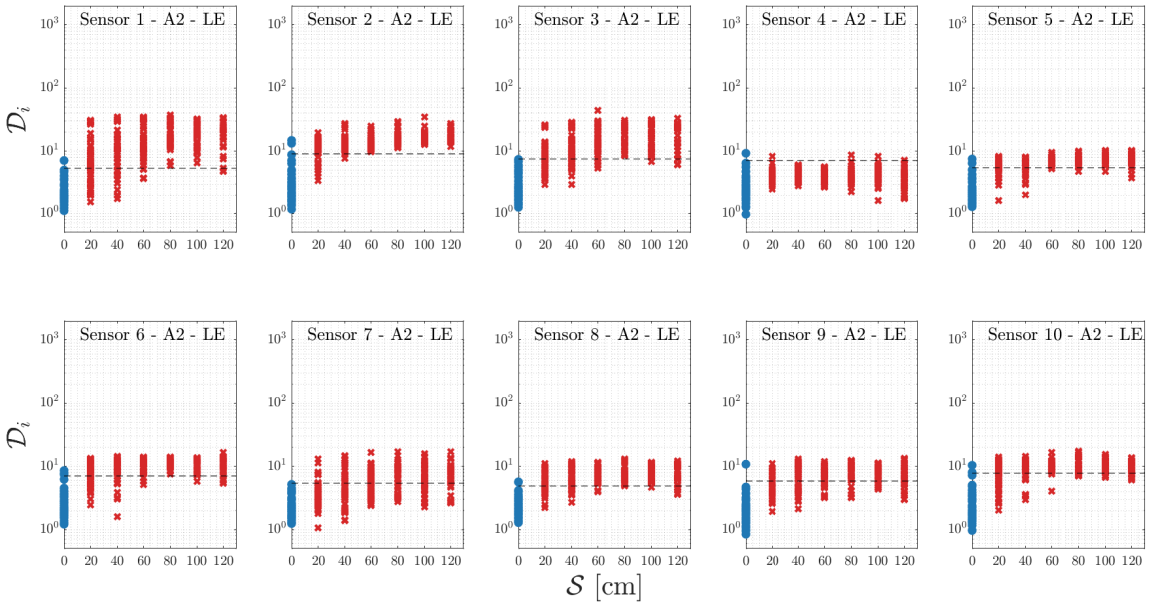

Source: Prepared by the author.

Figure 15: Damage index ($\mathcal{D}_i$) by damage size ($\mathcal{S}$) for accelerometers in the trailing edge (TE) with actuator in position A3. The damage index in the healthy (●) and damaged (x) conditions. The dashed line (---) corresponds to the threshold defined by a risk of false alarm probability equal set to $\kappa = 0.01$.

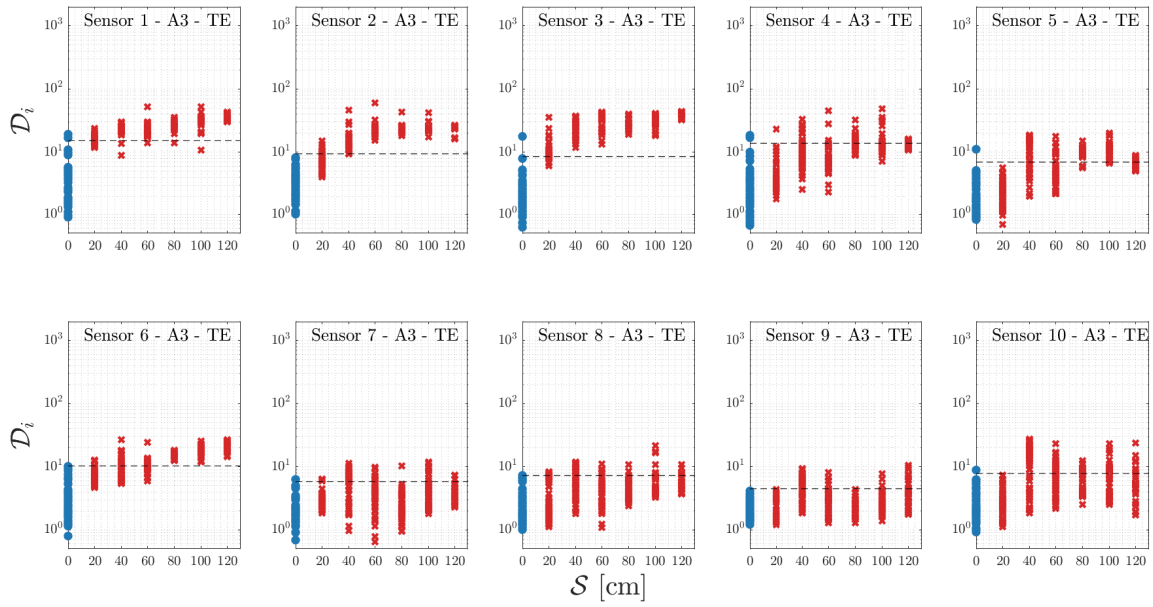

Source: Prepared by the author.

Figure 16: Damage index ($\mathcal{D}_i$) by damage size ($\mathcal{S}$) for accelerometers in the leading edge (LE) with actuator in position A3. The damage index in the healthy (●) and damaged (x) conditions. The dashed line (---) corresponds to the threshold defined by a risk of false alarm probability equal set to $\kappa = 0.01$.

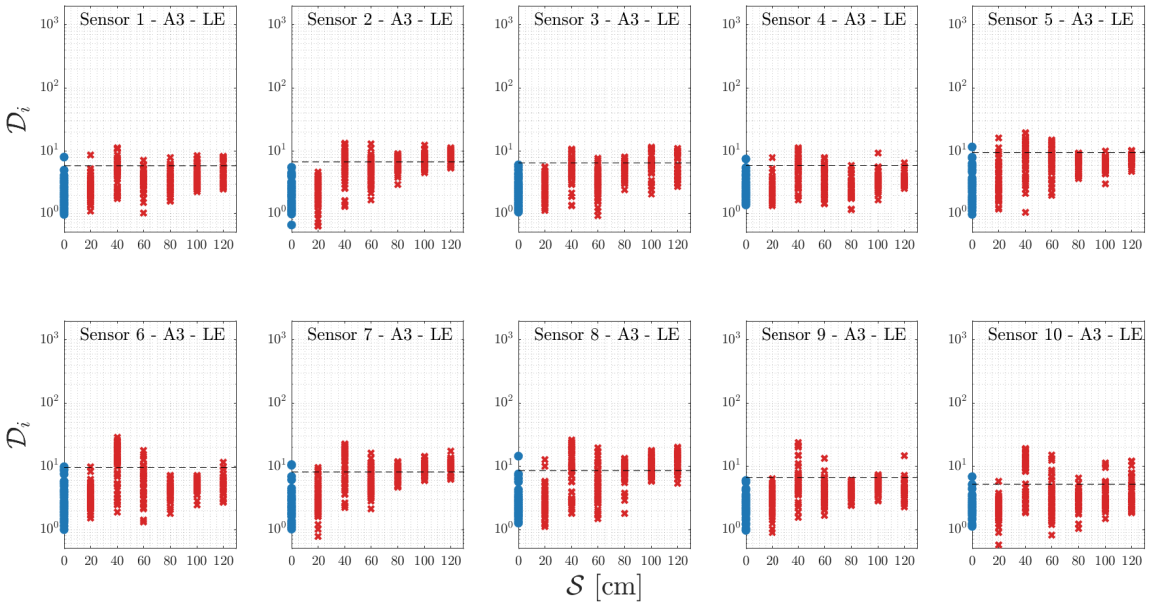

Source: Prepared by the author.

Figure 17: Damage index ($\mathcal{D}_i$) by damage size ($\mathcal{S}$) for accelerometers in the trailing edge (TE) with actuator in position A4. The damage index in the healthy (●) and damaged (x) conditions. The dashed line (---) corresponds to the threshold defined by a risk of false alarm probability equal set to $\kappa = 0.01$.

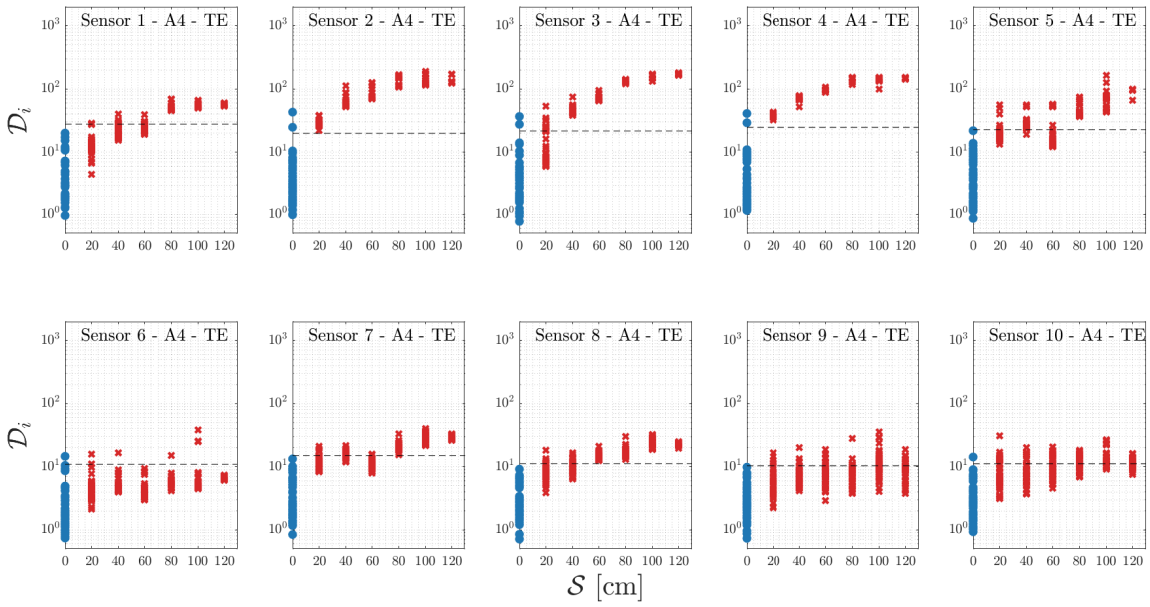

Source: Prepared by the author.

Figure 18: Damage index ($\mathcal{D}_i$) by damage size ($\mathcal{S}$) for accelerometers in the leading edge (LE) with actuator in position A4. The damage index in the healthy (●) and damaged (x) conditions. The dashed line (---) corresponds to the threshold defined by a risk of false alarm probability equal set to $\kappa = 0.01$.

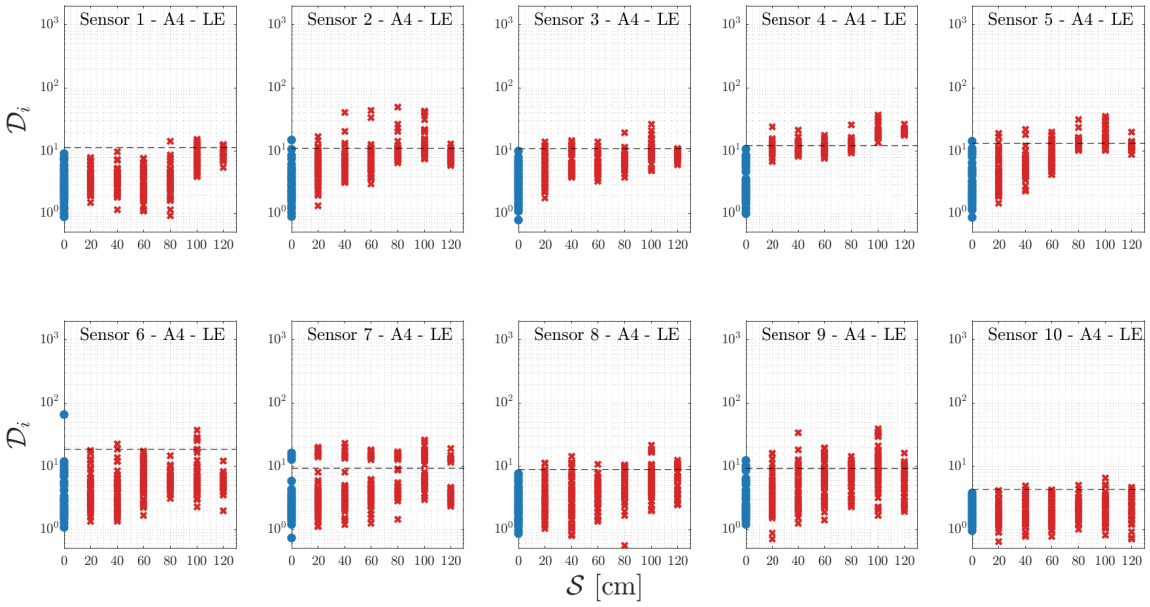

Source: Prepared by the author.

4.3.2 Damage quantification

The damage quantification methodology used is based on constructing a PC-Kriging metamodel, which obtains the debonding size as a function of the local damage index. The local damage index is used as input for building a PC-Kriging metamodel. The following conditions' local damage index are considered in the model learning stage: H, D40, D80, D100, and D120. The damaged conditions D20 and D60 are used in the test steps to validate the prediction of damage quantification using metamodel. The choice of conditions D20 and D60 for validation of the metamodel was due to the fact that they are conditions closer to the healthy state. Simulations were performed with different validation conditions and the results were similar. For the situation where fewer learning conditions are used, the metamodel has a higher cross-validation error.

The damage index is always positive, so in the PCE settings, the distribution used is lognormal, and the moments of the PCE settings are the mean and standard deviation of the learning data. In the Kriging configuration, a correlation function based on an exponential and ellipsoidal family is used to optimize the maximum likelihood estimate performed by a gradient method to define the GPR model (LATANIOTIS; MARELLI; SUDRET, 2015). The learned models represent a mean and 95% confidence interval of the predicted distribution. Figures 19 and 22 attests to the severity, that is, the size of the trailing edge debonding as a function of the damage index obtained by the PC-Kriging method for the sensors in the TE and LE in actuator position A1, Figures 25 and 28 to position A2, Figures 31 and 34 to position A3 and Figures 37 and 40 to position A4. These figures show that most of the damage indexes used in the learning and validation stages are within the region of the confidence interval, inferring an adequate selection of the training parameters. It is also noted that the PC-Kriging model captured the damage index trend adequately well. The sensors located in the TE also had a better performance for quantifying the damage. The results show that the sensor's location in the TE and LE influences the results. The sensors that fall under scenarios i) and ii) referred to in damage detection results (subsection 4.3.1) are the ones that present the best results.

The Root Mean Squared Error (RMSE) metric is chosen to validate the model prediction for test conditions D20 and D60. This metric frequently measures the differences between values estimated by a model or an estimator and the values measured. The RMSE in this work can be defined as

$$RMSE = \sqrt{\sum_{i=1}^{n} \frac{\left(\mathcal{S}_{est} - \mathcal{S}_{mea}\right)^2}{n}}, \tag{48}$$

where $\mathcal{S}_{est}$ are estimated values for the quantification of the debonding area, $\mathcal{S}_{mea}$ are measured values of the debonding area, and n is the number of observations.

The validations of the PC-Kriging model prediction for the validation conditions in the TE and LE for the four actuator locations are presented in Figures 20, 23, 26, 29, 32, 35, 38 and 41. Ideally, the points would concentrate on the diagonal line, as this is where the estimated damage size coincides with the measured damage size. The Figures 21, 24, 27, 30, 33, 36, 39, and 42 show the boxplot of the values estimated, by the PC-Kriging metamodel, for the test conditions D20 and D60. With the boxplot it is possible to analyze the dispersion of the values obtained and observe those that came closest to the values measured experimentally. In particular, it can be seen in Figure 39 that the values for sensors 1, 2, 3 and 4 have little dispersion and are very close to the measured values. For all sensors located in the LE, it is possible to observe a large dispersion of the estimated values. Tables 3-10 presents the RMSE values and the mean of the estimated value for the validation conditions, D20 and D60, for each sensor in the TE and LE in actuator location at A1, A2, A3, and A4.

As already mentioned, for all actuator positions, the accelerometers in the TE were able to obtain a better quantification of the severity of the year. For the actuator location at A1, the results show that sensor 4 was able to quantify the damage well for both validation conditions. Sensor 5 was able to quantify the damage well in the condition D60 and sensor 8 in the condition D20, as can be seen in the Figures 19 and 22, Figures 20 and 23 and Tables 3 and 4. As for the actuator in positions A2 and A3, it is observed that the sensors did not obtain a good quantification of the damage, even with low RMSE values (see Tables 5, 6, 7 and 8), the validation data present a lot of dispersion, as can be seen in the Figures 25, 28, 31 and 34. For actuator location at A4 in TE, sensors 2, 3, 4, and 8 had the best results. Sensor 10 had the worst effect on the TE, which did not detect the damage well (see Figure 37).

Figure 19: Damage severity ($\mathcal{S}$) by the damage index ($\mathcal{D}_i$) for accelerometers 1 to 10 on the trailing edge (TE) with actuator in position A1. The metamodel was learned using five conditions (●) and validated with two conditions (x). The bold line (—) corresponds to the trend mean and the gray-colored region (▬) to the 95 % of confidence interval.

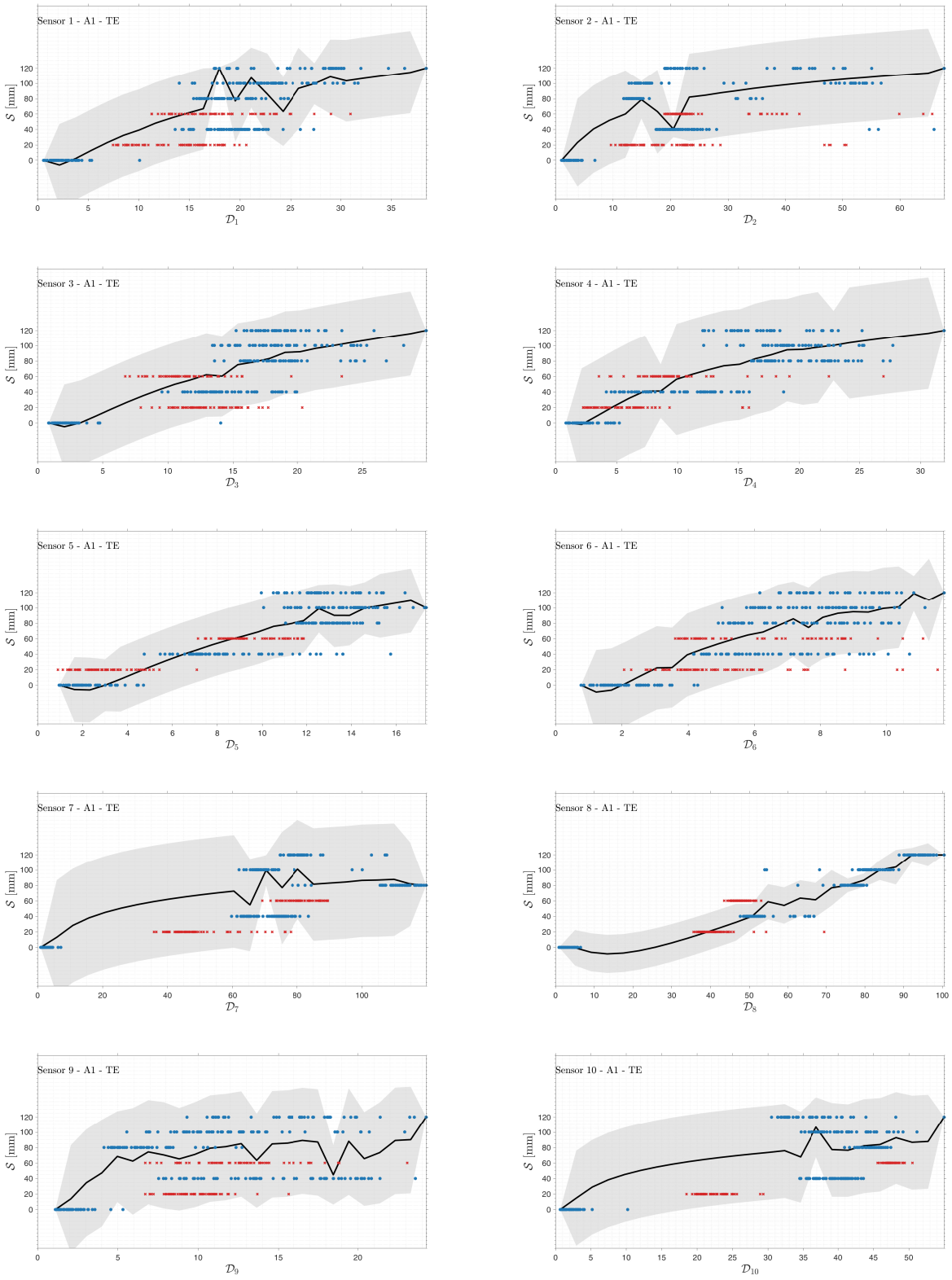

Source: Prepared by the author.

Figure 20: Validation of the estimated damage size for the test conditions (D20 and D60), using the PC-Kriging metamodel, by the actual damage size for each sensor in the TE with actuator in position A1. The estimated damage size for all damage indexes (●) and the mean of estimated damage size (●) for each test condition.

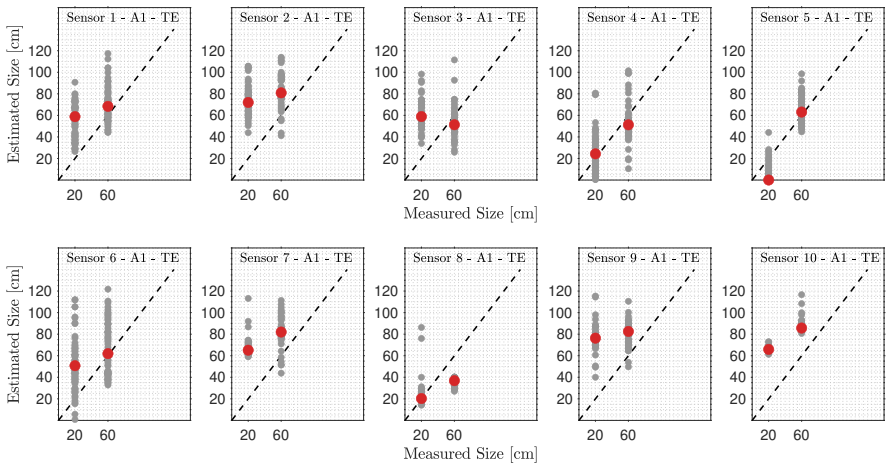

Source: Prepared by the author.

Figure 21: Boxplot of estimated values for test conditions D20 (■) and D60 (■) for each sensor along TE in actuator location at A1.

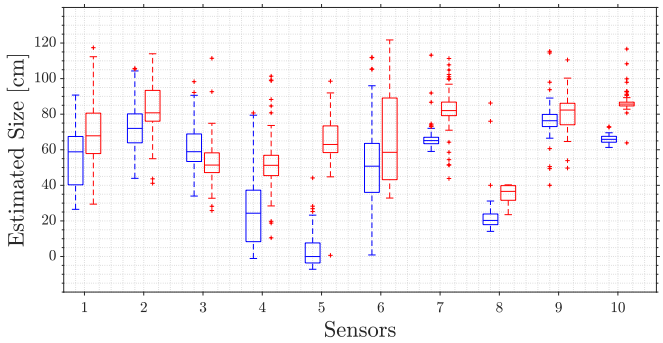

Source: Prepared by the author.

Table 3: Value of the root-mean-square error (RMSE) and the estimated values of the test conditions (D20 and D60) for each sensor along TE in actuator location at A1.

Sensor	1	2	3	4	5	6	7	8	9	10
RMSE	31.0	44.9	32.9	18.8	16.9	33.9	38.9	18.6	45.1	38.7
D20: mean est. [cm]	58.83	72.01	58.9	24.33	0.03	50.76	65.14	20.27	76.32	65.87
D60: mean est. [cm]	68.37	80.92	51.32	51.27	63.09	61.96	81.98	36.86	82.56	85.69

Source: Prepared by the author.

Figure 22: Damage severity ($\mathcal{S}$) by the damage index ($\mathcal{D}_i$) for accelerometers 1 to 10 on the leading edge (LE) with actuator in position A1. The metamodel was learned using five conditions (●) and validated with two conditions (x). The bold line (—) corresponds to the trend mean and the gray-colored region (▬) to the 95 % of confidence interval.

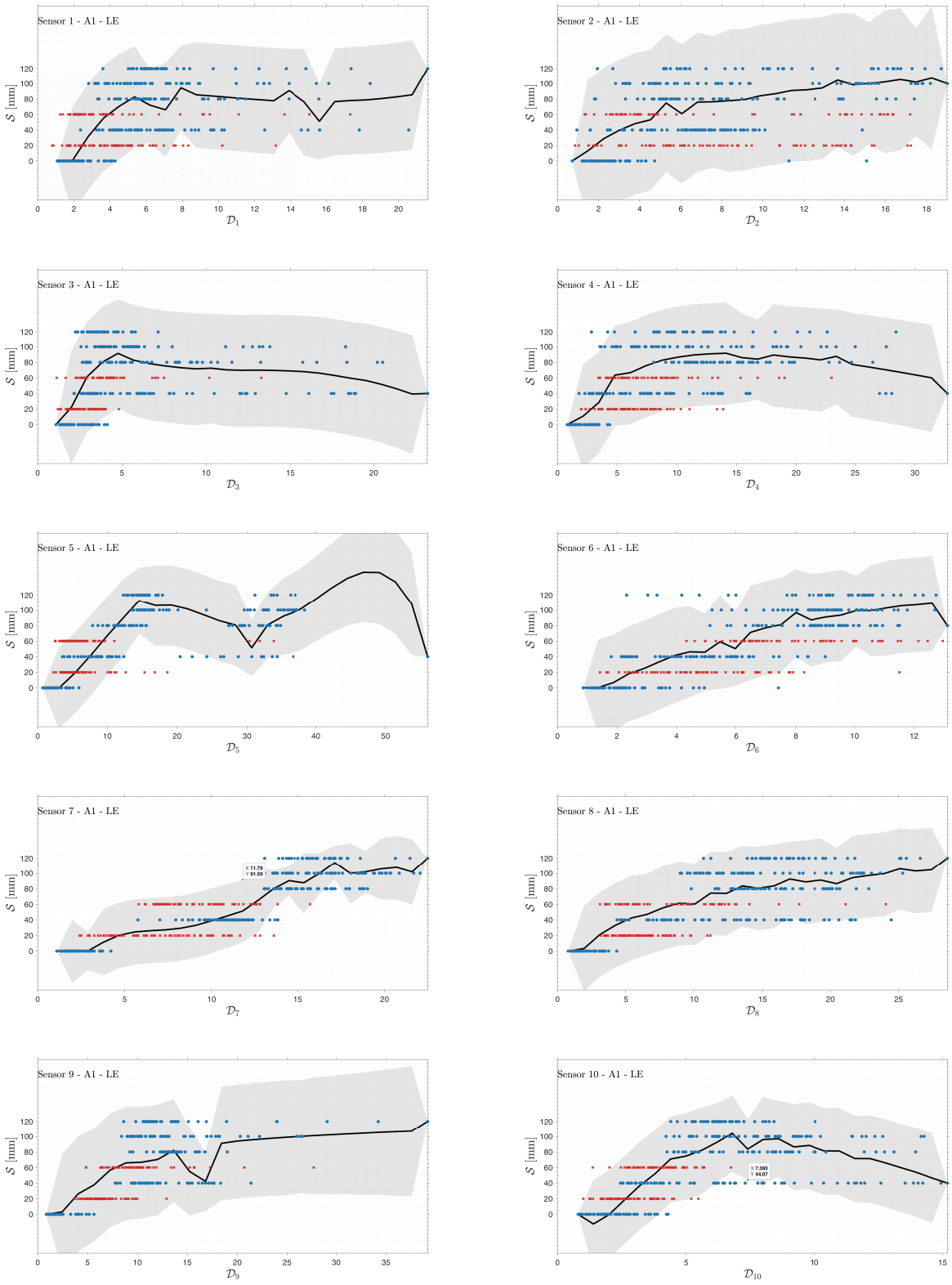

Source: Prepared by the author.

Figure 23: Validation of the estimated damage size for the test conditions (D20 and D60), using the PC-Kriging metamodel, by the actual damage size for each sensor in the LE with actuator in position A1. The estimated damage size for all damage indexes (●) and the mean of estimated damage size (●) for each test condition.

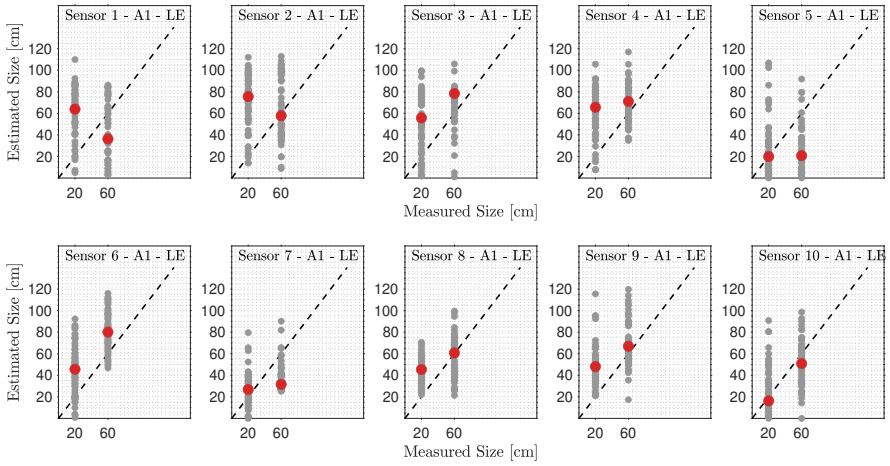

Source: Prepared by the author.

Figure 24: Boxplot of estimated values for test conditions D20 (■) and D60 (■) for each sensor along LE in actuator location at A1.

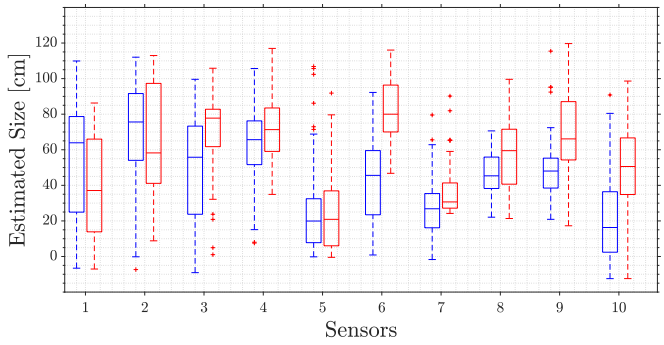

Source: Prepared by the author.

Table 4: Value of the root-mean-square error (RMSE) and the estimated values of the test conditions (D20 and D60) for each sensor along LE in actuator location at A1.

Sensor	1	2	3	4	5	6	7	8	9	10
RMSE	41.6	45.8	34.5	37.4	34.0	30.9	21.7	24.2	29.1	23.9
D20: mean est. [cm]	63.91	75.62	55.79	65.67	19.93	45.6	26.83	45.35	48.03	16.29
D60: mean est. [cm]	36.38	57.81	78.38	71.08	20.77	80.11	31.59	60.75	66.88	50.85

Source: Prepared by the author.

Figure 25: Damage severity ($\mathcal{S}$) by the damage index ($\mathcal{D}_i$) for accelerometers 1 to 10 on the trailing edge (TE) with actuator in position A2. The metamodel was learned using five conditions (●) and validated with two conditions (x). The bold line (—) corresponds to the trend mean and the gray-colored region (▬) to the 95 % of confidence interval.

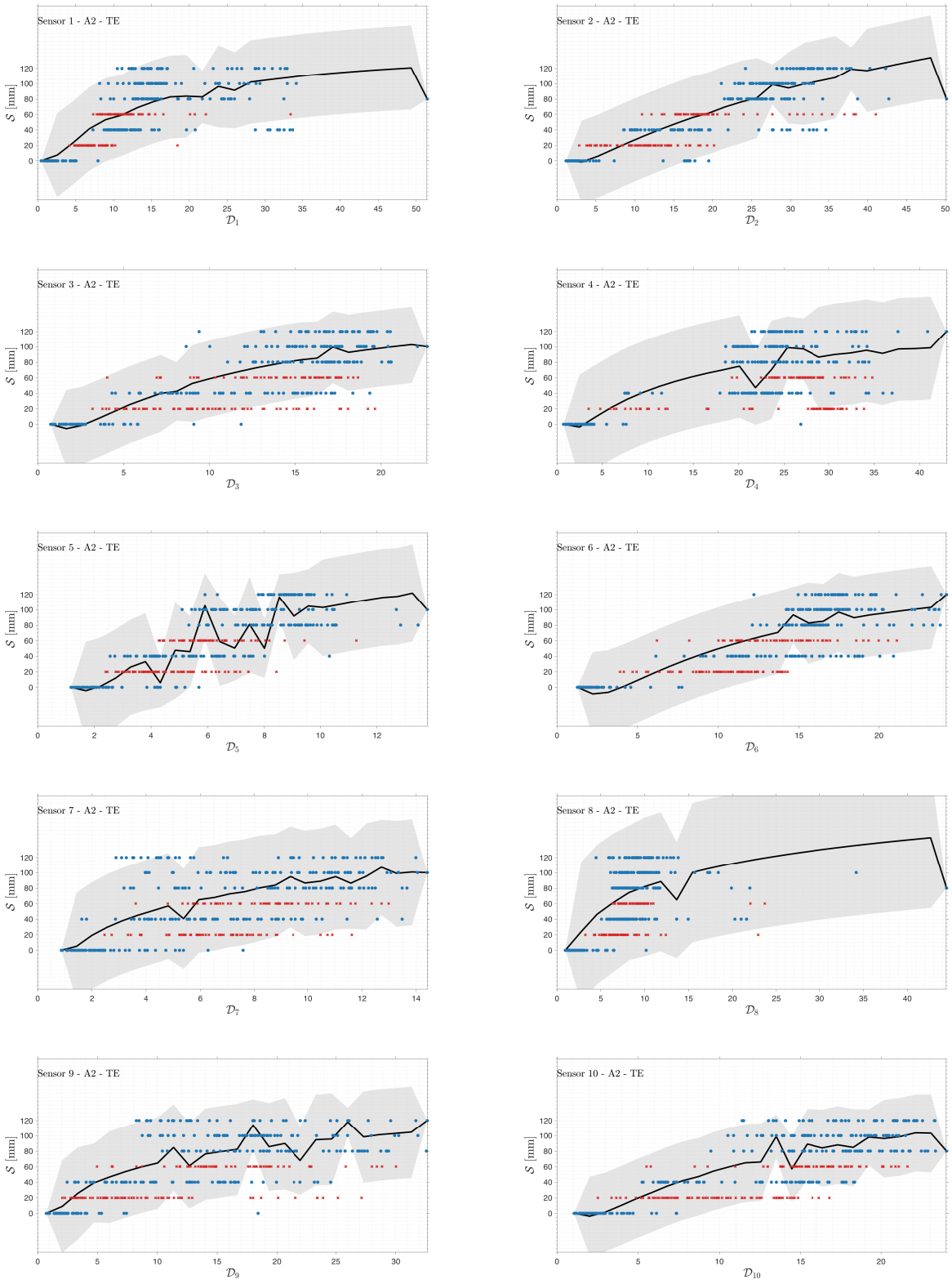

Source: Prepared by the author.

Figure 26: Validation of the estimated damage size for the test conditions (D20 and D60), using the PC-Kriging metamodel, by the actual damage size for each sensor in the TE with actuator in position A2. The estimated damage size for all damage indexes (●) and the mean of estimated damage size (●) for each test condition.

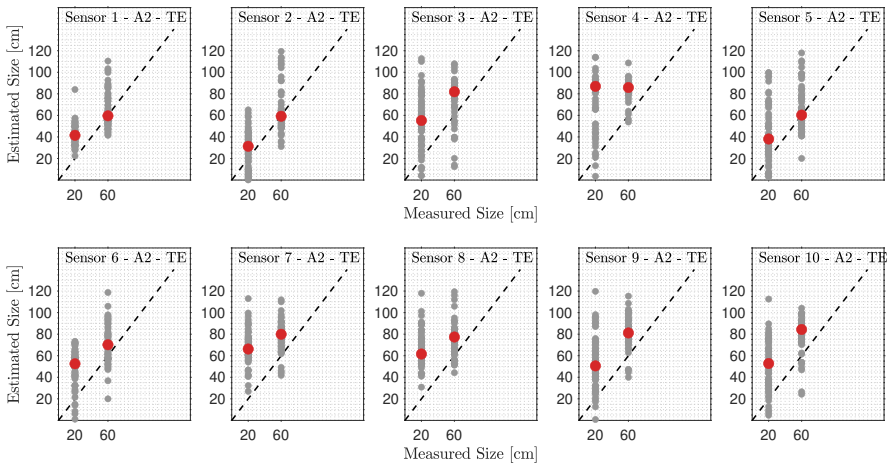

Source: Prepared by the author.

Figure 27: Boxplot of estimated values for test conditions D20 (■) and D60 (■) for each sensor along TE in actuator location at A2.

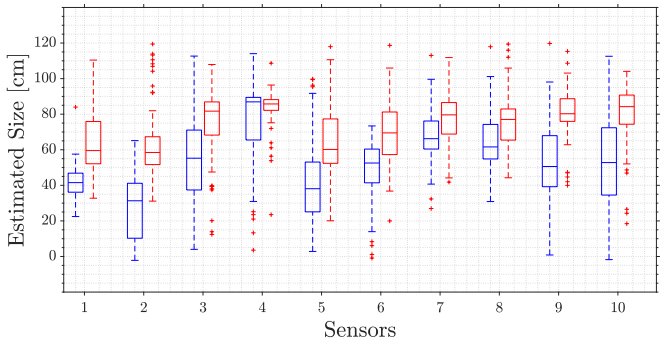

Source: Prepared by the author.

Table 5: Value of the root-mean-square error (RMSE) and the estimated values of the test conditions (D20 and D60) for each sensor along TE in actuator location at A2.

Sensor	1	2	3	4	5	6	7	8	9	10
RMSE	21.1	20.3	35.6	47.3	28.1	28.4	39.9	38.1	34.9	33.5
D20: mean est. [cm]	41.52	31.32	55.25	86.93	38.1	52.54	66.22	61.6	50.57	52.79
D60: mean est. [cm]	59.58	59.2	81.94	85.84	60.27	70.19	79.92	77.36	81.14	84.33

Source: Prepared by the author.

Figure 28: Damage severity ($\mathcal{S}$) by the damage index ($\mathcal{D}_i$) for accelerometers 1 to 10 on the leading edge (LE) with actuator in position A2. The metamodel was learned using five conditions (●) and validated with two conditions (x). The bold line (—) corresponds to the trend mean and the gray-colored region (▬) to the 95 % of confidence interval.

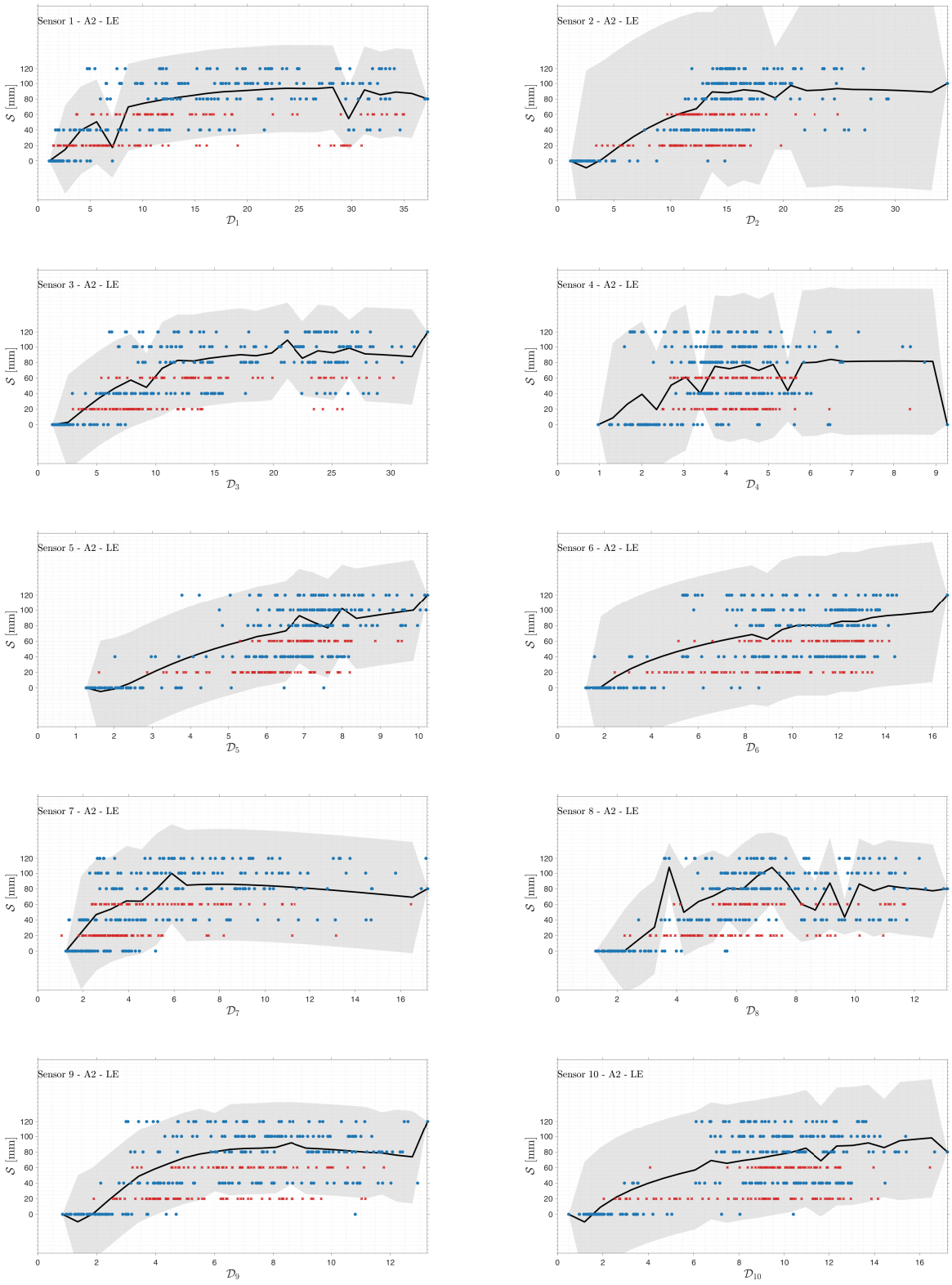

Source: Prepared by the author.

Figure 29: Validation of the estimated damage size for the test conditions (D20 and D60), using the PC-Kriging metamodel, by the actual damage size for each sensor in the LE with actuator in position A2. The estimated damage size for all damage indexes (●) and the mean of estimated damage size (●) for each test condition.

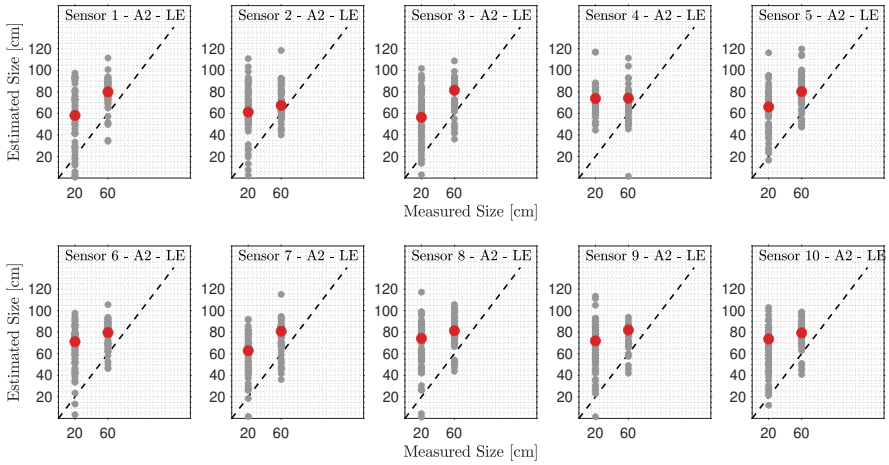

Source: Prepared by the author.

Figure 30: Boxplot of estimated values for test conditions D20 (■) and D60 (■) for each sensor along LE in actuator location at A2.

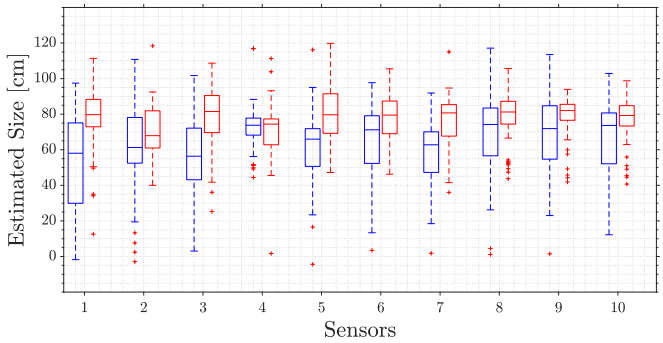

Source: Prepared by the author.

Table 6: Value of the root-mean-square error (RMSE) and the estimated values of the test conditions (D20 and D60) for each sensor along LE in actuator location at A2.

Sensor	1	2	3	4	5	6	7	8	9	10
RMSE	36.3	37.1	34.8	41.5	38.3	39.3	35.0	42.0	41.4	39.9
D20: mean est. [cm]	58.05	61.28	56.37	73.78	65.97	71.2	62.78	74.2	71.88	73.66
D60: mean est. [cm]	79.95	67.4	81.51	74.11	80.15	79.69	80.76	81.35	82.06	79.34

Source: Prepared by the author.

Figure 31: Damage severity ($\mathcal{S}$) by the damage index ($\mathcal{D}_i$) for accelerometers 1 to 10 on the trailing edge (TE) with actuator in position A3. The metamodel was learned using five conditions (●) and validated with two conditions (x). The bold line (—) corresponds to the trend mean and the gray-colored region (▬) to the 95 % of confidence interval.

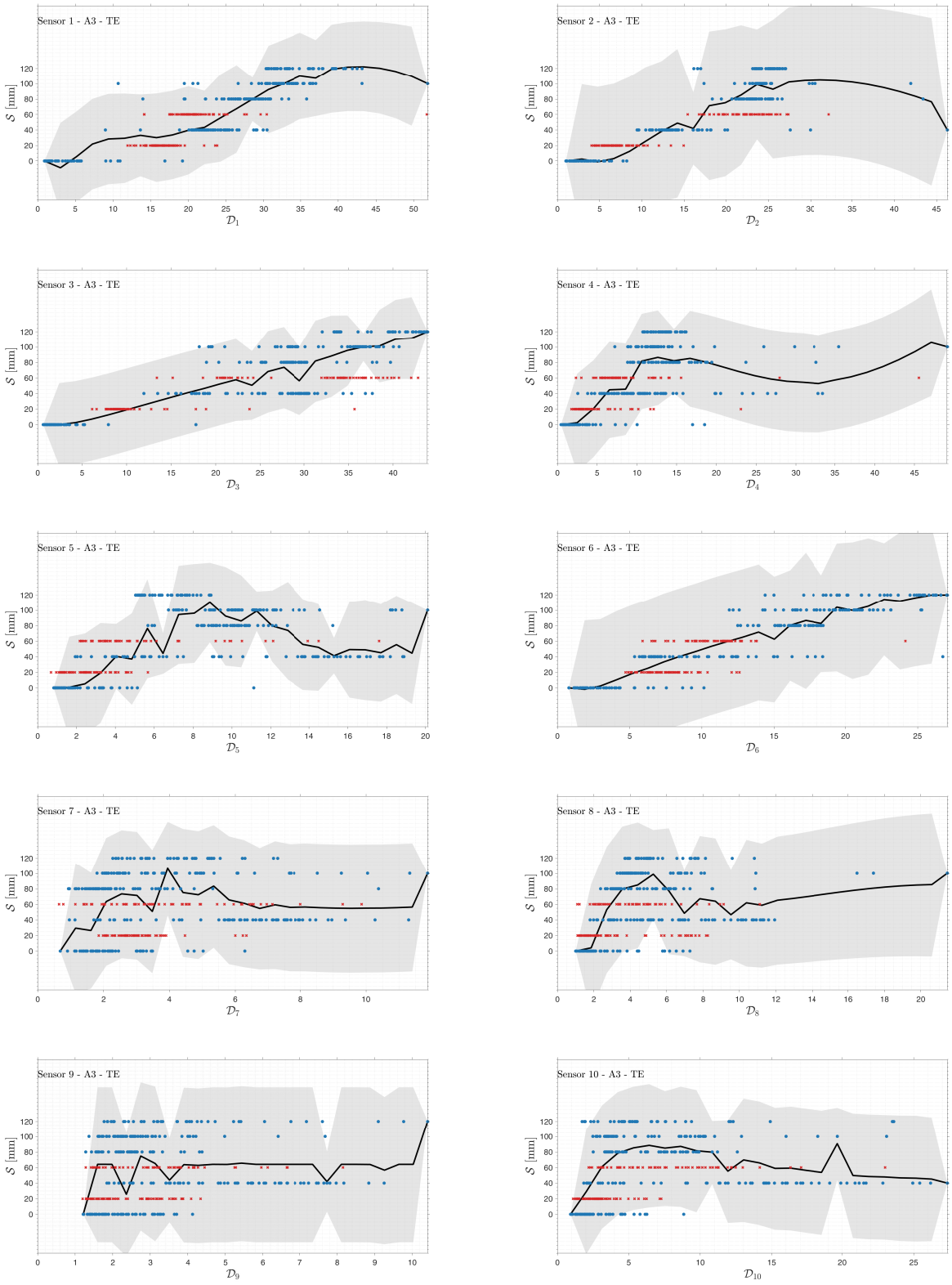

Source: Prepared by the author.

Figure 32: Validation of the estimated damage size for the test conditions (D20 and D60), using the PC-Kriging metamodel, by the actual damage size for each sensor in the TE with actuator in position A3. The estimated damage size for all damage indexes (●) and the mean of estimated damage size (●) for each test condition.

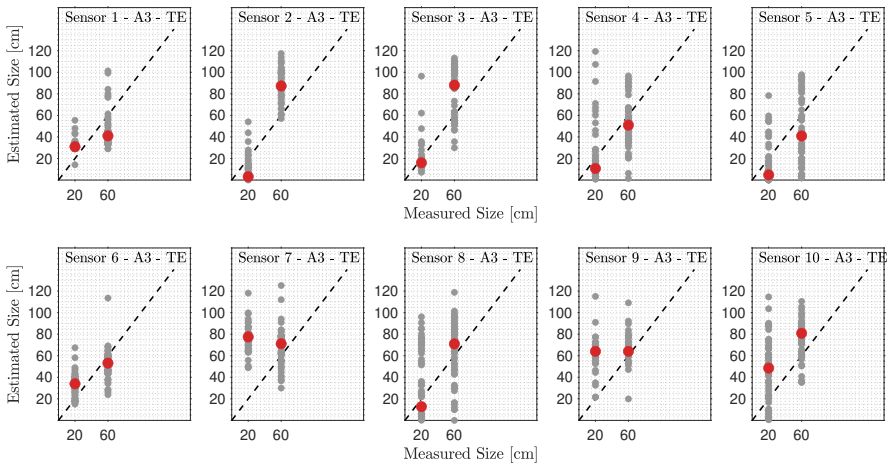

Source: Prepared by the author.

Figure 33: Boxplot of estimated values for test conditions D20 (■) and D60 (■) for each sensor along TE in actuator location at A3.

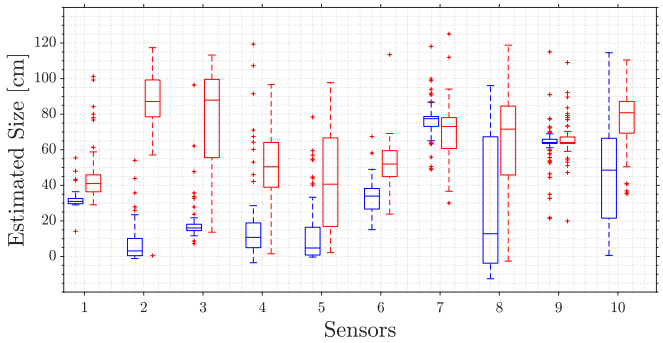

Source: Prepared by the author.

Table 7: Value of the root-mean-square error (RMSE) and the estimated values of the test conditions (D20 and D60) for each sensor along TE in actuator location at A3.

Sensor	1	2	3	4	5	6	7	8	9	10
RMSE	17.0	25.5	23.0	23.5	27.2	15.8	43.8	32.7	33.8	32.2
D20: mean est. [cm]	30.96	3.12	16.03	10.74	4.77	33.94	77.47	12.79	64.08	48.53
D60: mean est. [cm]	41.0	87.29	88.04	50.96	40.88	53.12	71.14	70.99	64.08	80.83

Source: Prepared by the author.

Figure 34: Damage severity ($\mathcal{S}$) by the damage index ($\mathcal{D}_i$) for accelerometers 1 to 10 on the leading edge (LE) with actuator in position A3. The metamodel was learned using five conditions (●) and validated with two conditions (x). The bold line (—) corresponds to the trend mean and the gray-colored region (▬) to the 95 % of confidence interval.

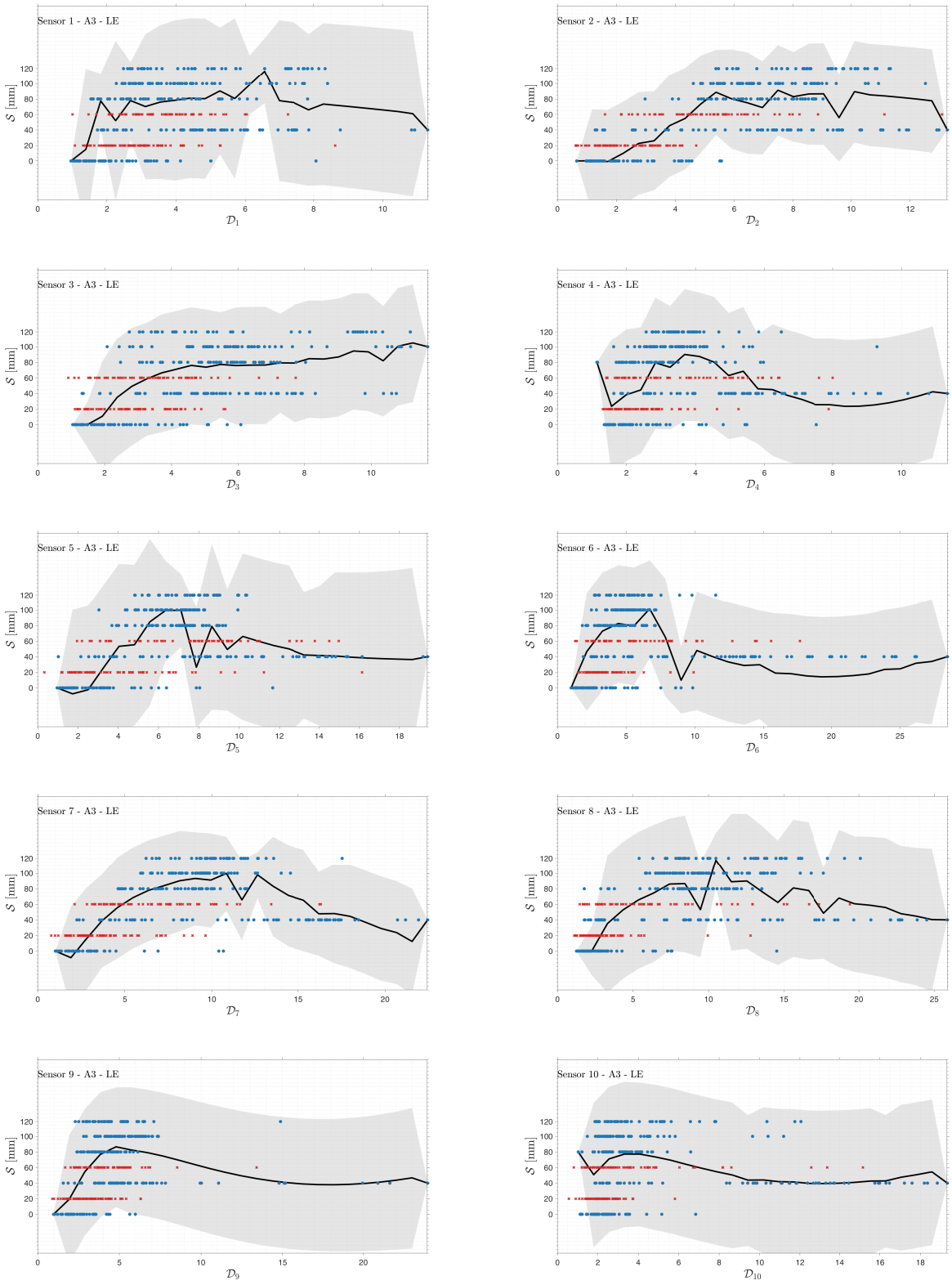

Source: Prepared by the author.

Figure 35: Validation of the estimated damage size for the test conditions (D20 and D60), using the PC-Kriging metamodel, by the actual damage size for each sensor in the LE with actuator in position A3. The estimated damage size for all damage indexes (●) and the mean of estimated damage size (●) for each test condition.

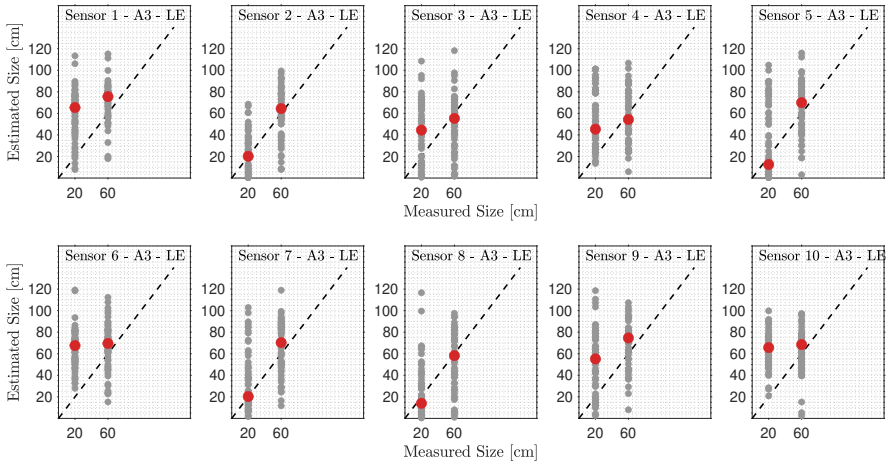

Source: Prepared by the author.

Figure 36: Boxplot of estimated values for test conditions D20 (■) and D60 (■) for each sensor along LE in actuator location at A3.

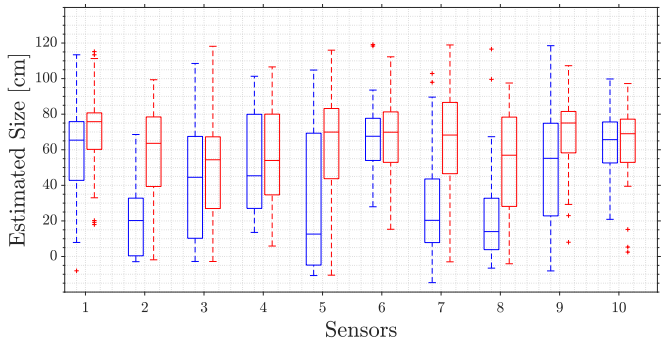

Source: Prepared by the author.

Table 8: Value of the root-mean-square error (RMSE) and the estimated values of the test conditions (D20 and D60) for each sensor along LE in actuator location at A3.

Sensor	1	2	3	4	5	6	7	8	9	10
RMSE	17.0	25.5	23.0	23.5	27.2	15.8	43.8	32.7	33.8	32.2
D20: mean est. [cm]	30.96	3.12	16.03	10.74	4.77	33.94	77.47	12.79	64.08	48.53
D60: mean est. [cm]	41.0	87.29	88.04	50.96	40.88	53.12	71.14	70.99	64.08	80.83

Source: Prepared by the author.

Figure 37: Damage severity ($\mathcal{S}$) by the damage index ($\mathcal{D}_i$) for accelerometers 1 to 10 on the trailing edge (TE) with actuator in position A4. The metamodel was learned using five conditions (●) and validated with two conditions (x). The bold line (—) corresponds to the trend mean and the gray-colored region (▬) to the 95 % of confidence interval.

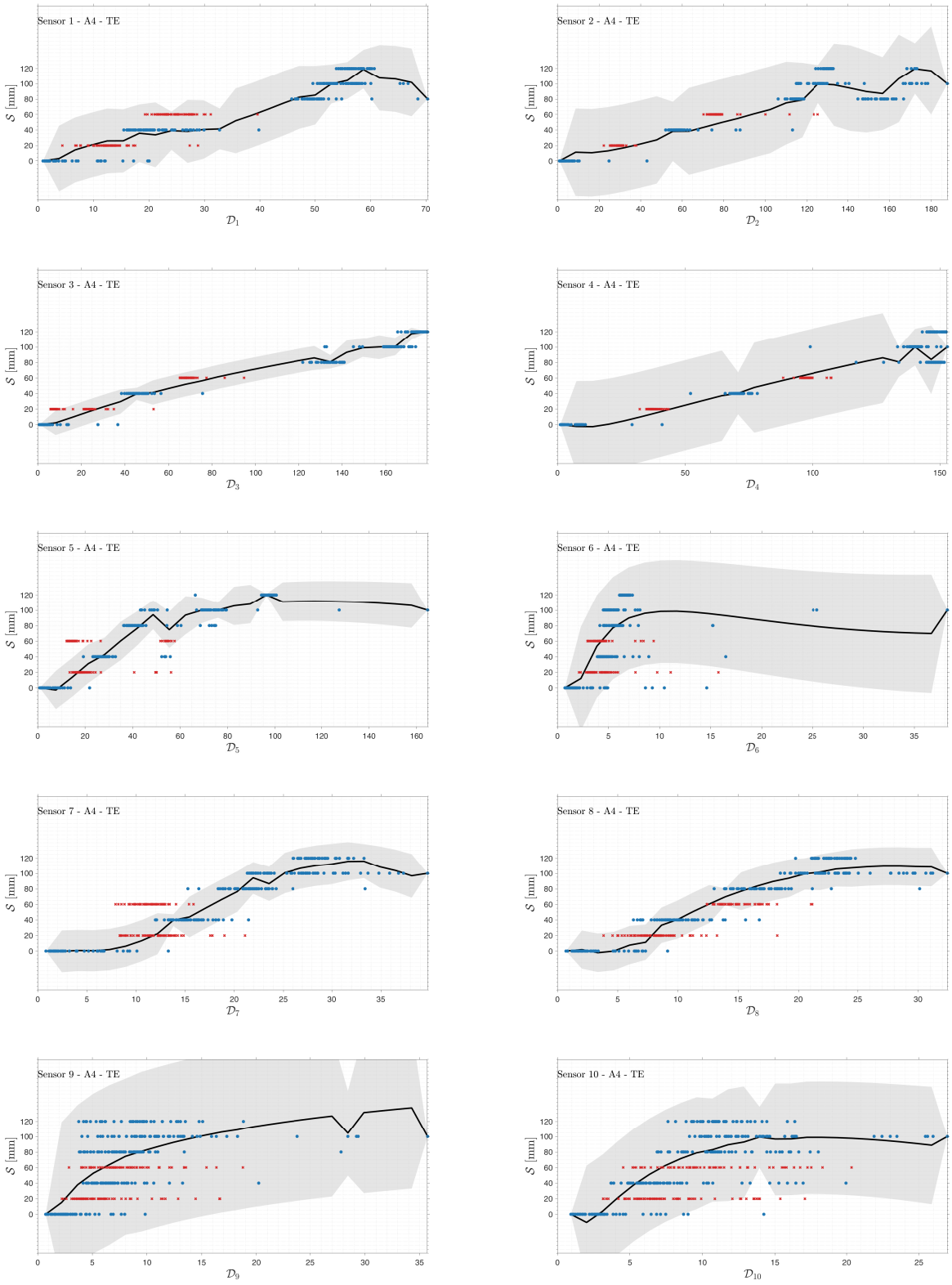

Source: Prepared by the author.

Figure 38: Validation of the estimated damage size for the test conditions (D20 and D60), using the PC-Kriging metamodel, by the actual damage size for each sensor in the TE with actuator in position A4. The estimated damage size for all damage indexes (●) and the mean of estimated damage size (●) for each test condition.

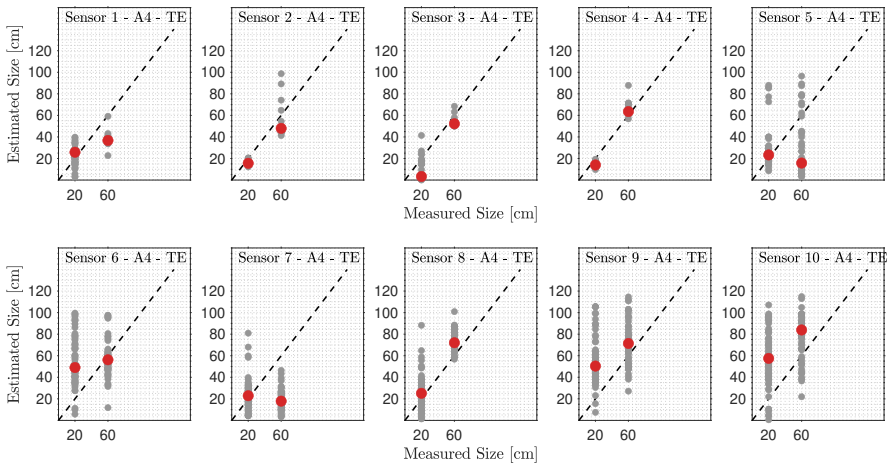

Source: Prepared by the author.

Figure 39: Boxplot of estimated values for test conditions D20 (■) and D60 (■) for each sensor along TE in actuator location at A4.

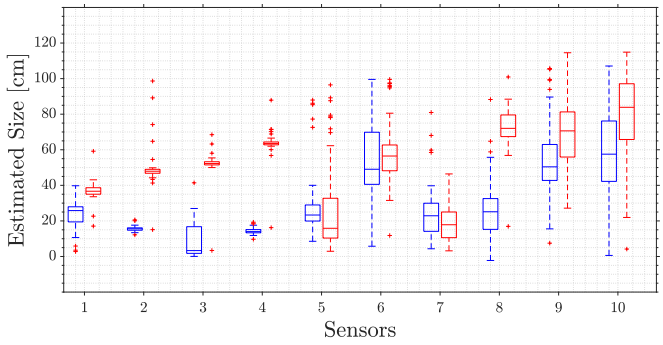

Source: Prepared by the author.

Table 9: Value of the root-mean-square error (RMSE) and the estimated values of the test conditions (D20 and D60) for each sensor along TE in actuator location at A4.

Sensor	1	2	3	4	5	6	7	8	9	10
RMSE	16.8	10.0	11.4	5.83	31.1	32.0	30.6	16.4	33.6	38.5
D20: mean est. [cm]	25.81	15.58	3.31	13.99	23.31	49.04	22.89	25.14	50.40	57.52
D60: mean est. [cm]	36.77	47.95	52.25	63.54	15.78	56.23	17.86	72.04	71.38	83.89

Source: Prepared by the author.

Figure 40: Damage severity ($\mathcal{S}$) by the damage index ($\mathcal{D}_i$) for accelerometers 1 to 10 on the leading edge (LE) with actuator in position A4. The metamodel was learned using five conditions (●) and validated with two conditions (x). The bold line (—) corresponds to the trend mean and the gray-colored region (▬) to the 95 % of confidence interval.

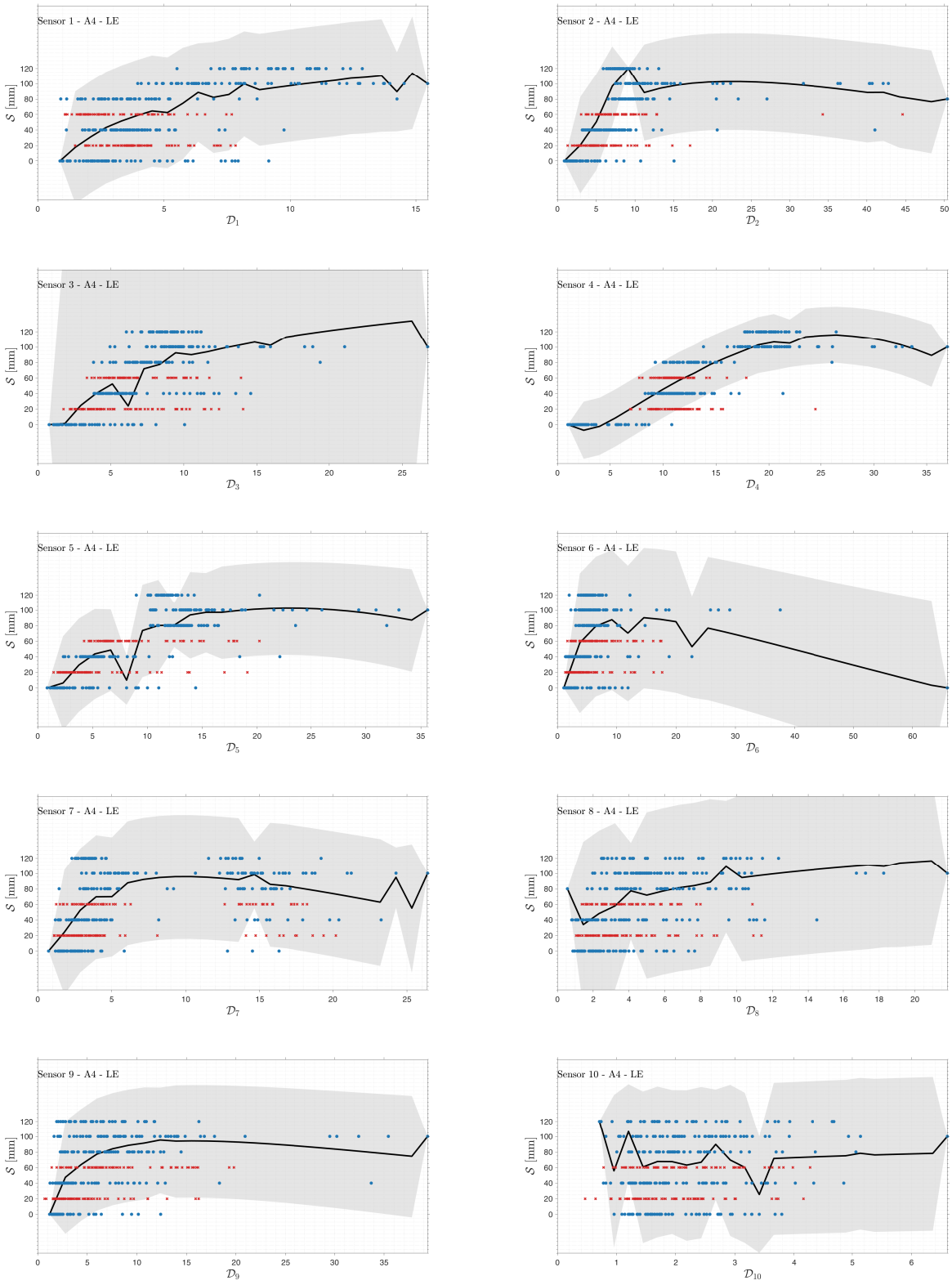

Source: Prepared by the author.

Figure 41: Validation of the estimated damage size for the test conditions (D20 and D60), using the PC-Kriging metamodel, by the actual damage size for each sensor in the LE with actuator in position A4. The estimated damage size for all damage indexes (●) and the mean of estimated damage size (●) for each test condition.

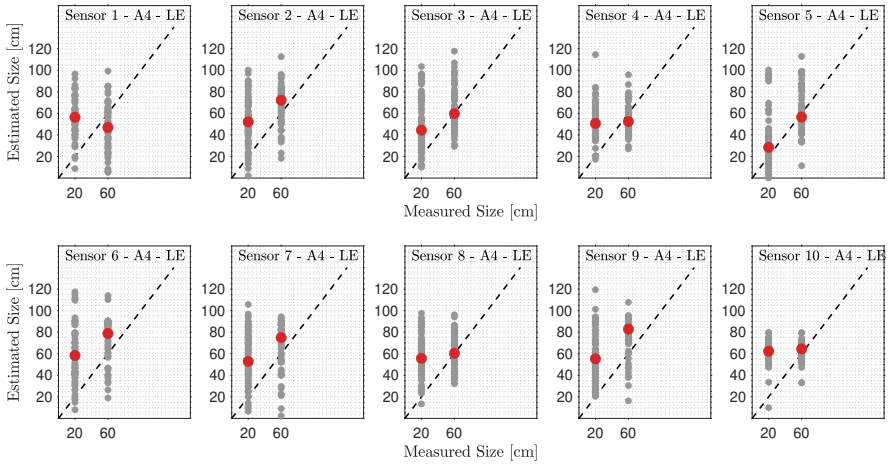

Source: Prepared by the author.

Figure 42: Boxplot of estimated values for test conditions D20 (■) and D60 (■) for each sensor along LE in actuator location at A4.

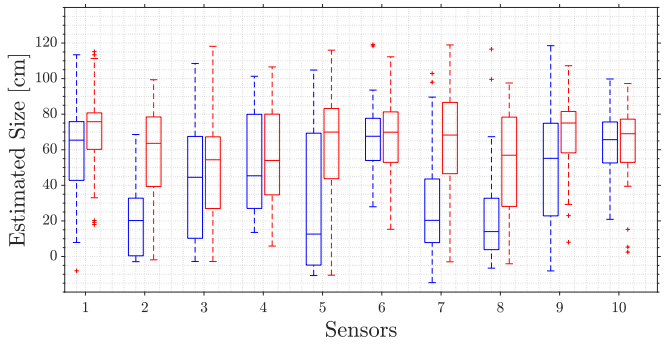

Source: Prepared by the author.

Table 10: Value of the root-mean-square error (RMSE) and the estimated values of the test conditions (D20 and D60) for each sensor along LE in actuator location at A4.

Sensor	1	2	3	4	5	6	7	8	9	10
RMSE	34.3	32.3	32.3	28.5	26.5	38.5	35.5	32.9	36.1	32.4
D20: mean est. [cm]	56.40	52.14	44.43	50.69	28.47	58.38	52.94	55.69	55.33	62.37
D60: mean est. [cm]	46.99	72.16	59.80	52.44	56.62	78.79	74.91	60.41	82.85	64.50

Source: Prepared by the author.

4.4 FINAL REMARKS

This chapter approached the debonding area's quantification due to the debonding in wind turbine blades, using a new methodology considering the uncertainties and interpolation through a metamodel obtained by the Polynomial Chaos-Kriging (PC-Kriging) method. The metamodel obtained relates the damage indexes to trailing edge debonding. To obtain the damage indexes, the methodology presented in Cava and Tcherniak (2019) was used. This methodology was applied to an SSP 34 m wind turbine blade, instrumented with one actuator, in positions A1, A2, A3, and A4, with ten accelerometers in the TE and ten in the LE. It is observed that the accelerometers located in the TE detected the damage better than those found in the LE. The excellent performance of accelerometers 1, 2, 3, and 4 in the TE with the actuator in position A4 stands out. These sensors showed low RMSE values and little dispersion of validation data. It is also noted that the damage introduced is situated in the TE, where the accelerometers obtained more favorable results for all actuator positions.

The PC-Kriging method was used to obtain a metamodel that relates the damage index with severity to quantify the trailing edge debonding considering the uncertainties. This relationship's trend curve was received, considering a 95% confidence interval. The PCE method captures the computational model's global behavior, while the Kriging method of the interpolation type captures local variations. For this reason, PC-Kriging, which is the combination of the two approaches, presents itself as a more robust method for obtaining metamodels. The PC-Kriging trend curve, in general, managed to capture a monotonic increase in damage indexes, showing promising results for quantification. The advantages observed in the use of PC-Kriging were its simplicity and ease in constructing the metamodel since the toolbox UQLab is available, which allows an easy implementation of the method. It is also observed the low computational cost to obtain the results. The processor of the computer on which the simulations were performed is an Intel(R) Core(TM) i5-5200U CPU @ 2.20GHz. On this computer, the time to perform damage detection simulations was approximately 3 minutes and to obtain the PC-Kriging metamodel, for damage quantification, was approximately 2.5 minutes.

This study contributes to the data-driven SHM methodology regarding the quantification of damages in mechanical structures. It addresses the use of a method that is not yet widely explored in this area. This study collaborates with research development in damage quantification so that better results are always obtained.

5 SENSITIVITY ANALYSIS OF SENSOR LOCATION AND USE OF TRANSMISSIBILITY FUNCTION FOR DAMAGE DETECTION IN A WIND TURBINE BLADE

The study presented in this chapter is carried out with the same data from the composite wind turbine blade shown in chapter 4. The methodology developed in this chapter follows the steps described below:

i) Using the methodology available in Cava and Tcherniak (2019), a global damage index is obtained, using data from the ten sensors located on the TE of the composite wind turbine blade and considering two locations for the actuator, A1 and A4. It was chosen in this study to present only the results with the data of the TE and for actuator location at A1 and A4, because the damage index of the data of the sensors located in the TE are better (CAVA; TCHERNIAK, 2019),

ii) Using the global damage index, a metamodel is obtained using the Polynomial Chaos-Kriging (PC-Kriging) method to quantify the damage size, as performed in chapter 4. The metamodel generates a trend curve related to the global damage indexes. To validate the metamodel, the RMSE was used.

iii) Afterwards, the sensitivity analysis of global DI is performed, using Sobol' indices for actuator location at A1 and A4. From the results of the Sobol' indices, a new DI is obtained, considering only the data from the sensors that are most influential. A new metamodel for damage quantification is obtained with this new DI and its RMSE calculated. Thus comparing the damage quantification results considering the global DI with data from the ten sensors and the DI evaluating the data only from the most influential sensors, according to the Sobol' indices.

iv) Finally, with the sensitivity analysis results, the most influential sensors are used to calculate the transmissibility function of healthy data of the blade. A Kriging metamodel is obtained from the healthy transmissibility function, which has a confidence interval of 95%, and is used as a threshold for damage detection. Metamodel validation is performed using the damaged data of the blade.

This chapter is organized as follows: section 5.1 presents the methodology used to perform sensitivity analysis of the location of sensors on the blade; section 5.2 shows the methodology for damage detection using the transmissibility function; section 5.3 presents

the results obtained for the sensitivity analysis and damage detection; and in section 5.4 the main conclusions of chapter are highlighted.

5.1 METHODOLOGY FOR SENSITIVITY ANALYSIS

To perform the sensitivity analysis of the sensors' influence on the damage index, it is necessary to use a global damage index, that is, with information from the 10 accelerometers. Then, the following global damage index is proposed:

$$\mathcal{DI} = \frac{1}{N_s} \sum_{i=1}^{N_s} \mathcal{D}_i, \tag{49}$$

where N_s is the number of sensors used to monitor the structure and $\mathcal{D}_i$ is the local damage index.

The idea of applying PC-Kriging at the damage quantification level used in this chapter is similar to the concept used in chapter 4. Still, now the metamodel captures the trend between a global damage index and damage severity. The global damage index is used as an input, and the damage size is used as an output for building a PC-Kriging model. In this case, PC-Kriging is described as

$$\mathcal{S} \cong \sum_{\alpha \in \mathcal{A}} y_\alpha \Psi_\alpha(\mathcal{DI}) + \sigma^2 \mathcal{Z}(\mathcal{DI}, \Omega), \tag{50}$$

where $\mathcal{DI} \in \mathbb{R}$ is the global damage index with a given Probability Density Function (PDF) f_X, $\mathcal{S}$ is the damage size, with $\mathcal{S} \in \mathbb{R}$. The $\sum_{\alpha \in \mathcal{A}} y_\alpha \Psi_\alpha(\mathcal{DI})$ is a weighted sum of orthonormal polynomials that describes the PC-Kriging model trend, where $\Psi_\alpha(\mathcal{DI})$ are orthonormal polynomials in relation to f_X, $\alpha \in \mathcal{A}$ are the indices and y_α are the corresponding coefficients; σ^2 is the variance of the process, and $\mathcal{Z}((\mathcal{DI}), \Omega)$ is a Gaussian random process with zero mean. Ω describes outcomes of the underlying probability space with a correlation family $\mathcal{R}$ and its hyperparameters θ. That is, the correlation function $\mathcal{R} = \mathcal{R}(x, x', \theta)$ describes the correlation between two samples of the input space. For example, x and x' depends on the hyperparameters θ (SCHÖBI; SUDRET, 2014).

With the global damage index $\mathcal{DI}$, the sensitivity analysis is performed using the Sobol' indices. The data from the ten accelerometers in the TE that make up the global DI are the model's input, where the sobol' indices show the influence of each of them on the output, that is, on the global DI. The distributions of each input data are determined by statistical inference. The metamodel used to obtain the Sobol' indices is via PCE. The implementation of the PC-Kriging algorithms and sensitivity analysis is performed using

the UQLab.

5.2 METHODOLOGY FOR DAMAGE DETECTION USING TRANSMISSIBILITY

According to Zhou *et al.* (2015a), if we consider a linear multiple-degree of-freedom system, the dynamic equilibrium equation can be written by the well-known second order differential equation:

$$\mathbb{M}\ddot{x}(t) + \mathbb{C}\dot{x}(t) + \mathbb{K}x(t) = f(t), \tag{51}$$

where $\mathbb{M}$ is the mass, $\mathbb{C}$ is the damping, and $\mathbb{K}$ is the stiffness matrices of the system. $f(t)$ is the input force vector, and $x(t)$ contains the responses of each degree of freedom of the system. For a harmonic applied force at a given coordinate, the transmissibility between point i and a reference point j can be defined as:

$$T_{(i,j)} = \frac{X_i(\omega)}{X_j(\omega)}, \tag{52}$$

where, X_i and X_j are complex amplitudes of the system responses $x_i(t)$ and $x_j(t)$, respectively, and ω is the frequency.

To calculate the transmissibility, no matter in real engineering or experiment analysis, apart from direct extracting from the two responses, it can be derived in several ways (MAIA *et al.*, 2011). For example, using the frequency response function (FRF),

$$T_{(i,j)} = \frac{X_i(\omega)/F_l(\omega)}{X_j(\omega)/F_l(\omega)} = \frac{H_{(i,l)}(\omega)}{H_{(j,l)}(\omega)}, \tag{53}$$

where l is the excitation point and H represents the FRF. Note that in this case, the transmissibility is a norm that estimates the structural dynamic responses (ZHOU *et al.*, 2015a).

The applied forces do not have to be necessarily harmonic. Although the expressions for the transmissibility have been deduced assuming harmonic forces, they remain valid for other types of excitation, including those of an impulsive or random nature (MAIA *et al.*, 2011).

The advantage of using transmissibilities to detect damage is local quantities. This local feature has a higher sensitivity to detect changes in dynamic behavior due to some type of damage (MAIA *et al.*, 2011). In this work, the transmissibility functions between the healthy data of two sensors located on a damaged wind turbine blade are used to

obtain a Kriging metamodel with a confidence interval of 95%, which is the threshold for damage detection. In this case, the transmissibility function is defined as:

$$T_{(s_i,s_j)} = \frac{X_{s_i}(\omega)}{X_{s_j}(\omega)}, \tag{54}$$

where s_i and s_j are the sensors i and j, with $i = 1:9$ and $j = 2:10$, and X_{s_i} and X_{s_j} the corresponding output responses.

5.3 RESULTS AND DISCUSSIONS

This section presents global DI sensitivity analysis and damage detection using the transmissibility function.

5.3.1 Sensitivity analysis of sensor location in a wind turbine blade

Sensitivity analysis aims to identify the accelerometers with the most significant influence on global DI and analyze whether an optimized DI improves the metamodel for damage quantification with only influential sensor data. The damage quantification methodology used is based on constructing a PC-Kriging metamodel, which obtains the trailing edge debonding size as a function of the global damage index. The global damage index is used as input for building a PC-Kriging metamodel. The following conditions' local damage index is considered in the model learning stage: H, D40, D80, D100, and D120. The damaged conditions D20 and D60 are used in the validation steps to validate the prediction of damage quantification using metamodel, as performed in chapter 4. In this study, the RMSE metric is also chosen to validate the model prediction for validation conditions D20 and D60.

In this study, the locations A1 and A4 of the actuator for the sensors in the TE are analyzed. These locations were chosen because they are the actuator positions with the best results for quantifying the damage. A schematic of the blade with the analyzed actuator positions can be seen in Figure 43.

After obtaining a global DI, the methodology used in chapter 4 to quantify damage is also used in this chapter. Figure 44 attests to the severity, that is, the size of the trailing edge debonding as a function of the damage index obtained by the PC-Kriging method for the global DI with all ten sensors in the TE at actuator position A1. Figure 45 shows the results obtained for the actuator in position A4. The trained models represent the predicted distribution's mean and 95% confidence interval.

Figure 43: Accelerometers, damage and actuator locations scheme in SSP 34 meters wind turbine blade to perform the sensitivity analysis of the global damage index.

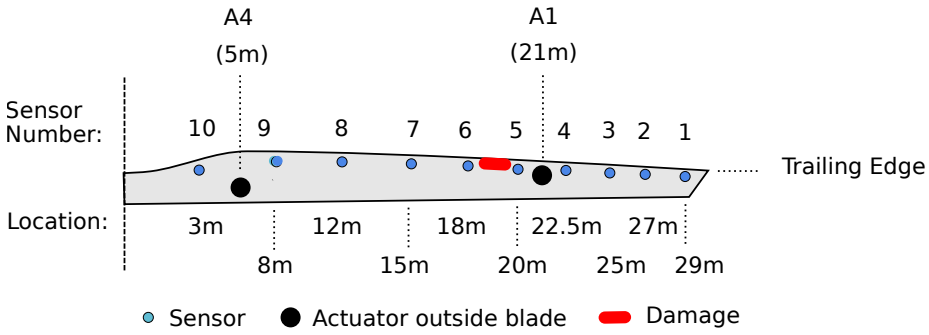

Source: Prepared by the author.

Figure 44: Polynomial Chaos-Kriging metamodel for damage quantification and validation of the estimated damage size with actuator location at A1 and the ten accelerometers in TE.

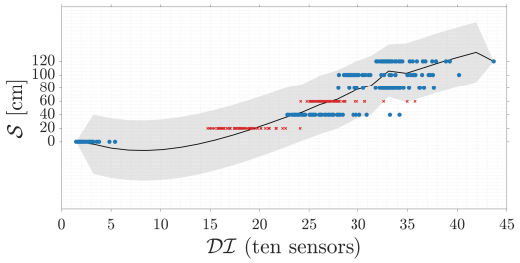

(a) Damage severity ($\mathcal{S}$) by the global damage index ($\mathcal{DI}$). The metamodel was learning using five conditions (●) and validated with two conditions (x). The bold line (—) corresponds to the trend mean and the gray-colored region (▬) to the 95% of confidence interval.

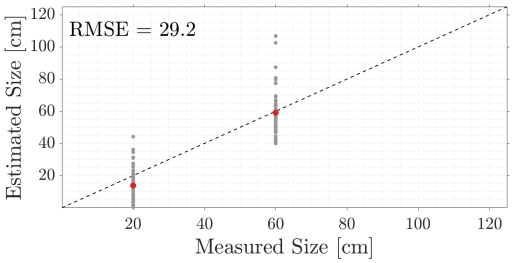

(b) The estimated damage size for all damage indexes (●) and the mean of estimated damage size (●) for each validation condition.

Source: Prepared by the author.

The objective now is to perform a sensitivity analysis of the global DI to identify the accelerometers that have the most significant influence on the DI. With the information from the sensitivity analysis, a new DI will be obtained, with only the data from the influential sensors. Then it will be analyzed if the metamodel generated from this new DI is as good as the metamodel obtained from the global DI with the data of the ten sensors. To perform the sensitivity analysis of the global DI, the Sobol' indices were used, using a surrogate model based on PCE. In Figure 46 it is possible to observe the results of Sobol' indices order 1 and total for the global DI for the actuator in position A1. Remembering that the closer to the value 1, the greater the influence of the parameter on the output response. At actuator position A1, the Sobol' indices show that sensors 6, 7, 8, and 10

Figure 45: Polynomial Chaos-Kriging metamodel for damage quantification and validation of the estimated damage size with actuator location at A4 and the ten accelerometers in TE.

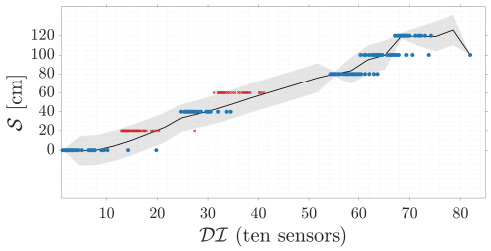

(a) Damage severity ($\mathcal{S}$) by the global damage index ($\mathcal{DI}$). The metamodel was learning using five conditions (●) and validated with two conditions (x). The bold line (—) corresponds to the trend mean and the gray-colored region (▬) to the 95 % of confidence interval.

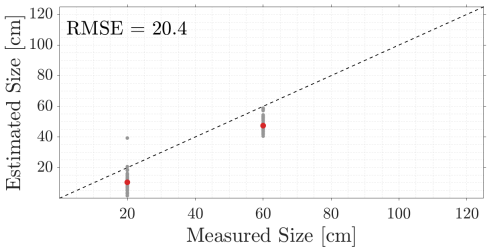

(b) The estimated damage size for all damage indexes (●) and the mean of estimated damage size (●) for each validation condition.

Source: Prepared by the author.

influence the global damage index, not showing much difference for the order 1 and total Sobol' indices. We also analyzed the influence of sensors on the global DI according to the damage condition. In Figure 47 it is possible to observe the results obtained for the six damage conditions (D20, D40, D60, D80, D100 and D120), that is, the influence of sensors on the global DI as the damage grows.

Figure 46: Sobol' indices of order 1 and total for the global damage index with the ten sensors in TE, with all conditions, with actuator location at A1.

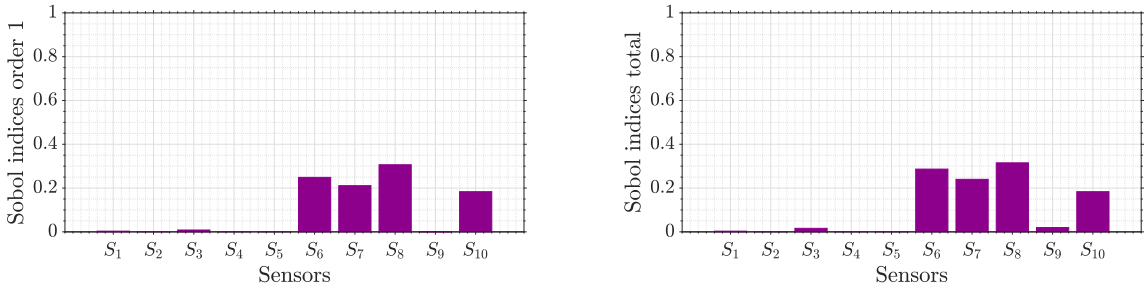

Source: Prepared by the author.

In the Figures, 48 and 49 is possible to observe the results of the Sobol' indices for the actuator in position A4. The Sobol' indices show that sensors 1, 2, 3, and 8 have the greatest influence on the global DI for this actuator position. However, as the damage

Figure 47: Sobol' indices of order 1 for the global damage index with the ten sensor in TE, for the six damage conditions, with actuator location at A1.

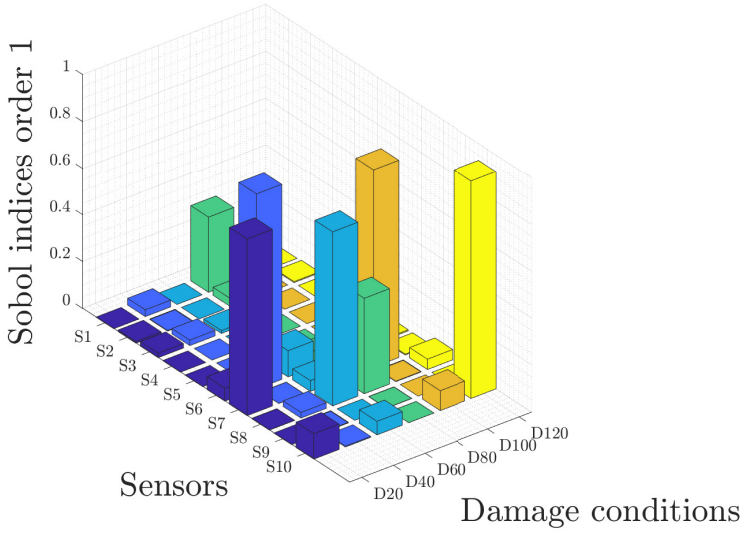

Source: Prepared by the author.

grows, it is observed that sensor 8 has no effect, which makes a lot of sense, as it is not in the path of damage.

Figure 48: Sobol' indices of order 1 and total for the global damage index with the ten sensors in TE, with all conditions, with actuator location at A4.

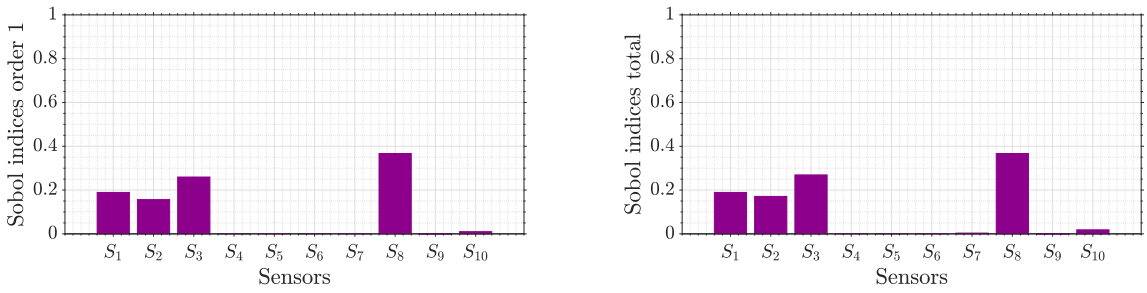

Source: Prepared by the author.

To validate the results obtained by the Sobol' indices, we performed a new damage quantification, obtaining a new DI containing only the data of the most influential sensors. For actuator position A1, the Sobol' indices show that sensors 6, 7, 8, and 10 have a greater influence on DI. We chose to use information from only sensors 6, 7, and 8, as sensor 10 is not in the path between actuator A1 and the damage, thus ruling out a possible negative influence of this sensor. Figure 50 shows the new damage quantification obtained. In this

Figure 49: Sobol' indices of order 1 for the global damage index with the ten sensors in TE, for the six damage conditions, with actuator location at A4.

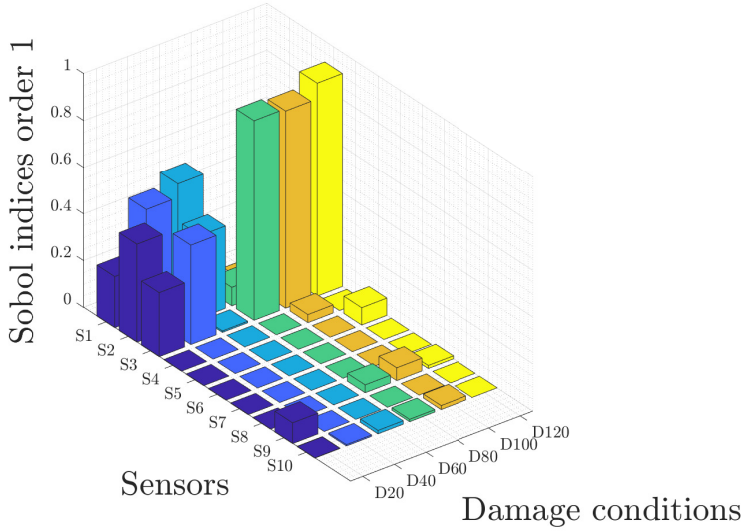

Source: Prepared by the author.

case, the RMSE equals 22.6, while with the global DI, with all sensors, the RMSE is 29.2.

Figure 50: Polynomial Chaos-Kriging metamodel for damage quantification and validation of the estimated damage size with actuator location at A1 and accelerometers 6, 7 and 8 in TE.

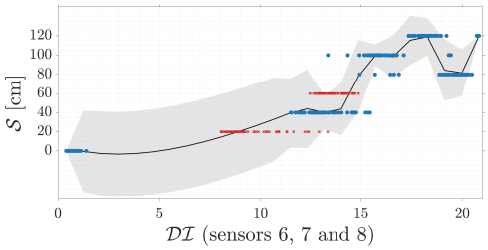

(a) Damage severity ($\mathcal{S}$) by the damage index ($\mathcal{D}_i$). The metamodel was trained using five conditions (●) and validated with two conditions (x). The bold line (—) corresponds to the trend mean and the gray-colored region (▬) to the 95 % of confidence interval.

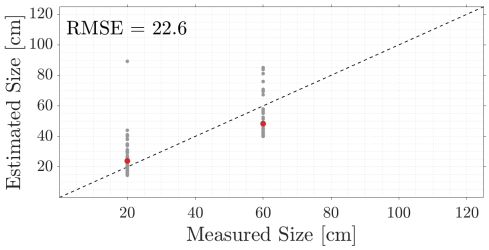

(b) The estimated damage size for all damage indexes (●) and the mean of estimated damage size (●) for each validation condition.

Source: Prepared by the author.

For actuator position A4, we obtain a new DI using the data from sensors 1, 2, and 3. As much as the results of the Sobol' indices show the influence of sensor 8, we decided to discard the DI, as sensor 8 is not in the path from actuator A4 to the damage, which may have some negative influence. In Figure 51, it is possible to observe the new damage

quantification obtained. In this case, the RMSE equals 19.9, while with the global DI, with all sensors, the RMSE is 20.4.

Figure 51: Polynomial Chaos-Kriging metamodel for damage quantification and validation of the estimated damage size with actuator location at A4 and accelerometers 1, 2 and 3 in TE.

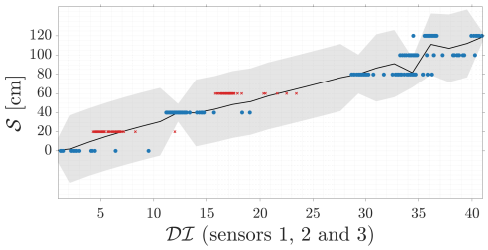

(a) Damage severity ($\mathcal{S}$) by the damage index ($\mathcal{D}_i$). The metamodel was trained using five conditions (●) and validated with two conditions (x). The bold line (—) corresponds to the trend mean and the gray-colored region (▬) to the 95 % of confidence interval.

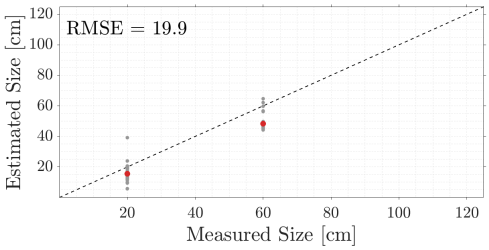

(b) The estimated damage size for all damage indexes (●) and the mean of estimated damage size (●) for each validation condition.

Source: Prepared by the author.

5.3.2 Transmissibility function for damage detection in a wind turbine blade

This subsection presents the results obtained from the proposed methodology for damage detection in the blade, using the transmissibility function. To carry out the method, it was chosen to analyze the data of sensor 3 with the actuator location at A4 because, according to the sensitivity analysis performed, this sensor was the one that had the greatest influence on the DI for such location of the actuator.

In Figure 52, it is possible to see the behavior of the acceleration data of sensor 3 over time, from healthy condition and damage condition D12O. The sampling frequency of the data is relatively high, 16384 Hz (CAVA; TCHERNIAK, 2019). Doing a decimation by 2 and obtaining the data in the frequency domain, it is observed that the primary information is concentrated up to approximately 1000 Hz, as can be seen in Figure 53.

The transmissibility function was obtained from Equation 53. The transmissibility between sensors 3 and 10 was chosen because, according to the sensitivity analysis, sensor 3 has a lot of influence and is in the path of damage. In contrast, sensor 10 does not influence the DI and is not in the damage path. Figure 54 shows the transmissibility function between sensors 3 and 10 for healthy condition and condition D120. Due to

Figure 52: Signal of acceleration in time of sensor 3 with actuator location at A4. - signal healthy (H) and – signal of condition D120.

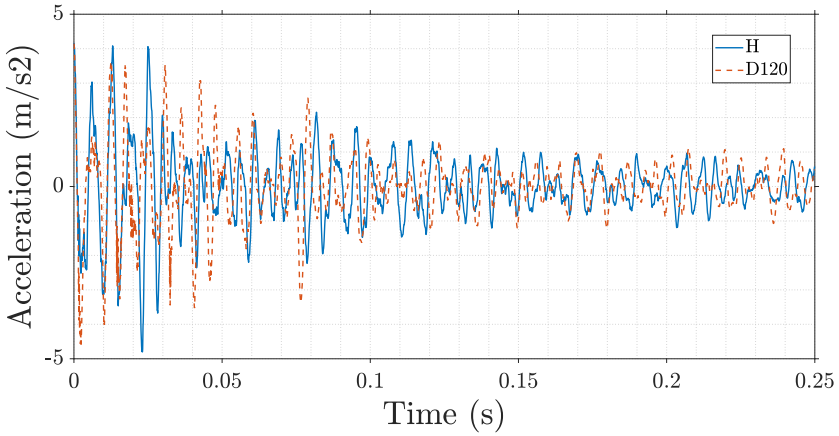

Source: Prepared by the author.

Figure 53: Fast Fourier Transform (FFT) of sensor 3 with actuator location at A4. - signal healthy (H) and – signal of condition D120.

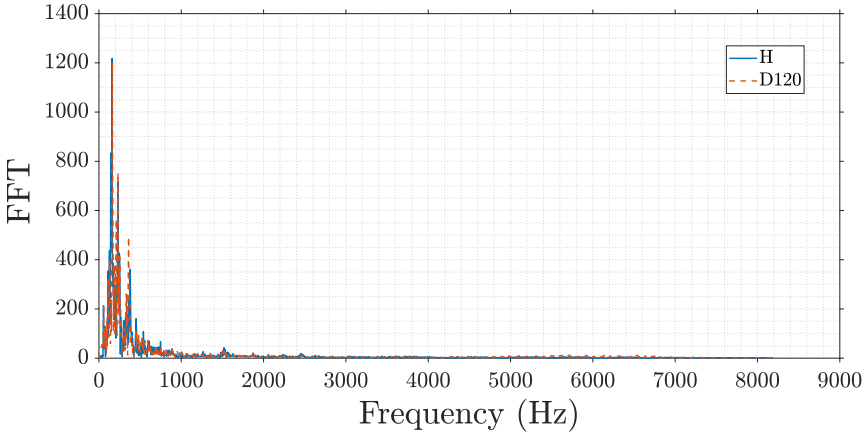

Source: Prepared by the author.

the fact that the structure has an impact excitation, it is known that the most relevant information is obtained at low frequency. For this reason, a decimation was performed to improve the resolution in the frequency range we want to analyze. After plotting the transmissibilities, healthy and damaged, it was observed that the range from 0 to 60 Hz was the range of frequency in which the transmissibilities showed greater sensitivity to damage. Figure 55 shows the transmissibility for all conditions (H, D20, D40, D60, D80, D100 and D120) of blade in the range of 0 to 60 Hz. In this figure is possible to see that the transmissibility is sensitive to damage in this frequency range and that the transmissibility presents an increasing in amplitude according to the damage condition.

Figure 54: Transmissibility function between sensors 3 and 10. - transmissibility with healthy data (H) and – transmissibility with the data of condition D120.

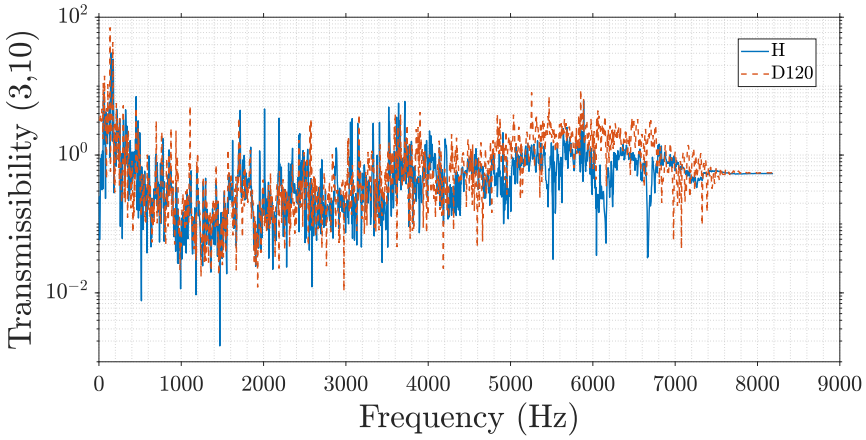

Source: Prepared by the author.

Figure 55: Transmissibility function between sensors 3 and 10 for all conditions, healthy and damage, and in the lower frequency range.

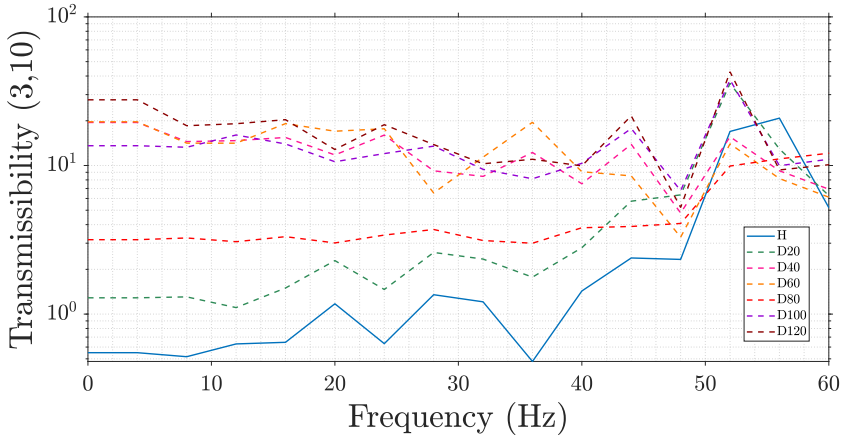

Source: Prepared by the author.

With the transmissibility function between sensors 3 and 10 of the healthy data, a GPR model was obtained using the Kriging method and a confidence interval of 95%. The model was learned with healthy data and validated with damage conditions. The idea is to use the confidence interval as a threshold for damage detection. Figure 56 shows the GPR model obtained and the confidence interval in gray. Data on the transmissibilities of damage conditions D20, D40, D60, D80, D100, and D120 were plotted. Table 11 shows the damage detection probabilities for each of the conditions. It is observed that with the small damage, the probability of detecting the damage was very low; as the damage increases, the detection probability increases.

Figure 56: Kriging metamodel of the transmissibility between sensors 3 and 10. The metamodel was learned with the data in the healthy condition (H) and validated with the damage conditions (D20, D40, D60, D80, D100 and D120). The confidence interval (CI) is 95%.

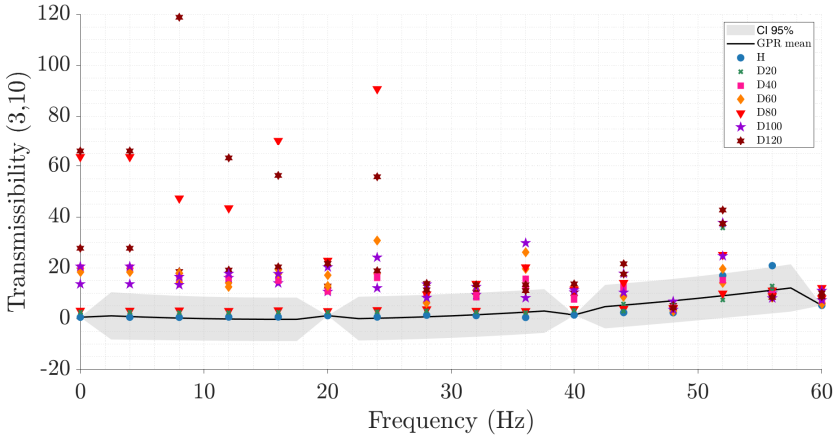

Source: Prepared by the author.

Table 11: Detection probabilities for each of the damage conditions (D20, D40, D60, D80, D100, and D120).

Damage conditions	D20	D40	D60	D80	D100	D120
Detection probability (%)	31.25	84.37	75	65.62	81.25	87.5

Source: Prepared by the author.

5.4 FINAL REMARKS

The study developed in this chapter approached the sensitivity analysis of sensors in a global damage index, used to quantify the area damaged due to the debonding in wind turbine blades. The damage quantification is obtained by a methodology that considers uncertainties and interpolation through a metamodel obtained by the Polynomial Chaos-Kriging (PC-Kriging) method (PAVLACK *et al.*, 2022). The metamodel obtained relates the damage indexes to trailing edge debonding, as seen in chapter 4. To get the damage indices, the methodology presented in Cava and Tcherniak (2019) was used. This methodology was applied to a 34 m SSP wind turbine blade, which was described in chapter4. We only used data from accelerometers located in the TE in this work. Previous works show that the results obtained for these accelerometers are better than those obtained for the accelerometers located in the LE. We consider the actuator's locations at A1 and A4 for the sensitivity analysis.

The Sobol' indices were used to perform the sensitivity analysis using the surrogate model based on Polynomial Chaos Expansion (PCE). The results obtained by the Sobol' indices were satisfactory, as this method was able to identify the sensor data with the greatest influence on the global damage index. To validate the information obtained by the Sobol' indices, new PC-Kriging metamodels were obtained to quantify damage, considering a new ID only with the data from the most influential sensors. For locating the actuator in positions A1 and A4, validation data dispersion and RMSE values for the new damage quantification improve. In this way, the DI with only the most influential sensor data is as good as the global DI containing the information of the ten sensors.

After performing the sensitivity analysis, it was observed that sensor 3 with the actuator location at A4 was the sensor with the most influence on the DI. For this reason, it was chosen to analyze the sensitivity for detecting damage to the transmissibility function of sensor 3 with the actuator location at A4. The transmissibility function was obtained from the data of sensors 3 and 10, as sensor 3 showed a lot of influence on the DI, while sensor 10 is not even in the way of the actuator and the damage. The results show that the transmissibility function has a sensitivity to damage in a frequency range of up to 60 Hz, which is the range chosen for the analysis. Transmissibility with healthy data from sensors 3 and 10 was used to learn a Kriging model with a confidence interval of 95%. This confidence interval is considered a threshold for damage detection. To validate the methodology, transmissibilities data under damage conditions were plotted. It was observed that the detection probability for the minor damage (D20) was relatively low, while the detection probability for the significant damage (D120) was reasonable.

This study contributes to the data-driven SHM methodology regarding sensor location optimization. With sensitivity analysis is possible to identify the sensors with the most influential data to obtain a good damage index. Consequently, it is possible to reduce experimental costs, which is of great industrial interest.

The detection of structural damage under operational conditions still encounters some difficulties, especially at an early stage, as environmental varieties pose challenges in real engineering applications and may require great computational efforts in monitoring structural health and potential maintenance. Therefore, the study of new methodologies to detect damage contributes to the advancement of research in this area.

6 FINAL CONCLUSIONS

This thesis addressed SHM methodologies in a composite wind turbine blade considering the uncertainties. More specifically, the topics of damage quantification were addressed using a PC-Kriging metamodel and the sensitivity analysis of the influence of sensors on a global DI to improve damage quantification and optimize the location of sensors in the experiment. Finally, from the sensitivity analysis, the thesis proposes a methodology for damage detection using a confidence interval of a Kriging model learned with the health data of the transmissibility function.

In this chapter, the study's main conclusions developed and the results obtained in the work will be summarized. Thus, section 6.1 presents the main findings of the approach and the results shown in this work. Additionally, section 6.2 gives suggestions for future works and applications in the research.

6.1 SUMMARY

- A brief state-of-the-art was presented on the topics of damage quantification in a wind turbine blade, the use of the PC-Kriging metamodel to propagate uncertainties, and sensitivity analysis using Sobol' indices, and the use of the transmissibility function for damage detection. With this, it became clear that there are gaps in the literature on SHM methodologies, considering the uncertainties and how much this subject is of great interest to society. This topic approaches problem situations in real engineering.

- A practical application was carried out to obtain the debonding area's quantification due to the debonding in wind turbine blades, using a new methodology considering the uncertainties and interpolation through a metamodel obtained by the PC-Kriging method. The metamodel received related the damage indexes to trailing edge debonding. The PCE method captures the computational model's global behavior, while the Kriging method of the interpolation type captures local variations. To get the damage indexes, the methodology presented in Cava and Tcherniak (2019) was used. This methodology was applied to an SSP 34 m wind turbine blade, instrumented with one actuator in four positions (A1, A2, A3, and

A4), ten accelerometers in the trailing edge (TE), and ten in the leading edge (LE). For all actuators, it is observed that the accelerometers located in the TE detected the damage better than those located in the LE. This result was already expected, as the simulated damage is located in the TE. The PC-Kriging method obtained a metamodel that relates the damage index with severity to quantify the trailing edge debonding. This relationship's trend curve was obtained, considering a 95% confidence interval. The results show that the accelerometers that better detected the damage obtained better damage indexes and consequently resulted in a good performance for the quantification. It is also observed that the location of the accelerometers and actuator influences the results. Actuator locations at A1 and A4 achieved the best results. For this reason, PC-Kriging, which is the combination of the two methods, presents itself as a more robust method for obtaining metamodels. To conclude, it was observed that the PC-Kriging trend curve, in general, managed to capture a monotonic increase in damage indexes, showing promising results for quantification. It is also observed the low computational cost to obtain the results. The advantages observed in the use of PC-Kriging were its simplicity and ease in constructing the metamodel since the toolbox UQLab is available, which allows an easy implementation of the method.

- To improve the damage quantification obtained by the methodology proposed, a sensitivity analysis of the influence of accelerometers on the global DI was performed. To perform the sensitivity analysis, the Sobol' indices were used. The accelerometers in the TE with the actuator location at A1 and A4 were chosen for the study because, as already mentioned, they were the situations with the best results. For the actuator in position A1, the Sobol' indices indicated that sensors 6, 7, and 8 have more influence on the global DI. A new DI was obtained only with the data from these accelerometers. After that, a new PC-Kriging metamodel was obtained for the damage quantification, where the RMSE result improved and reduced the dispersion of the validation data. In the same way, the analysis was performed for the actuator in position A4. In this location, the Sobol' indices showed the more significant influence of sensors 1, 2, and 3. The new DI obtained with the data from these accelerometers also improved the results of damage quantification. The second and higher-order Sobol' indices were irrelevant; therefore, only the first order and total results were shown in this work.

- The sensitivity analysis results for the actuator location at A4 showed the significant influence of sensor 3. For this reason, this sensor was chosen to carry out a study on

the use of the transmissibility function for damage detection. First, an analysis of the frequency response of the data from these accelerometers was performed. The transmissibility function between sensors 3 and 10 was obtained with the actuator location at A4. This choice was because sensor 3 has a lot of influence, and sensor 10 has no effect on the DI and is not in the way of the actuator and the damage. Observing the transmissibility function of sensors 3 and 10 for the healthy condition and damage condition D120, it is observed that the transmissibility is sensitive to damage at low frequencies. Therefore, the range from 0 to 60 Hz is chosen to perform the analysis. A Kriging metamodel is obtained, which is learned from the healthy data of the transmissibility between sensors 3 and 10 and has a confidence interval of 95%. The idea was to use the confidence interval as a threshold for damage detection. Data on the transmissibilities of the damage conditions were used to validate the methodology. It is observed that the detection probability was very low for minor damage. As the damage increases, the detection probability increases. The contribution of this methodology proposal is based on the fact that it considers the uncertainties for damage detection and the low computational cost of obtaining the Kriging metamodel.

- This work presents a contribution to the data-driven SHM methodologies, as it addresses the use of methods that is not yet widely explored in this area. This study collaborates with research development in damage quantification and uncertainty quantification, always trying to improve to apply in real situations.

6.2 FUTURE WORK

As future work we intend to apply the damage detection, damage quantification and sensitivity analysis methodologies, presented in this thesis, in other composite material structures. Below are some suggestions for future work that explore the idea of SHM methodologies extended to other composite material structures and nonlinear dynamical systems:

- Use PCE-based Sobol' indices as a metric for damage. The experimental application will be made using a Carbon Fiber Reinforced Polymer (CFRP) plate and Sobol' indices to analyze the sensitivity concerning temperature and the influence of damage. Through the sensitivity of the excitation point, it is believed that it is possible to obtain information on the location of the damage;

- Obtain a GPR model with two input variables, temperature, and damage index, related to the severity of the damage, using data from the CFRP plate;
- Use Co-Kriging modeling for delamination quantification in laminated composites. Kriging is already used to quantify the damage; however, using the Co-Kriging method will allow combining a small amount of data (from experimental tests or calibrated models) with cheap data from a simple model without a previous calibration;
- Use recent techniques, such as Sparse Identification of Nonlinear Dynamics (SINDy) and Dynamic Mode Decomposition (DMD) to identify the governing equations, from data, of nonlinear dynamical systems.

REFERENCES

ABSIL, C. O.; RICCARDI, A.; VASILE, M.; TARDIOLI, C. SMART-UQ : uncertainty quantification toolbox for generalised intrusive and non intrusive polynomial algebra. *In*: INTERNATIONAL CONFERENCE ON ASTRODYNAMICS TOOLS AND TECHNIQUES, 6., 2016. **Proceedings [...]**, [S.l.: s.n.], DEU, 2016.

ADAMS, D.; ADAMS, L. A tensile impact test apparatus for composite materials. **Experimental Mechanics**, New York, v. 29, p. 466–473, 1989.

ALMOHAMMADI, K. M.; INGHAM, D. B.; MA, L.; POURKASHANIAN, M. Cfd sensitivity analysis of a straight-blade vertical axis wind turbine. **Wind Engineering**, London, v. 36, n. 5, p. 571–588, 2012.

AVENDAÑO-VALENCIA, L. D.; BARAHONA, B.; HOELZL, C.; CHATZI, E. Operational regime clustering for the construction of PCE-based surrogates of operational wind turbines. *In*: INTERNATIONAL CONFERENCE ON ADVANCES IN EXPERIMENTAL STRUCTURAL ENGINEERING (AESE), 7., 2017, Pavia. **Proceedings [...]**, Pavia: [s.n.], v. 17, p. 961–964, 2017.

AVENDAÑO-VALENCIA, L. D.; CHATZI, E.; SPIRIDONAKOS, M. Non-stationary random coefficient models for vibration-based SHM in structures influenced by strong operational and environmental variability. **International Workshop On Structural Health Monitoring**, Stanford, v. 9, 2015.

BLATMAN, G. **Adaptive sparse polynomial chaos expansion for uncertainty propagation and sensitivity analysis**. 2009. Thesis (Ph. D.) — Université Blaise Pascal, Clermont-Ferrand, France, 2009. Doutorado em Engenharia Mecânica.

BLATMAN, G.; SUDRET, B. An adaptive algorithm to build up sparse polynomial chaos expansions for stochastic finite element analysis. **Probabilistic Engineering Mechanics**, London, v. 25, n. 2, p. 183 – 197, 2010. ISSN 0266-8920.

BODJONA, K.; LESSARD, L. Load sharing in single-lap bonded/bolted composite joints. part ii: Global sensitivity analysis. **Composite Structures**, v. 129, p. 276–283, 2015. ISSN 0263-8223.

BODJONA, K.; RAJU, K.; LIM, G.-H.; LESSARD, L. Load sharing in single-lap bonded/bolted composite joints. part i: Model development and validation. **Composite Structures**, London, v. 129, p. 268–275, 2015.

BOGOEVSKA, S.; SPIRIDONAKOS, M.; CHATZI, E.; DUMOVA-JOVANOSKA, E.; HöFFER, R. A data-driven diagnostic framework for wind turbine structures: a holistic approach. **Sensors**, Basel, v. 17, p. 720, 2017.

BORNN, L.; FARRAR, C. R.; PARK, G. Damage detection in initially nonlinear systems. **International Journal of Engineering Science**, Philadelphia, v. 48, n. 10, p. 909–920, 2010. ISSN 0020-7225.

BULL, T.; ULRIKSEN, M.; TCHERNIAK, D. **The effect of environmental and operational variabilities on damage detection in wind turbine blades**, [S.l.: s.n.], 2018.

CARNEIRO, G. das N.; ANTONIO, C. Sobol' indices as dimension reduction technique in evolutionary-based reliability assessment. **Engineering Computations**, Bingley, v. 37, p. 368–398, 2020.

CAVA, D. G.; TCHERNIAK, D. An experimental study on the data-driven structural health monitoring of large wind turbine blades using a single accelerometer and actuator. **Mechanical Systems and Signal Processing**, London, v. 127, p. 102 – 119, 2019. ISSN 0888-3270.

CAVA, D. G.; TCHERNIAK, D.; BRANNER, K. **Virtual prototyping of an actuator-based structural health monitoring system of wind turbine blades**, Leuven: [s.n.], 2018.

CHESNE, S.; DERAEMAEKER, A. Damage localization using transmissibility functions: A critical review. **Mechanical Systems and Signal Processing**, London, v. 38, n. 2, p. 569–584, 2013. ISSN 0888-3270.

CIANG, C. C.; LEE, J.-R.; BANG, H.-J. Structural Health Monitoring for a wind turbine system: a review of damage detection methods. **Measurement Science and Technology**, Bristol, v. 19, n. 12, p. 122001, oct 2008.

CRESPO, B. H. Damage sensing in blades. *In*: OSTACHOWICZ, W.; MCGUGAN, M.; SCHRÖDER-HINRICHS, J.-U.; LUCZAK, M. (ed.). **MARE-WINT: New Materials and Reliability in Offshore Wind Turbine Technology**, Cham: Springer International, p. 25–52, 2016. ISBN 978-3-319-39094-9.

CRESTAUX, T.; MAITRE, O. L.; MARTINEZ, J.-M. Polynomial chaos expansion for sensitivity analysis. **Reliability Engineering & System Safety**, London, v. 94, n. 7, p. 1161–1172, 2009. ISSN 0951-8320.

DU, X.; LEIFSSON, L. Multifidelity modeling by polynomial chaos-based cokriging to enable efficient model-based reliability analysis of NDT systems. **Journal of Nondestructive Evaluation**, New York, v. 39, p. 3, 2020.

DUBOURG, V. **Adaptive surrogate models for reliability analysis and reliability-based design optimization**. 2011. Thesis (Ph. D.), "Université" Blaise Pascal, Clermont-Ferrand, France, 12 2011.

DUBREUIL, S.; BARTOLI, N.; GOGU, C.; LEFEBVRE, T.; COLOMER, J. M. Extreme value oriented random field discretization based on an hybrid polynomial chaos expansion: Kriging approach. **Computer Methods in Applied Mechanics and Engineering**, Amsterdam, v. 332, p. 540 – 571, 2018. ISSN 0045-7825.

ECHEVERRÍA, F.; MALLOR, F.; MIGUEL, U. S. Global sensitivity analysis of the blade geometry variables on the wind turbine performance: Global sensitivity analysis of the blade geometry variables. **Wind Energy**, Oxford, v. 20, p. 5, 2017.

EDER, M.; BRANNER, K.; BERRING, P.; BELLONI, F.; TOFT, H.; SØRENSEN, J.; CORRE, A.; LINDBY, T.; QUISPITUPA, A.; PETERSEN, T. **Experimental Blade Research: Phase 2**. [S.l.]: DTU Wind Energy, 2015. (DTU Wind Energy E, 83).

FASSOIS, S.; SAKELLARIOU, J. Time-series methods for fault detection and identification in vibrating structures. **Philosophical Transactions of the Royal Society A**, London, v. 365, p. 411–48, 03 2007.

FRISWELL, M. I.; PENNY, J. E. T. Crack modeling for structural health monitoring. **Structural Health Monitoring**, v. 1, n. 2, p. 139–148, 2002.

GARCÍA-MACÍAS, E.; CASTRO-TRIGUERO, R.; FRISWELL, M. I.; ADHIKARI, S.; SáEZ, A. Metamodel-based approach for stochastic free vibration analysis of functionally graded carbon nanotube reinforced plates. **Composite Structures**, London, v. 152, p. 183 – 198, 2016. ISSN 0263-8223.

GHANEM, R.; OWHADI, H.; HIGDON, D. London: Springer International, 2017. 2053 p. *In*: GHANEM, R.; HIGDON, D.; OWHADI, H. (ed.).

GHANEM, R.; SPANOS, P. D. Polynomial chaos in stochastic finite elements. **Journal of Applied Mechanics**, Tehran, v. 57, n. 3, p. 197–202, 1990.

GHANEM, R. G.; SPANOS, P. **Stochastic finite elements: a spectral approach**. New York: Springer-Verlag, 1991.

GOGE, D.; SINAPIUS, M.; FULLEKRUG, U.; LINK, M. Detection and description of non-linear phenomena in experimental modal analysis via linearity plots. **International Journal of Non-Linear Mechanics**, Oxford, v. 40, n. 1, p. 27–48, 2005. ISSN 0020-7462.

HOMMA, T.; SALTELLI, A. Importance measures in global sensitivity analysis of nonlinear models. **Reliability Engineering and System Safety**, London, v. 52, n. 1, p. 1–17, 1996.

KAINTURA, A.; DHAENE, T.; SPINA, D. Review of polynomial chaos-based methods for uncertainty quantification in modern integrated circuits. **Electronics**, Basel, v. 7, n. 3, p. 21, 2018. ISSN 2079-9292.

KERSAUDY, P.; SUDRET, B.; VARSIER, N.; PICON, O.; WIART, J. A new surrogate modeling technique combining Kriging and polynomial chaos expansions: application to uncertainty analysis in computational dosimetry. **Journal of Computational Physics**, Maryland Heights, v. 286, p. 103 – 117, 2015. ISSN 0021-9991.

KERSCHEN, G.; WORDEN, K.; VAKAKIS, A. F.; GOLINVAL, J. Past, present and future of nonlinear system identification in structural dynamics. **Mechanical Systems and Signal Processing**, London, v. 20, n. 3, p. 505–592, 2006. ISSN 0888-3270.

KRIGE, D. G. A statistical approach to some basic mine valuation problems on the Witwatersrand. **The Journal of the Chemical, Metallurgical and Mining Society of South Africa**, Johannesburg, v. 52, n. 6, p. 119–139, 1951.

LARROSA, C.; LONKAR, K.; CHANG, F.-K. In situ damage classification for composite laminates using Gaussian discriminant analysis. **Structural Health Monitoring**, London, v. 13, n. 2, p. 190–204, 2014.

LARSEN, G. C.; BERRING, P.; TCHERNIAK, D.; NIELSEN, P. H.; BRANNER, K. Effect of a Damage to Modal Parameters of a Wind Turbine Blade. *In*: EUROPEAN WORKSHOP ON STRUCTURAL HEALTH MONITORING - EWSHM, 7., 2014, Nantes. **Proceedings [...]**, Nantes, 2014.

LATANIOTIS, C.; MARELLI, S.; SUDRET, B. **UQLAB User Manual: Kriging (Gaussian process modelling)**. Zurich, 2015. 53 p. Report UQLab-V0.9-105.

LIU, Q.; PAAVOLA, J. General analytical sensitivity analysis of composite laminated plates and shells for classical and first-order shear deformation theories. **Composite Structures**, London, v. 183, p. 21–34, 2018.

LOVE, B. Comparing supervised and unsupervised category learning. **Psychonomic bulletin & review**, New York, v. 9, n. 1, p. 829–835, 2002.

MAES, K.; ILIOPOULOS, A.; WEIJTJENS, W.; DEVRIENDT, C.; LOMBAERT, G. Dynamic strain estimation for fatigue assessment of an offshore monopile wind turbine using filtering and modal expansion algorithms. **Mechanical Systems and Signal Processing**, London, v. 76-77, p. 592 – 611, 2016. ISSN 0888-3270.

MAI, C. V. **Polynomial chaos expansions for uncertain dynamical systems – Applications in earthquake engineering**. 2016. Thesis (Ph. D.) — ETH Zürich, Zürich, Switzerland, 2016.

MAIA, N. M.; ALMEIDA, R. A.; URGUEIRA, A. P.; SAMPAIO, R. P. Damage detection and quantification using transmissibility. **Mechanical Systems and Signal Processing**, London, v. 25, n. 7, p. 2475–2483, 2011. ISSN 0888-3270.

MANDAL, D.; WADADAR, D.; BANERJEE, S. Health monitoring of stiffened metallic plates using nonlinear wave interaction and embedded pzt transducers. **Vibration Engineering and Technology of Machinery**, New York, v. 23, p. 629–638, 2015. ISSN 978-3-319-09917-0.

MARELLI, S.; SUDRET, B. UQLab: A framework for uncertainty quantification in matlab. *In*: INTERNATIONAL CONFERENCE ON VULNERABILITY AND RISK ANALYSIS AND MANAGEMENT - ICVRAM, 2., 2014, Liverpool. **Proceedings [...]**, Liverpool: University of Liverpool: [s.n.], p. 2554–2563, 2014.

MARELLI, S.; SUDRET, B. **UQLab user manual: Polynomial chaos expansions**. Zurich, 2015. 44 p.

MATHERON, G. **Traité de Géostatistique Appliquée, Tome II: Mémoires du Bureau de Recherches Géologiques et Minières**. [S.l.: s.n.], 1963.

MONTESANO, J.; CHU, H.; SINGH, C. V. Development of a physics-based multi-scale progressive damage model for assessing the durability of wind turbine blades. **Composite Structures**, London, v. 141, p. 50 – 62, 2016. ISSN 0263-8223.

NIELSEN, M.; ROCZEK-SIERADZAN, A.; JENSEN, F. M.; NIELSEN, P. H.; BERRING, P.; SIERADZAN, T.; ROUDNITSKI, V.; BITSCHE, R.; KNUDSEN, H. W.; RASMUSSEN, A. B.; RASMUSSEN, J. J. A.; ULDAHL, U.; ANDRLOVA, Z.; BRANNER, K.; BAK, C.; KALLESOE, B. S.; MCGUGAN, M.; LAGERBON, M.; WEDEL-HEINEN, J.; LINDBY, T.; RIBER, H. J.; JENSEN, C. **Full Scale Test SSP 34m blade, edgewise loading LTT. Extreme load and PoC_InvE Data report**. Roskilde, 2010. Danmarks Tekniske Universitet, Risø Nationallaboratoriet for Bæredygtig Energi.

NOËL, J.; KERSCHEN, G. Nonlinear system identification in structural dynamics: 10 more years of progress. **Mechanical Systems and Signal Processing**, London, v. 83, p. 2 – 35, 2017. ISSN 0888-3270.

ONU, O. d. N. U. **Objetivos de Desenvolvimento Sustentável**. 2015. Available from: `https://nacoesunidas.org/pos2015/`. Access on: 16 May 2022.

PAIXÃO, J.; SILVA, S. da; FIGUEIREDO, E. Damage quantification in composite structures using autoregressive models. *In*: INTERNATIONAL CONFERENCE ON DAMAGE ASSESSMENT OF STRUCTURES, 13, 2020, Singapore. **Proceedings** [**...**], Singapore: Springer, p. 804–815, 2020.

PAIXÃO, J.; SILVA, S. da; FIGUEIREDO, E.; RADU, L.; PARK, G. Delamination area quantification in composite structures using gaussian process regression and auto-regressive models. **Journal of Vibration and Control**, London, v. 27, n. 23-24, p. 2778–2792, 2021.

PAIXÃO, J. A. S.; SILVA, S. da. Extrapolation of autoregressive models for structural health monitoring in composite structures. *In*: INTERNATIONAL SYMPOSIUM ON SOLID MECHANICS (MECSOL), 7., 2019, São Carlos. **Proceedings** [**...**], São Carlos: [s.n.], 2019.

PALAR, P. S.; ZUHAL, L. R.; SHIMOYAMA, K.; TSUCHIYA, T. Global sensitivity analysis via multi-fidelity polynomial chaos expansion. **Reliability Engineering & System Safety**, London, v. 170, p. 175–190, 2018. ISSN 0951-8320.

PAVLACK, B.; PAIXÃO, J.; SILVA, S. da; CUNHA JR, A.; CAVA, D. G. Polynomial chaos-kriging metamodel for quantification of the debonding area in large wind turbine blades. **Structural Health Monitoring**, London, v. 21, n. 2, p. 666–682, 2022.

PAVLACK, B.; VILLANI, L. G. G.; SILVA, S. da; CUNHA JR, A. Vantagens da expansão em polinômio de caos na propagação de incertezas em sistemas mecânicos. **Proceeding Series of the Brazilian Society of Computational and Applied Mathematics, CNMAC 2019**, [S.l.: s.n.], v. 7, n. 1, 2020.

RASMUSSEN, C. E.; WILLIAMS, C. K. I. **Gaussian Processes for Machine Learning (Adaptive Computation and Machine Learning)**. [S.l.]: The MIT Press, 2005. ISBN 978-0-262-18253-9.

RASMUSSEN, C. E.; WILLIAMS, C. K. I. **Gaussian Processes for Machine Learning**. Cambridge: MIT Press, 2006. 248 p. ISBN 026218253X.

RIZOS, D.; FASSOIS, S.; MARIOLI-RIGA, Z.; KARANIKA, A. Vibration-based skin damage statistical detection and restoration assessment in a stiffened aircraft panel. **Mechanical Systems and Signal Processing**, London, v. 22, n. 2, p. 315–337, 2008. ISSN 0888-3270.

RYTTER, A. **Vibrational Based Inspection of Civil Engineering Structures**. 1993. Thesis (Ph. D.), Denmark, 1993. Ph.D.-Thesis defended publicly at the University of Aalborg, April 20, 1993 PDF for print: 206 pp.

SACKS, J.; WELCH, W. J.; MITCHELL, T. J.; WYNN, H. P. Design and analysis of computer experiments. **Statistical Science**, Shaker Heights, v. 4, n. 4, p. 409–423, 11 1989.

SALTELLI, A.; RATTO, M.; ANDRES, T.; CAMPOLONGO, F.; CARIBONI, J.; GATELLI, D.; SAISANA, M.; TARANTOLA, S. **Global Sensitivity Analysis: The Primer**. New York: John Wiley & Sons Inc, 2008.

SANTNER, T.; WILLIAMS, B.; NOTZ, W. **The Design and Analysis Computer Experiments**. [S.l.]: Springer, 2003. ISBN 978-1-4419-2992-1.

SARGSYAN, K. Surrogate models for uncertainty propagation and sensitivity analysis. *In*: GHANEM, R.; HIGDON, D.; OWHADI, H. (ed.). **Handbook of Uncertainty Quantification**, Cham: Springer International, p. 673–698, 2017. ISBN 978-3-319-12385-1.

SCHÖBI, R.; KERSAUDY, P.; SUDRET, B.; WIART, J. **Combining polynomial chaos expansions and Kriging**. ETH Zurich, Switzerland ; Orange Labs research, 2014.

SCHÖBI, R.; MARELLI, S.; SUDRET, B. **UQLab User Manual: polynomial chaos Kriging**. Zurich, 2017. 19 p. Report # UQLab-V1.4-109.

SCHÖBI, R.; SUDRET, B. **PC-Kriging**: A new metamodelling method combining polynomial chaos expansions and kriging. Rouen: [s.n.], 2014.

SCHÖBI, R.; SUDRET, B.; MARELLI, S. Rare event estimation using polynomial-chaos Kriging. **ASCE-ASME Journal of Risk and Uncertainty in Engineering Systems, Part A: Civil Engineering**, v. 500, p. D4016002, 03 2016.

SCHÖBI, R.; SUDRET, B.; WIART, J. Polynomial-chaos-based Kriging. **International Journal of Uncertainty Quantification**, Danbury, v. 5, p. 2, 2015.

SILVA, S. da; PAIXÃO, J.; RÉBILLAT, M.; MECHBAL, N. Extrapolation of ar models using cubic splines for damage progression evaluation in composite structures. **Journal of Intelligent Material Systems and Structures**, London, v. 0, n. 0, p. 1045389X20963171, 2020.

SOBOL, I. M. Sensitivity estimates for nonlinear mathematical models. **Mathematical and Computer Modelling**, Oxford, v. 1, p. 407–414, 1993.

SOIZE, C.; GHANEM, R. Physical systems with random uncertainties: Chaos representations with arbitrary probability measure. **SIAM Journal on Scientific Computing**, v. 26, n. 2, p. 395–410, 2004.

SOIZE, C.; ORCESI, A. Machine learning for detecting structural changes from dynamic monitoring using the probabilistic learning on manifolds. **Structure and Infrastructure Engineering**, Abingdon, v. 0, n. 0, p. 1–13, 2020.

SPIRIDONAKOS, M.; CHATZ, E. Polynomial chaos expansion models for SHM under environmental variability. *In*: INTERNATIONAL CONFERENCE ON STRUCTURAL DYNAMICS, 2014, Porto. **Proceedings [...]**, Porto: [s.n.], 2014.

SPIRIDONAKOS, M.; CHATZI, E.; SUDRET, B. **Polynomial Chaos Expansion Models for the Monitoring of Structures under Operational Variability**. [S.l.]: American Society of Civil Engineers, 2016.

STEIN, M. L. **Interpolation of Spatial Data: Some Theory for Kriging**. New York: Springer Science & Business Media, 1999. 247 p. ISBN 0-387-98629-4.

SUDRET, B. Recent developments in surrogate modelling for uncertainty quantification. **Proc. 3rd Int. Conf. on Vulnerability, Risk Analysis and Management (ICVRAM2018)**, Florianópolis, Brasil, 2018.

TANG, B.; BRENNAN, M. J.; LOPES, V. J.; SILVA, S. d.; RAMLAN, R. Using nonlinear jumps to estimate cubic stiffiness nonlinearity: an experimental study. **Proceedings of the Institution of Mechanical Engineers, Part C**, London, v. 0, n. 0, p. 1–7, 2015.

TCHERNIAK, D.; MØLGAARD, L. L. Vibration-based SHM system: Application to wind turbine blades. **Journal of Physics: Conference Series**, Bristol, v. 628, p. 012072, jul 2015.

TCHERNIAK, D.; MøLGAARD, L. L. Active vibration-based structural health monitoring system for wind turbine blade: Demonstration on an operating vestas v27 wind turbine. **Structural Health Monitoring**, London, v. 16, n. 5, p. 536–550, 2017.

THAPA, M.; MISSOUM, S. Uncertainty quantification and global sensitivity analysis of composite wind turbine blades. **Reliability Engineering & System Safety**, London, v. 222, p. 108354, 2022. ISSN 0951-8320.

TRIPATHY, R. K.; BILIONIS, I. Deep UQ: Learning deep neural network surrogate models for high dimensional uncertainty quantification. **Journal of Computational Physics**, Maryland Heights, v. 375, p. 565 – 588, 2018. ISSN 0021-9991.

ULRIKSEN, M. D.; TCHERNIAK, D.; DAMKILDE, L. Damage detection in an operating vestas v27 wind turbine blade by use of outlier analysis. *In*: WORKSHOP ON ENVIRONMENTAL, ENERGY, AND STRUCTURAL MONITORING SYSTEMS – EESMS. **Proceedings [...]**, New York: IEEE, p. 50–55, 2015.

ULRIKSEN, M. D.; TCHERNIAK, D.; KIRKEGAARD, P. H.; DAMKILDE, L. Operational modal analysis and wavelet transformation for damage identification in wind turbine blades. **Structural Health Monitoring**, London, v. 15, n. 4, p. 381–388, 2016.

UMESH, K.; GANGULI, R. Material uncertainty effect on vibration control of smart composite plate using Polynomial chaos expansion. **Mechanics of Advanced Materials and Structures**, New York, v. 20, p. 1–12, 2013. ISSN 1537-6494.

VILLANI, L. G. G.; SILVA, S. da; CUNHA JR, A. Application of a stochastic version of the restoring force surface method to identify a duffing oscillator. **First International Nonlinear Dynamics Conference (NODYCON 2019)**, Roma, Italy, v. 1, p. 335–336, 2019.

VILLANI, L. G. G.; SILVA, S. da; CUNHA JR, A.; TODD, M. D. Damage detection in an uncertain nonlinear beam based on stochastic volterra series: An experimental application. **Mechanical Systems and Signal Processing**, London, v. 128, p. 463 – 478, 2019. ISSN 0888-3270.

VILLANI, L. G. G.; SILVA, S. da; CUNHA JR, A. Damage detection in uncertain nonlinear systems based on stochastic volterra series. **Mechanical Systems and Signal Processing**, London, v. 125, p. 288 – 310, 2019. ISSN 0888-3270.

VIRGIN, L. N. **Introduction to Experimental Nonlinear Dynamics**. Cambridge University Press: [s.n.], 2000.

WANG, R.; JIANG, S. Mathematical methods for uncertainty quantification in nonlinear multi-physics systems and their numerical simulations. **Scientia Sinica Mathematica**, Beijing, p. 723–738, 2015.

WIENER, N. The homogeneous chaos. **American Journal of Mathematics**, Baltimore, v. 60, n. 4, p. 897–936, 1938.

WORDEN, K.; CROSS, E. J.; DERVILIS, N.; PAPATHEOU, E.; ANTONIADOU, I. Structural health monitoring: from structures to systems-of-systems. *In*: SYMPOSIUM ON FAULT DETECTION, SUPERVISION ANDSAFETY FOR TECHNICAL PROCESSES - SAFEPROCESS, 9., 2015, [s. l.]. **Proceedings [...]**, [S.l.]: IFACPapersOnLine, v. 48, n. 21, p. 1 – 17, 2015. ISSN 2405-8963.

WORDEN, K.; TOMLINSON, G. R. **Nonlinearity in Structural Dynamics - Detection, Identification and Modelling**. [S.l.]: University of Sheffield: Institute of Physics Publishing, 2001.

XIU, D. **Numerical Methods for Stochastic Computations: a Spectral Method Approach**. New Jersey: Princeton University, 2010.

XIU, D.; KARNIADAKIS, G. The Wiener-Askey polynomial chaos for stochastic differential equations. **SIAM Journal on Scientific Computing**, Philadelphia, v. 24, p. 619–644, 2002.

ZENG, M.; YANG, Y.; ZHENG, J.; CHENG, J. Normalized complex teager energy operator demodulation method and its application to fault diagnosis in a rubbing rotor system. **Mechanical Systems and Signal Processing**, London, v. 50-51, p. 380–399, 2015. ISSN 0888-3270.

ZHANG, J.; YIN, J.; WANG, R. Basic framework and main methods of uncertainty quantification. **Mathematical Problems in Engineering**, London, v. 2020, p. 1–18, 2020.

ZHOU, C.; LI, C.; ZHANG, H.; ZHAO, H.; ZHOU, C. Reliability and sensitivity analysis of composite structures by an adaptive kriging based approach. **Composite Structures**, London, v. 278, p. 114682, 2021. ISSN 0263-8223.

ZHOU, Y.; FIGUEIREDO, E.; MAIA, N.; PERERA, R. Damage detection and quantification using transmissibility coherence analysis. **Shock and Vibration**, London, v. 2015, p. 1–16, 2015.

ZHOU, Y.; FIGUEIREDO, E.; MAIA, N.; SAMPAIO, R.; PERERA, R. Damage detection in structures using a transmissibility-based mahalanobis distance. **Structural Control and Health Monitoring**, Oxford, v. 22, 2015.

ZHOU, Y.-L.; MAIA, N. M.; SAMPAIO, R. P.; WAHAB, M. A. Structural damage detection using transmissibility together with hierarchical clustering analysis and similarity measure. **Structural Health Monitoring**, London, v. 16, n. 6, p. 711–731, 2017.

ZHOU, Y.-L.; MAIA, N. M.; WAHAB, M. A. Damage detection using transmissibility compressed by principal component analysis enhanced with distance measure. **Journal of Vibration and Control**, London, v. 24, n. 10, p. 2001–2019, 2018.

A POLYNOMIAL CHAOS-KRIGING CODE IN MATLAB

```
clc
clear
close all

display('Damage quantification using the Polynomial Chaos-Kriging metamodel in a large wind turbine blade')

load processed_data/setup % Loading the data collected from the blade
load(strcat(setup.save_path,'/damage_index')) % Loading of local damage indices

uqlab; % Starting UQLab

% CONFIGURATION INFORMATION POLYNOMIAL CHAOS-KRIGING METAMODEL

InputOpts.Marginals.Type    = 'Lognormal'; % Distribution of model learning data
InputOpts.Marginals.Moments = [mean, std]; % Moments of the learning data

myInput = uq_createInput(InputOpts);

OptPCKOpts.Type     = 'Metamodel';
OptPCKOpts.MetaType = 'PCK'; % PC-Kriging metamodel
OptPCKOpts.Mode     = 'optimal'; % Specifies the PC-Kriging model type

OptPCKOpts.Kriging.Display     = 'quiet'; % Display information
OptPCKOpts.Kriging.EstimMethod = 'ML'; % Estimation method
OptPCKOpts.ExpDesign.Sampling  = 'user'; % Experimental design options

% Correlation function options
OptPCKOpts.PCE.Method             = 'LARS';
OptPCKOpts.PCE.Degree             = 3:10; % Range of degree to be tested
OptPCKOpts.Kriging.Corr.Family    = 'exponential'; % Correlation family
OptPCKOpts.Kriging.Corr.Type      = 'ellipsoidal'; %
OptPCKOpts.Kriging.Corr.Isotropic = 0;

% Hyperparameters optimization method
OptPCKOpts.Kriging.Optim.Method  = 'HCMAES'; % Hybrid Covariance Matrix Adaptation-Evolution Strategy
OptPCKOpts.Kriging.Optim.Display = 'none'; % Limits

% MODEL LEARNING AND VALIDATION

 for actuator=1:4
     for sensor=1:10

         di_train  = []; % Vector with the data of the DI for learning
         sev_train = []; % Vector with the severity data for learning
         di_test   = []; % Vector with the data of the DI for validation
         sev_test  = []; % Vector with the severity data for validation

         for cond=[1 3 5 6 7] % Learning conditions (H, D40, D80, D100, and D120)
             train     = D(cond,actuator,sensor).data;
             di_train  = [di_train train];
             sev_train = [sev_train ones(1,length(train))*setup.severity(cond)];
         end

         for cond=[2 4] % Validation conditions (D20 and D60)
             test     = D(cond,actuator,sensor).data;
             di_test  = [di_test test];
             sev_test = [sev_test ones(1,length(test))*setup.severity(cond)];
          end

       OptPCKOpts.ExpDesign.X = di_train'; % Input of the PC-Kriging metamodel
       OptPCKOpts.ExpDesign.Y = sev_train'; % Output of the the PC-Kriging metamodel

       myOptPCK = uq_createModel(OptPCKOpts);

```

```
65        PCK(actuator,sensor).model = myOptPCK;
66
67
68         % Settings for the confidence interval of 95%
69         x = linspace(min(di_train), max(di_train), 25)
70
71         [ypred_ref,std_pred2,C] = uq_evalModel(myOptPCK, x');
72         [pred_test,std_pred,C]  = uq_evalModel(myOptPCK,di_test');
73
74         u_band = ypred_ref + 1.96*sqrt(std_pred2);
75         l_band = ypred_ref - 1.96*sqrt(std_pred2);
76         x_conf = [x, fliplr(x)];
77         y_conf = [u_band', fliplr(l_band')];
78
79         % Definitions for the obtained PCK metamodel, to facilitate figure settings, for example
80         PCK(actuator,sensor).pred          = ypred_ref;
81         PCK(actuator,sensor).x             = x;
82         PCK(actuator,sensor).x_conf        = x_conf;
83         PCK(actuator,sensor).y_conf        = y_conf;
84         PCK(actuator,sensor).di_train      = di_train;
85         PCK(actuator,sensor).sev_train     = sev_train;
86         PCK(actuator,sensor).di_test       = di_test;
87         PCK(actuator,sensor).sev_test      = sev_test;
88         PCK(actuator,sensor).sev_pred_test = pred_test;
89
90     end
91 end
```